Porphyrin-based porous organic polymers enriched with Fe_3O_4 nanoparticles as electrosensors for the detection of endocrine disrupting chemicals in water

by

Lu-Nita Berrangé

Submitted in fulfilment of the requirements for the degree

Master of Science in Chemistry

In the Faculty of Natural & Agricultural Sciences

University of Pretoria

November 2023

Declaration

I, Lu-Nita Berrangé, declare that the dissertation, which I hereby submit for the degree Master of Science in Chemistry at the University of Pretoria, is my own work and has not previously been submitted by me for a degree at this or any other tertiary institution.

SIGNATURE: …… DATE: ……

Dedication

To my future husband and loving parents

Claude du Plessis,

Lukas and Anita Berrangé

Acknowledgments

Thank you, Lord, for blessing me with many great talents perfectly suited to who I am. I thank you for your wisdom and strength throughout this chapter in my life.

I would like to thank my supervisor, Dr N Nombona, for everything I have learned. Thank you for all the invaluable advice, continuous support, and patience during my MSc Studies. Thank you to our research group for always being willing to help and give advice and for your encouragement over the past years.

I wish to thank the University of Pretoria and the Department of Chemistry for providing a conducive environment to carry out this research. Thank you to University of Johannesburg's electron microscopy lab for helping me analyze my samples.

I am so grateful to my family and friends for your support throughout this chapter in my life. Thank you for celebrating all my small or big achievements with me and lending a shoulder when facing difficulty. May we all write the next chapter together.

Abstract

Endocrine disrupting chemicals (EDCs) are commonly found in products such as pesticides, plastics, and pharmaceuticals. These chemicals are of significant concern due to their potential to disrupt the endocrine system, which plays essential roles in growth and reproduction. The detection of EDCs in water requires extensive equipment training and is expensive; therefore, it remains a significant challenge. Various catalysts such as multiwalled carbon nanotubes and graphene has been used as sensors to detect EDCs but porous organic polymers (POPs) and Porphyrin-based POPs (Py-POPs) have gained interest in electrochemical research owing to their porosity, stability, and tuneable structure. The structure of POPs depends on the synthetic method, the monomer used, and reaction conditions. Porphyrins are cyclic tetrapyrroles that consist of a conjugated π-electron system. Due to this conjugation, Py-POPs are stable structures that can coordinate metal ions. Metalated porphyrin-based POPs (MPy-POPs) are redox-active and chemically stable with improved electrochemical performance.

In light of this, metalated porphyrin-based POPs (MPy-POPs) were used as sensing platforms for the detection of 2-phenylphenol, an endocrine disrupting chemical. Iron and zinc Py-POPs were synthesized and enriched with Fe_3O_4 nanoparticles to form nanocomposite materials. The morphological and structural characteristics of the composites were analysed using a variety of techniques, which includes ultraviolet-visible (UV-Vis) spectroscopy, Fourier transform infrared spectroscopy (FTIR), powder X-ray diffraction (PXRD), scanning electron microscopy (SEM), tunnel electron microscopy (TEM) and energy dispersive X-ray (EDX) analysis. The synthesized composites had spherical morphology.

The Fe_3O_4@MPy-POP catalysts were used for the electrocatalytic detection of 2-phenylphenol. Catalytic currents ranged between 24.7 µA and 41.5 µA, with peak potentials between 0.61 V and 0.65 V. The limit of detection ranged from 0.75 mM to 2.6 mM for the redox active catalysts. Real sample analysis using sunblock and apple peels were analyzed for the detection abilities of the synthesized catalysts. This study shows that these composites are promising materials for the detection endocrine disrupting chemicals in water.

Table of Contents

List of abbreviations

CMPs	Conjugated microporous polymers
CNG	Compression at high pressure
COFs	covalent organic frameworks
CS	Chitosan
CTFs	covalent triazine frameworks
CV	Cyclic voltammetry
DCM	Dimethyl chloride
DNA	Deoxyribonucleic acid
DPV	Differential pulse voltammetry
EDCs	Endocrine disrupting chemicals
EDLC	Electrostatic double layered capacitors
EIS	Electrochemical Impedance Spectroscopy
FeP-CMP	Iron (III) porphyrin CMPs
FTIR	Fourier transform infrared spectroscopy
GCE	Glassy carbon electrode
H-Fe_3O_4@C/GNS /GCE	3D carbon encapsulated hollow Fe_3O_4 nanoparticles anchored on graphene oxide nanosheet
$HMPF_6$	n-hexyl-3-methylimidazolium hexafluorophosphate
HOMO	Highest occupied molecular orbital
HCPs	Hyper-crosslinked polymers
ITO	indium tin oxide

LNG	Liquefaction at low temperatures
LUMO	Lowest unoccupied molecular orbital
MIP	Molecular imprinted polymers
MnPc-TA	Terminal alkyne substituted manganese phthalocyanine thin film
MOFs	Metal organic frameworks
MPY-POPs	Metalated porphyrin porous organic polymers
MP-POP	Magnetic porphyrin-based porous organic polymers
MWCNT/MWNT	Multiwall carbon nanotubes
N_3-PANI	4-azido polyaniline
NP	Nanoparticle
PAFs	Porous aromatic frameworks
PC	Pseudocapacitors
PCP	Porous coordination polymers
PdNPs	Pd nanoparticles
POPs	Porous organic polymers
Py-POPs	porphyrin-based porous organic polymers
rGO	reduced graphene oxide
SEM	Scanning electron microscopy
SFP	Nitrogen self-doped sunflower plate-derived carbon
SPE	Screen printed electrodes
SWV	Square wave voltammetry
TA	Tannic acid

TEM	Transmission electron microscopy
THF	Tetrahydrofuran
TMPs	triptycene-based microporous polymers
TPES	Thermoplastic elastomers
TTSBI	5,5′,6,6′-tetrahydroxy-3,3,3′,3′-tetramethyl-1,1′-spirobisindane
UV-Vis	Ultraviolet-visible spectroscopy
XRD	X-ray diffraction

List of symbols

µ	Micro
g	Gram
L	Liter
cm	Centimeter
m	Meter
mL	Milliliters
nm	Nanometer
mM	Millimolar
µM	Micromolar
α	Electron transfer coefficient
ν	Scan rate
R	Gas constant
T	Temperature
F	Faraday’s constant
n	Number of electrons

I_p	Peak current
E_{pa}	Anodic potential
I_{pa}	Anodic current

List of Figures

List of tables:

List of schemes

Chapter 1: Introduction

1.1. Background

Endocrine disrupting chemicals (EDCs) pose a significant threat to human health, and unfortunately, they are present in various sources such as the environment, food, plasticizers, pharmaceuticals, and personal care products (Bergman et a., 2013). EDCs are compounds that interfere with the proper functioning of the endocrine system, including metabolism, hormone biosynthesis, and reproduction (Diamanti-Kandarakis et al., 2009). Although several analytical methods have been developed to detect EDCs like phthalates, bisphenols, and parabens over the past decade, it still remains a big challenge because these chemicals are present in very low concentrations. Additionally, the available analytical methods for detection are often expensive (Scognamiglio et al., 2016).

Porous organic polymers (POPs) are a unique type of polymers due to their organic porous structure made from light elements. This characteristic contributes to their high surface area, structural tunability, and thermal stability (Song et al., 2023). Structurally ordered POPs are known as covalent organic frameworks (COFs) and are highly crystalline. Semicrystalline covalent triazine frameworks (CTFs) consist of crystalline and amorphous domains. Lastly, various groups of amorphous POPs include hypercrosslinked polymers (HCPs), polymers of intrinsic properties (PIMs), conjugated microporous polymers (CMPs), and porous aromatic frameworks (PAFs) (Giri et al., 2022).

Porphyrins are a class of compounds that consist of an 18-π aromatic macrocycle. Due to their rigidity, planar geometry, and chemical stability they are used as monomers for POP synthesis (Xia et al., 2010). Metalated porphyrin-POPs (MPy-

POPs) can be synthesized to produce highly crystalline or amorphous structures. The porous nature of POPs allows them to interact with target molecules in a specific environment, making them promising materials for various applications, such as electrochemical research.

Metal oxide nanoparticles, like magnetite (Fe_3O_4), have several advantageous characteristics including chemical and photochemical stabilities, low-cost synthesis, good electrochemical activity, and magnetic properties. These properties make them highly desirable for creating sensor materials (Hwang et al., 2014). By combining metal nanoparticles with MPy-POPs, new multifunctional composites can be created (Fe_3O_4@MPy-POP) that combines the properties of both MPy-POP and the nanoparticles. The use of nanoparticles to enrich POPs has become increasingly popular due to their enhanced performance in various applications (Lee et al., 2023). However, nanoparticle aggregation can be detrimental to performance as it can reduce surface area and electrical conductivity (Li & Kaner, 2006). To prevent this, metal oxide nanoparticles have been incorporated into the POP structures to improve performance (Kathiresan, 2023).

POPs have a wide range of applications which includes catalysis, absorption, separation, sensing and energy storage (Song et al., 2023). Amongst the various categories of POP-based sensors, fluorescence sensors are most popular for the detection of explosives, metal ions, small molecules, and biological molecules (Wang et al., 2022). Metals, such as copper, have been incorporated in Py-POPs for non-enzymatic electrochemical detection of glucose. This method has achieved a limit of detection of 0.9 µM and a sensitivity of 415. 87 µA. $mM^{-1}.cm^{-2}$ (Sun et al, 2018). Additionally, porous coordination polymers (PCP) have been doped with Fe_3O_4 nanoparticles for the detection of diethylstilbesterol and 17β-estradiol in toner (Chen

et al., 2018). However, Fe_3O_4 nanoparticles are susceptible to oxidation and can cause agglomeration issues (Pintor Simamora et al., 2018). To overcome this, researchers have incorporated Fe_3O_4 nanoparticles into the nanoporous PCP composite. The PCP composite achieved a LOD of 4.65 nM and 4.9 nM for diethylstilbesterol and 17β-estradiol respectively (Chen et al., 2018). The nanoparticles were monodispersed within the PCP structure, displaying a high surface area and catalytic activity, as well as fast electron transfer on the electrode surface. Efficient electrochemical sensors require electrodes and signal tags that are highly specific, as well as electrodes with exceptional sensitivity and stability (Yang et al., 2022). The combination of Fe_3O_4 nanoparticles with a coordination polymer has shown promising results and contributes to enhanced performance of the electrochemical sensor.

This study aims to use MPy-POPs and Fe_3O_4@MPy-POPs as sensing platforms to detect 2-phenylphenol, an endocrine disrupting chemical. The MPy-POPs will be enriched with Fe_3O_4 nanoparticles. The use of MPy-POPs in conjunction with Fe_3O_4 is to reduce agglomeration of nanoparticles and enhance the composite sensitivity of the electrode, leading to improved electrochemical detection of 2-phenylphenol.

1.2. Problem statement

Endocrine disrupting chemicals are present in everyday household items. EDC exposure to humans has increased due to its presence in portable water as a result of agricultural activities and their presence in cosmetic products (Kahm et al., 2020). They are also present in food containers and wrappers and can leach into the food stuff and pose a danger to humans (Ong et al., 2020). These chemicals have potential to interfere with physiological processes namely sexual development, normal hormone function and fertility (Hlisníková, 2020). Due to the serious health implications of

exposure to endocrine disrupting chemicals, it is crucial to develop a more straightforward and cheaper method for their detection.

1.3. Hypothesis

If MPy-POPs are successfully synthesized and enriched with Fe_3O_4 nanoparticles, it will form Fe_3O_4@MPy-POP nanocomposites that reduce agglomeration of Fe_3O_4. The synergistic advantages of these electrocatalysts will produce a sufficient electrode with increased sensitivity and selectivity for detection of an EDC, 2-phenylphenol.

1.4. Aim and objectives

This work aims to synthesize and characterize FePy-POP, ZnPy-POP, Fe_3O_4@ZnPy-POP, and Fe_3O_4@FePy-POP. These compounds will be used as catalysts on a modified glassy carbon electrode (GCE) to enhance electrochemical detection of 2-phenylphenol in water and real samples.

Objectives:

i. Synthesize and characterize metalated porphyrin-based porous organic polymers (ZnPy-POP and FePy-POP).
ii. Synthesize and characterize metalated porphyrin-based porous organic polymers enriched with Fe_3O_4 nanocomposites (Fe_3O_4@ZnPy-POP and Fe_3O_4@FePy-POP).
iii. Electrochemical detection of 2-phenylphenol in aqueous solution
iv. Electrochemical detection of 2-phenylphenol in real samples

Chapter 2: Literature review

2.1. Discovery and general properties of porous organic polymers (POPs)

Porous polymers have been synthesized since the early 1960s using multitopic monomers in a chain-growth polymerization process (Hollis, 1966). In the 1990, microporous organic polymers were synthesized with more complex monomer building blocks to better the molecular recognition features (Sebati & Ray, 2018). Microporous polymers were further investigated for their application in storage, catalysis, and separation (Kaur et al., 2011). Porous materials can be classified by their pore size as microporous (pore diameter smaller than 2 nm), mesoporous (pore diameter between 2 nm and 50 nm), and macroporous (pore diameter larger than 50 nm) (Thommes et al., 2015). Furthermore, porous materials can be classified on their building blocks as inorganic (zeolites), inorganic-organic hybrids (metal-organic frameworks), and organic porous materials (porous organic polymers). Based on the long-range order of porous materials they are found to be either crystalline (zeolites, metal-organic frameworks, covalent organic frameworks, or H-bonded organic frameworks), semi-crystalline (covalent triazine frameworks) or amorphous materials (conjugated microporous polymers, hypercrosslinked polymers, polymers of intrinsic microporosity and porous aromatic frameworks) (Girri et al., 2022).

Porous organic polymers have emerged as designer materials combining the best features of heterogeneous and homogeneous catalysts with exceptional thermal and chemical stability (Yang et al., 2023). They can withstand high pressure and temperatures and exhibit great catalytic behavior and structural tunability by utilizing a wide range of organic building blocks (Tanabe et al., 2014). The combined features

in one framework allow POPs to be designed for specific functionalities and analyte-specific interactions which were not previously achievable.

POPs have highly polymeric backbones and are generally made of organic building blocks linked with covalent solid bonds forming 2-D or 3-D structures (Li et al., 2018). POPs can be synthesized as either crystalline, semicrystalline, or amorphous, each structurally unique but related by specific characteristics like high porosity, structural tunability, use of lightweight elements, and strong covalent bonds that can form particular shapes such as nanospheres, nanotubes or nanosheets (Sarkar et al., 2021). Metalloporphyrin complexes have been used as building blocks for the synthesis of POPs and have shown to have exceptional thermostability due to mononuclear active sites providing better sustainability, recyclability, and robustness in single-atom catalysis (Shultz et al., 2011). For this reason, these POP materials can be used not only as heterogenous support systems but also in gas storage (Cousins & Zhang, 2019), chemical sensing (Liu et al., 2020), adsorption and electrocatalysis (Zhu et al., 2019).

2.2. Classification and structure of POPs

Porous organic polymers can be divided into three main categories based on the long-range ordering and morphology of POPs as shown in Figure 2.1 (Giri et al., 2022).

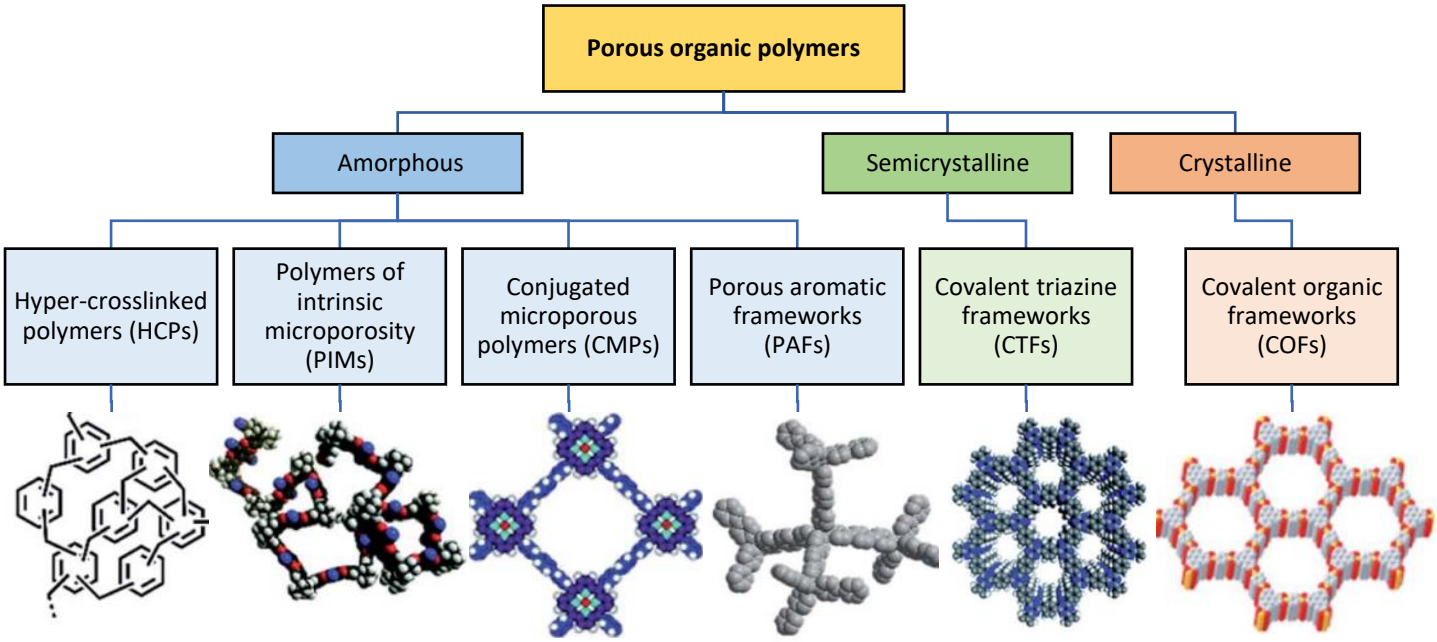

Figure 2.1: *Schematic presentation of the three main classes of porous organic polymers (Giri et al., 2022)*

Crystalline networks are defined by the long-range positional order of symmetrical 3-D building blocks in a distinct space. Amorphous structures are limited to long-range positional orders due to improper bond angles, bond lengths and dihedral angles between repetitive 3-D units (Geng et al., 2020). Crystalline POPs are structurally ordered, exhibiting uniform and periodic pore sizes. Amorphous POPs contain interconnected hierarchical and deformed pore architectures that are easier to synthesize with a larger variety of building blocks available. Although CTFs have been

previously described as crystalline, they are classified as semicrystalline POPs because they consist of both crystalline and amorphous domains (Giri et al., 2022).

2.2.1. Amorphous porous organic polymers

Many known POPs are amorphous, as the crystallization process is a major challenge (Guo et al., 2018). Amorphous POPs are synthesized using various synthetic strategies with abundant monomers that contribute to structural diversity. This plays a crucial role in designing functional and pore filled materials. The amorphous arrangement lacks long-range order causing a periodically repetitive pattern of POPs over short distances. This structural design and functionalization allow increased flexibility and adaptability of POPs (Giri et al., 2022).

2.2.1.1. Hyper-crosslinked polymers (HCPs)

HCPs are microporous, 3-D networks constructed from irreversible covalent linkages of various organic building blocks. HCPs are highly hydrophobic, conjugated structures. They are often used in adsorption applications due to their high affinity for aromatic compounds (Liu et al., 2015).

Several organic monomers can be used for the fairly easy and cost-effective synthesis of HCPs to achieve a variety of pore architectures built for specific functions (Tan & Tan, 2017). Three synthetic strategies are used for the synthesis of HCPs which aid in controlled reactions and contributes to structural diversity. Firstly, post-crosslinking synthesis involves external crosslinking agents like electrophiles in the presence of a Lewis acid and a suitable solvent to preserve spatial distributions. This method has been used to synthesize post-crosslinked polymeric adsorbents (Germain et al., 2007). Secondly, a one-pot synthesis polycondensation of bifunctional monomers, with more building blocks to produce controllable pore size and surface area (Wood

et al., 2007). The third synthetic strategy involves external crosslinkers that attach multiple low-cost, rigid aromatic building blocks contributing to high surface area HCPs. This is as greener synthetic strategy with methanol as the only by-product (Li et al., 2011). More research has been focussed on the external crosslinking strategy due to exceptional advantages namely structural tuneability, mild and cost-effective synthetic conditions, high surface area and production of various pore structures. HCPs are often used in adsorption applications to remove benzene (Xia et al., 2021) and 2-naphthol from water (Cao et al., 2023).

To obtain optimum adsorption, the pore size of the adsorbents must be 2-6 times larger than the adsorbate molecular size (Li et al., 2011). HCP synthesis generally leads to packed microporous frameworks which limits the removal of bulky aromatic pollutants. Adsorption efficiency is increased by incorporating mesopores and micropores into the HCP structure to ensure more sufficient connecting channels (Seo et al., 2015). This can be done by using hyperbranched polystyrene (TPES) as a precursor in the Friedel-Craft reaction to obtain HCPs with high surface area and hierarchical pores. The general synthesis is displayed in Figure 2.2, where incorporated mesopores in HCPs increased the adsorption efficiency.

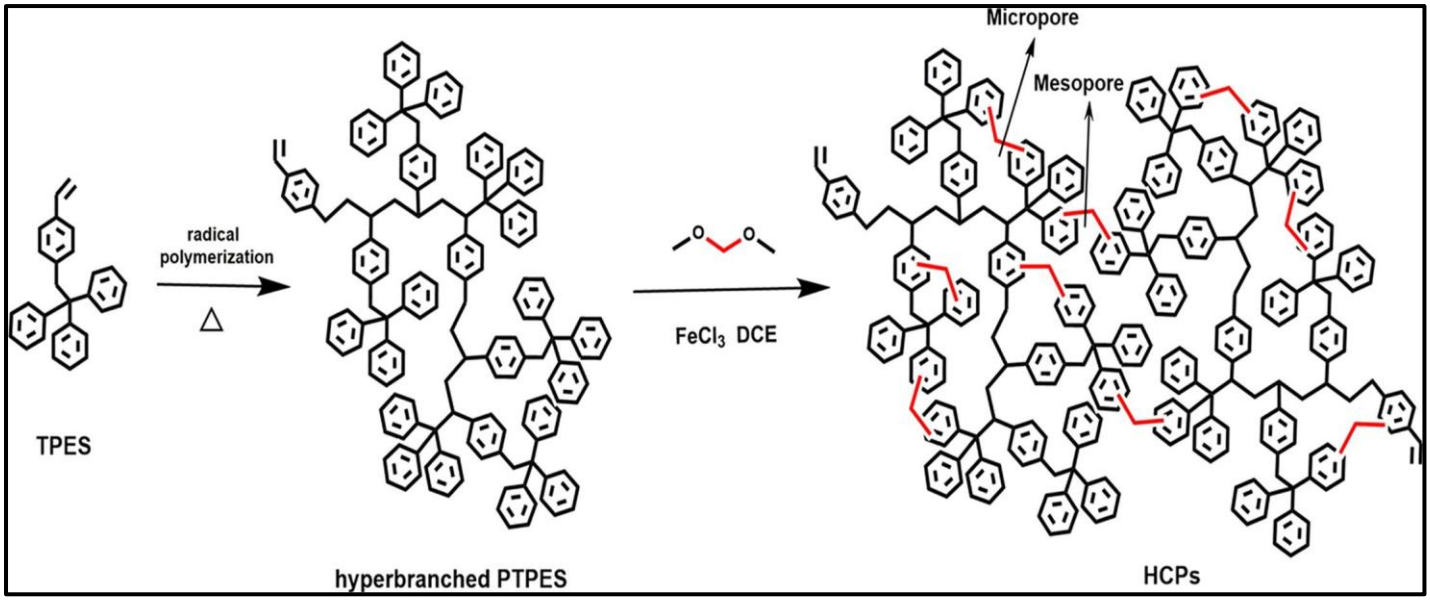

Figure 2.2: *Synthesis of HCPs containing hierarchical pores from hyperbranched polystyrene precursors via Friedel-Craft chemistry (Cai et al., 2021).*

2.2.1.2. Polymers of intrinsic microporosity (PIMs)

PIMs are a class of amorphous POPs that do not have a macromolecular network structure and, therefore, are highly soluble in organic solvents. Generally, PIMs are synthesized using soluble polymers as building blocks, and through insufficient packing, they display randomly distorted shapes that create pores inside the polymer (McKeown, 2017). PIMs are made of a structural component that possesses concavities to introduce contortion into the polymer chain. They also have a linking group component that fuses the structural units together during polymerization which prevents rotation of one unit relative to the neighbouring unit. Due to their solubility in organic solvents, PIMs can be processed into films with high permeability and distinct gas pair selectivity in gas separation (Foster et al., 2020).

PIMs are derived from three types of reaction strategies which are based on PIM polymerisation using either (a) dibenzodioxane formation, (b) Tröger's base formation

and (c) imide formation called PIM-polyimides. These methodologies have been used to generate a wide range of PIMs, with Tröger's base being the most popular because it can serve as both the linking group and the structural unit (McKeown, 2020). In order to maintain microporosity, the selection of both conformationally locked monomer building blocks and a polymerization reaction is important to enforce steric hindrance to prevent or severely restrict bond rotation. Monomers containing spiro-centres, linking groups like Tröger's base, or both can be used to avoid a linear structure. PIM's structure cannot pack efficiently as they have rigid and contorted backbones which contributes to its microporosity and high selectivity. Because of this, PIMs are suitable for formation of polymer membranes for gas separation (Foster et al., 2020), heterogenous catalysis, hydrogen storage (McKeown & Budd, 2006) and electrochemical applications (Marken et al., 2020).

The properties of PIMs depend on the acidity/basicity of functional groups, molecular weight, aging process, exposure to air and light, as well as the guest species that can produce various structures (Marken et al., 2020). As seen in Figure 2.3, PIMs can consist of various topologies due to insufficient packaging during synthesis.

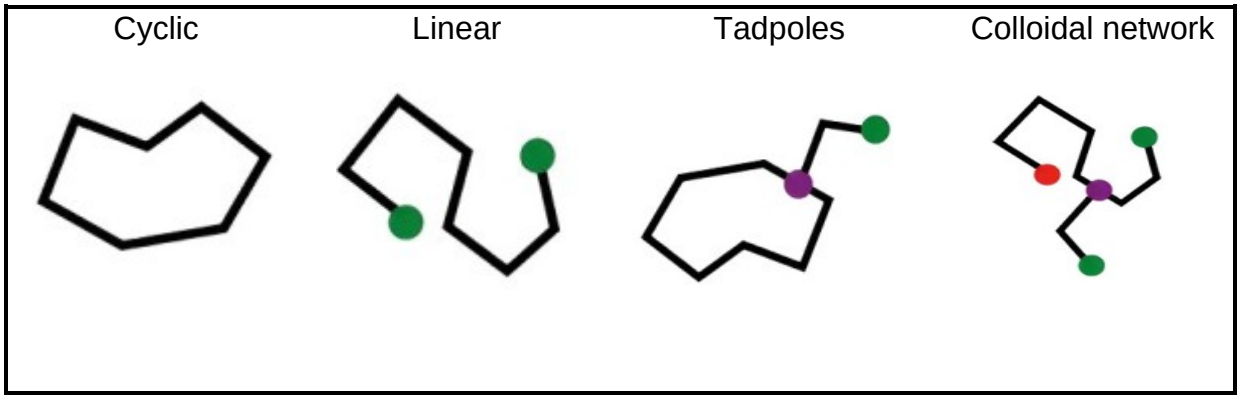

Figure 2.3: *Various topologies of PIMs (Foster et al., 2020).*

2.2.1.3. Conjugated microporous polymers (CMPs)

CMPs are a class of amorphous POPs first reported in 2007 (Jiang et al., 2007). These porous materials have been developed extensively and are unique with their broad π-conjugated linking of various building blocks to achieve a 3-D network. Optimization of the skeleton and properties are easily achievable due to little limitations of geometry, size and functional groups that contributes to tuneable π-conjugated porous structural designs (Xu et al., 2013). Conjugation arise from building blocks like phenyl units, arenes, heterocyclic aromatics or macrocycles, linked together by double or triple bonds throughout the extended network. These covalent bonds are formed kinetically by several irreversible reactions like Sonogashira-Hagihara coupling, Suzuki-Miyaura coupling, Yamamoto coupling, Heck coupling and oxidative coupling (Lee & Cooper, 2020). The combination of various synthetic strategies along with the broad range of monomers available for use, yields conjugated skeletons with nanopores that shows great potential in gas adsorption, chemosensors, heterogenous catalysis, light harvesting, and electric energy storage. CMPs show great potential as sensors due to their large surface area exceeding 1000 m^2g^{-1} that provides a bigger area for analyte interaction with increased response time and sensitivity (Liu et al., 2012).

Iron (III) porphyrin CMPs (FeP-CMP) have been reported for heterogeneous catalysis having large surface areas and inherent nanopores accessible to substrates for highly selective oxidation reactions under mild conditions. The amorphous structure of FeP-CMP consists of an inherent porous framework with catalytic sites build into the skeleton (Figure 2.4). FeP-CMP showed to be chemoselective which allows for large scale transformations of sulphides to sulfoxides. These CMPs are also readily recycled; therefore, they can be valuable as photocatalysts (Chen et al., 2010).

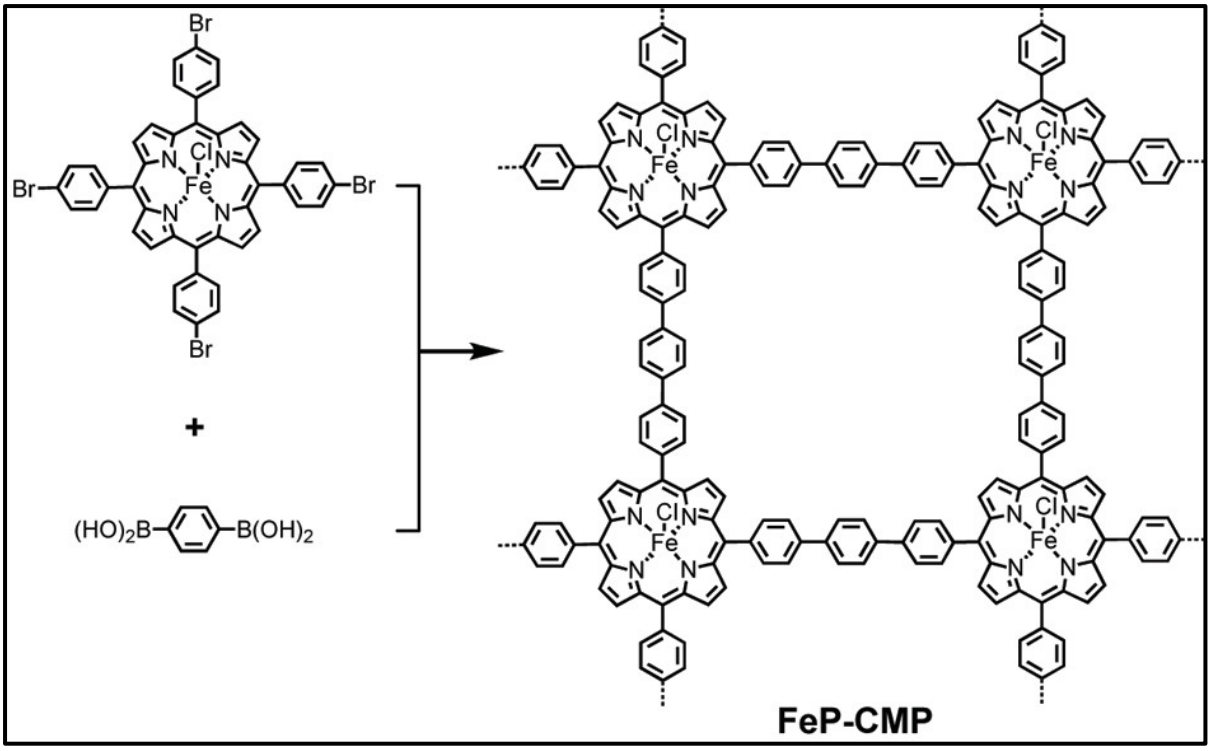

Figure 2.4: *Synthesis of CMP nanoporous polymer with built-in metalloporphyrin skeleton used in heterogeneous catalysis (Chen et al., 2010).*

2.2.1.4. Porous aromatic frameworks (PAFs)

Porous organic frameworks are also known as porous polymer networks and are synthesized using similar coupling reactions as CMPs but lack π-conjugation as they are generally linked to tetrahedral tetraphenylmethane nodes (Lu et al., 2010). This class of POPs is seen as a 'framework' and originates from using building blocks with predesigned geometries in an irreversible coupling reaction. PAFs display flexible frameworks, tunability, chemical stability and are extremely hydrophobic. This separates them from other framework-based classes like metal organic frameworks (MOFs) and zeolites (Ben at al., 2009). The first recorded porous aromatic framework (PAF-1) was applauded for exceptional surface area (7 100 m^2g^{-1}), possibly due to Yamamoto-type Ullmann coupling reaction that eliminates unreacted starting material (Yuan & Zhu, 2019). PAF-1 has a diamond like framework as seen in Figure 2.5 and

has robust covalent carbon bonds connecting the whole framework (Yuan & Zhu, 2019). Additionally, postsynthetic treatments are possible due to the exceptional thermal and chemical stability (Tian & Zhu, 2020).

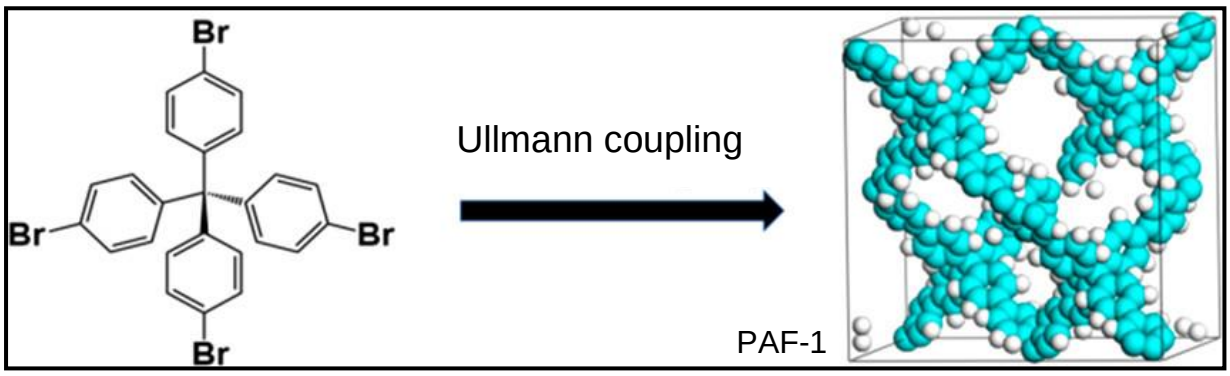

Figure 2.5: *PAF-1 building block used in a Yamamoto-type Ullmann coupling reaction displaying the diamond-like structure of PAF-1. (Tian & Zhu, 2020).*

2.2.2. Semicrystalline covalent triazine frameworks (CTFs)

CTFs have been reported as semicrystalline due to ultra-strong bond formation by dynamic condensation reactions to make ordered structures while having amorphous domains (Kuhn et al., 2008). CTFs are unique from other POPs as they consist of aromatic C=N linkages which leads to semicrystalline structures when strong aromatic covalent bonds are formed in a highly dynamic polymerization reaction (Liao et al., 2023).

This class of polymers are constructed using 1,3,5-triazine rings and contains planar π-conjugated properties between aromatic rings and triazine rings reducing the total energy in the framework, ultimately improving chemical stability. CTF offers a long service life and are not prone to aging, although reversable covalent bond formation leads to crystallization, it has limited stability (Zhang et al., 2018). Nitrogen rich CTFs comes from contributing triazine linkages but also from various selected groups used in synthesis which gives them an advantage compared with other POPs. Various

synthetic strategies involve ionothermal trimerization, Friedel-Craft reactions and amidine based polycondensation methods. The most established synthetic route to obtain semicrystalline structures is ionothermal synthesis at high temperatures (Qian et al., 2021). The type of monomer and temperature used in synthesis ultimately influences CTF crystallinity, surface area, porosity, light absorption ability and chemical stability.

Figure 2.6 shows the various monomers used at different reaction conditions leading to amorphous, semicrystalline, and crystalline CTF structures. The first strategy in Figure 2.6a leads to amorphous CTFs, as a result of very mild temperature conditions. The second strategy in Figure 2.6b uses microwave assisted conditions to form semicrystalline structures, and the last strategy (Figure 2.6c) forms crystalline structures through interfacial polymerization (Liu et al., 2019). CTFs have been explored in various applications like photocatalysis, fluorescent probe detection, adsorption and separation (Liao et al., 2023).

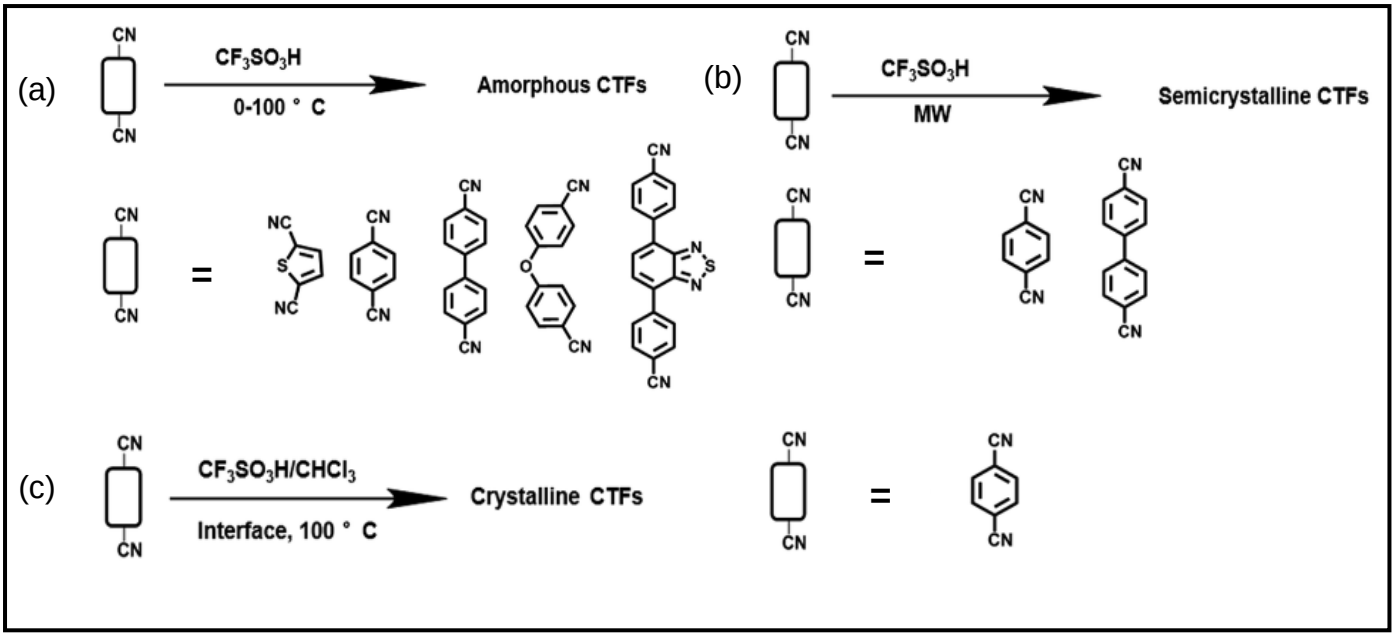

Figure 2.6: *Synthetic strategies of forming CTFs (a) amorphous, (b) semicrystalline and (c) crystalline structures (Liu et al., 2019).*

2.2.3. Crystalline covalent organic frameworks (COFs)

Crystalline POP synthesis requires highly symmetrical building blocks contributing to more uniform and ordered pore size, as a result, the synthesis of crystalline POPs remains a great challenge. COFs are highly crystalline structures, synthesized by reversable reactions that allows thermodynamically stable products which have long-range order (Liu et al., 2018). COFs first appeared in 2005 and are porous structures composed of light elements connected by strong covalent bonds to form highly crystalline structures. Various synthetic routes have been explored such as ionothermal synthesis, microwave synthesis and room temperature synthesis while solvothermal synthesis being the most preferred method.

The reversable nature of covalent bonds is vital to the formation of COF structures as it allows to check for errors during synthesis. Imine containing building blocks have been successfully used to synthesize highly crystalline COF nanofibers through solvothermal synthesis. The unique reversable nature of imines revealed a morphological transformation from microspheres to crystalline nanofibers that was controlled by a dissolution-recrystallization growth mechanism (Wei et al., 2013). Porphyrin-based crystalline COF cubes were synthesized from highly soluble monomers under solvothermal conditions. Morphology of COFs is affected by the reaction media, and the size and pore diameter can be controlled by adjusting the reaction time. This allows for precise control over both the macroscopic structure and the pore parameters of COFs (Feng et al., 2011).

There are four major crystalline COF structures that can be formed based on the rigid structure of the monomers. Polymerization of building blocks can be achieved by interpenetration, weaving, or interlocking as showed in Figure 2.7 leading to various COF structures. The crystallinity of COFs has defined pores that provides an ideal

environment for energy storage, catalysis, and gas storage of chemicals like hydrogen, methane, ammonia, and carbon dioxide (Ding &Wang, 2013).

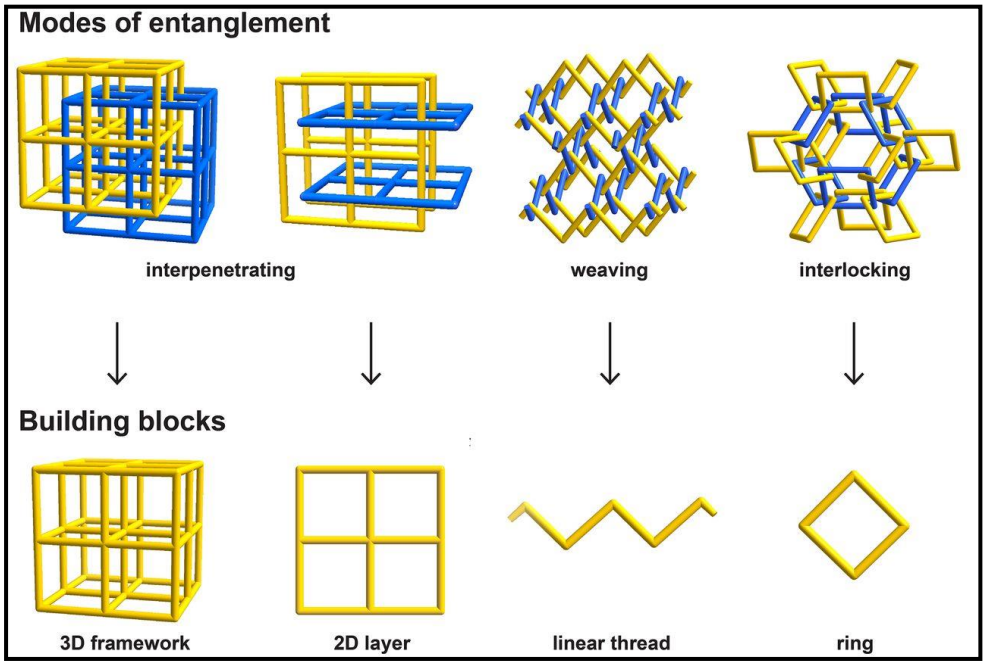

Figure 2.7: *COF structural designs (Diercks & Yaghi, 2017).*

2.3. Porphyrin-based porous organic polymers (Py-POPs)

A porphyrin macrocycle contains 26 electrons, of which 18 are electrons that contribute to the delocalization of electrons within the planar structure (Soury et al., 2019). Furthermore, porphyrins are nitrogen-rich, which results in highly conjugate systems. These molecules have excellent coordination ability, allowing metal ions to be incorporated within the macrocycle. The synthesis of Py-POPs has become popular due to its tunability, structural activity, and high porosity (Ji et al., 2021).

Py-POPs are classified as aromatic, heteroatom macrocyclic compounds containing nitrogen-rich atoms that can accommodate metal ions (Wang et al., 2016). Py-POPs are generally found to have CMPs or COFs like morphology. They can expand into 2-D atomic layers due to their π-conjugated solid system that coordinate the uniform distribution of metal sites. The structural composition of Py-POPs can be adjusted by

regulation of the central metals, modification of macrocyclic molecules with different amounts and types of substituents and adjusting the way units connect. Py-POPs can be synthesized as films, nanosheets, or powders (Ji et al., 2021).

In porphyrin-based COFs, the crystalline materials are acquired by connecting reversibly formed bonds using building blocks such as boroxine, carbonyl ester, triazine or imine. In contrast, porphyrin-based CMPs are formed through irreversible reactions using monomers that consist of two or more reactive terminal groups (Hynek et al., 2016). The first 2-D metalated porphyrin COF was synthesized through boronic esterification reaction under solvothermal conditions. The crystallinity and morphology depended on the reaction media, while the size and pore parameters depended on the reaction time. The uniform mesopores observed in this zinc porphyrin-based COF (ZnP-COF) were due to the reversibility of the growth process. ZnP-COF showed platelet-like objects of cubic shape has a similar size with mesoporous cavities (Feng et al., 2011). Imine-linked porphyrin COFs exhibited different topologies with rhombic and tetragonal shapes having micropores or mesopores; these 2-D polymer sheets were stacked to form layered frameworks (Chem et al., 2015). Iron porphyrin-based CMPs (FeP-CMPs) were constructed using covalent bonds that yielded amorphous polymers without long-range porphyrin ordering. The FeP-CMP displayed plate-shaped monoliths with a rough surface and nanometer cavities (Hynek et al., 2016). The structural composition of various POPs play an essential role in the possible applications of these polymers.

2.3.1. Py-POP synthetic methodology

The synthesis of Py-POPs occurs through a network of reactions. POPs can have various morphologies depending on the synthetic method, monomer structure, and reaction conditions. Amorphous POPs are generally said to be formed through irreversible reactions like Friedel Crafts Alkylation (HCPs), C-C coupling (PAFs), or imine formation (CMPs). Crystalline POPs, like COFs involve reversible reactions, but CTFs are synthesized by reversible or irreversible cyclotrimerization reactions (Gamal Mohamed et al., 2022).

Porphyrin-based POPs in powder form have been extensively studied, acknowledging their simple, controllable reaction conditions, and can be built from a wide range of monomer building blocks (Ji et al., 2021). As Py-POPs are classified as either conjugated microporous polymers (CMP) or covalent organic polymers (COF), it is essential to investigate various synthetic routes previously used in synthesizing porphyrin-based CMPs and COFs. Porphyrin-based COFs have been synthesized using a condensation reaction between tetra-amine and tetra-aldehyde under solvothermal conditions. These synthesized porphyrin-based COFs were shown to have tetragonal micropores with exceptional crystallinity and chemical stability (Xu et al., 2020).

Porphyrin-based CMPs can be synthesized through reflux in a one-pot process, which is cost-effective, but can result in uncertainty in the reaction process and the formation of unwanted by-products (Ju et al., 2019). However, recent advancements have been made in the synthesis of porphyrin-based CMPs using milder and simpler conditions, such as solvent-free synthesis (Cheung et al., 2019), room-temperature (Nath et al., 2016) and liquid-liquid interface synthesis (Zhou ET al., 2019). Several reaction types for porphyrin-based CMPs include phenazine ring fusion, Schiff base formation,

Yamamoto, Heck, Sonogashira-Hagihara, and Suzuki-Mataura cross-coupling. Iron porphyrin-based CMP was synthesized in 2010 using Suzuki-Miyaura cross-coupling polycondensation for the heterogeneous catalysis of sulfide to sulfoxide (Chen et al., 2010). Later studies explored the catalytic epoxidation of olefins at ambient temperatures (Chen et al., 2011) using metalloporphyrin POPs (Chen et al., 2011). Cobalt porphyrin-based CMP was synthesized in 2014 using a Yamamoto homocoupling reaction for oxygen reduction (Wu et al., 2013). A bifunctional copper porphyrin-based CMP electrocatalyst was synthesized, showing promising applications for hydrogen and oxygen evolution via the Yamamoto homocoupling reaction (Cui et al., 2016). The solvothermal synthesis of porphyrin-based CMPs allows for impeccable selectivity, suitable reaction conditions, simple one-pot synthesis modifications, high-yield production, and high surface area (Gamal Mohamed et al., 2022).

2.3.2. Metalated porphyrin-based POPs (MPy-POPs)

CMPs containing porphyrin units have gained popularity due to their redox activity, permanent porosity, and ability to coordinate various metals. This allows them to act as catalytic centers (Oliveras-Gonzalez et al., 2015). Combining metal-containing porphyrin units with organic carbonyl compounds, which function as redox-active groups and linking units, creates unique organic composites. According to a study by Shu et al. in 2022, using cobalt porphyrin-based CMPs as anodes in lithium-organic batteries has been shown to produce a giant, conjugated skeleton with improved electrochemical performance. The metal incorporation into the N_4 conjugated macrocycle is the reason behind this improvement (Shu et al., 2022). These polymers are chemically and thermally stable as they do not undergo any dissolution or decomposition, this can be attributed to their highly π-conjugated skeletons.

Construction of metalloporphyrin-based CMPs using nickel as a metal results in materials with unique microporous properties, large surface area, and pore volume with exceptional stability and reversible adsorption capacity for iodine vapor (Sigen et al., 2014).

MPy-POPs have been investigated as heterogeneous catalysts, particularly for the cycloaddition of epoxides and CO_2 to form cyclic carbonate. The synthesis involves a multi-step polymerization of tetraphenyl porphyrin monomers followed by metalation using metals such as Co, Zn, and Fe results in better activity and recyclability (Dai et al., 2016). Amorphous Ni (II)-α-diimine-POP was synthesized and used as a heterogeneous catalyst to promote Suzuki-Miyaura cross-coupling reaction. While homogeneous metal catalysts are often used for C-C bond formations, this has proven to be highly active and reusable, making it an excellent alternative to Pd-based catalysts (Dong et al., 2019). Many MPy-POPs have been studied for catalyzing organic reactions, including C-C coupling, C-H arylation of heteroarenes, hydrogen atom transfers, C-3 alkylation of indoles, and oxidation reaction (Kathiresan, 2023).

Another form of heterogenous catalysis is where MPy-POPs have been used as electrochemical sensors. The most well-known application of this type of catalysis is the glucose sensor. Recently, researchers have employed copper porphyrin-based POPs for nonenzymatic electrochemical detection of glucose with an LOD of 0.9 μM. The electrocatalyst's spherical morphology and amorphous nature enhances the selectivity for glucose, making it a promising option for low-cost and fast glucose detection (Bhaduri et al., 2023). Iron-porphyrin-based COFs were synthesized to be used to mimic peroxidase for the electrochemical reduction of hydrogen peroxide. These COFs are spherical and crystalline, demonstrating good electrochemical redox and proton activity for reducing hydrogen peroxide, achieving an LOD of 2.06 nM (Xie

et al., 2020). Considering the positive outcomes of previous research, they are worth investigating further since very few metalloporphyrin-based porous organic polymers have been explored as sensors.

2.4. UV-Visspectroscopy of porphyrin and metalloporphyrins

Porphyrins are naturally occurring macrocyclic compounds found in biological compounds like chlorophyll. They play an important role in nature having unique absorption, emission, and charge transfer because of their ring structure that is abundant with conjugated double bonds (Maria & Smith, 2023). Porphyrin's highly conjugated π-electron systems also contribute to their recognizable color. The porphyrin structure in Figure 2.8(a) is made up of four pyrrole rings connected by methine bridge. Figure 2.8(b) shows a typical UV-Visspectrum of porphyrin, with an intense band in the 380-500 nm range called the Soret or B band, and Q bands in the 500-750 nm range. The impeccable spectroscopic features of porphyrins are due to the conjugated system which makes it easy to monitor guest-binding process using UV-Vis (Giovannetti, 2012).

The porphyrin absorption bands arise from transitions between HOMOs and LUMOs as illustrated in Figure 2.8(c). The HOMO orbitals include $a1_u$ and $a2_u$, while the LUMOs are calculated to be a degenerate set of e_g orbitals. The Soret or B band in the electronic absorption spectrum corresponds to the transition from the ground state to the second excited state, while the Q bands correspond to a weak transition from the ground state to the first excited state (Giovannetti, 2012).

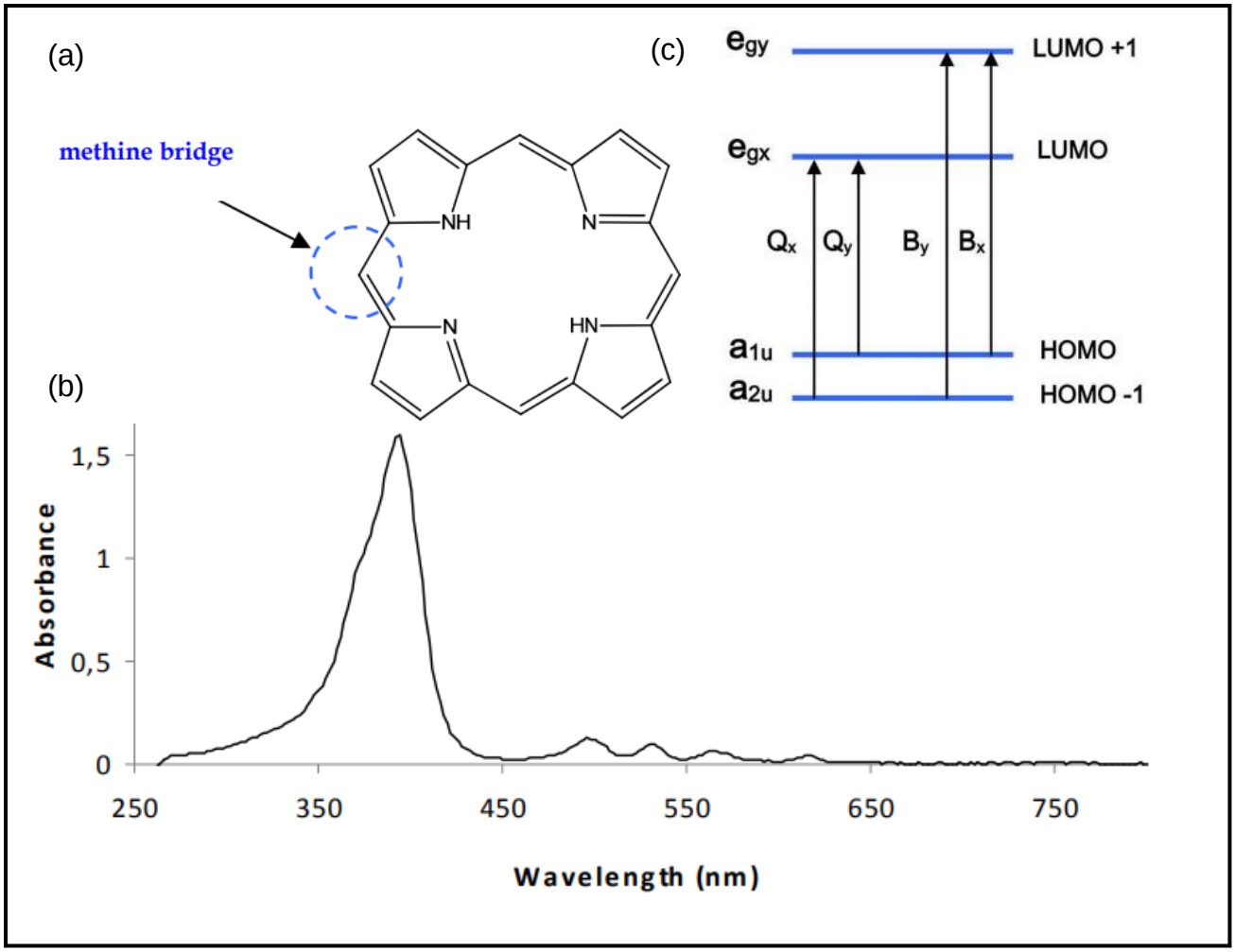

Figure 2.8: *(a) Basic structure of a porphyrin unit and (b) UV-Visspectrum of porphyrin (c) Energy levels of orbitals*

Porphyrins are generally synthesized in a metal-free form but can be synthesized by inserting metal ions. When the metal ion (M^{n+}) is inserted in porphyrin H_2P, it will form the metalloporphyrin $MP^{(n-2)+}$, where the amine protons are dissociated from pyrrole and reported in equation 2.1.

$$M^{n+} + H_2P \leftrightarrow MP^{(n-2)+} + 2H^+ \qquad \textbf{Equation 2.1}$$

Metals can be inserted in the porphyrin ring. An octahedral structure may form depending on the type of metal incorporated. Fe (II) for example, forms a distorted octahedral structure when it has two axial ligands, as seen in Figure 2.9(a) (Biesaga,

2000). Other iron porphyrins have a square pyramidal geometry located out of the plane (Figure 2.9(b)) forming a sitting-atop metalloporphyrin complex, as a result of one axial ligand.

(a) (b)

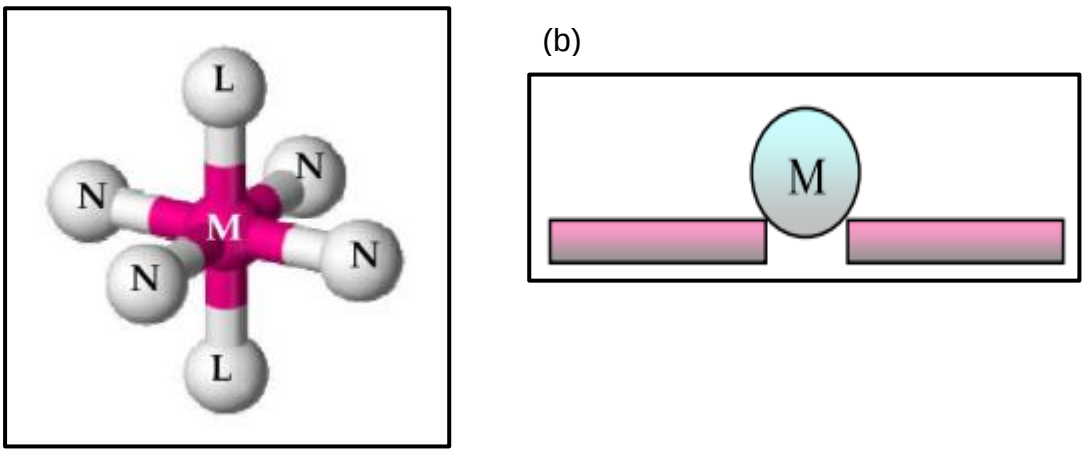

Figure 2.9: *Schematic representation of (a) octahedral structure and (b) sitting-atop metalloporphyrin (Giovannetti, 2012).*

Sitting-atop metalloporphyrins exhibit unique photochemical properties such as photoinduced charge transfer from the porphyrin ligand to the metal centre, or vice versa (Horváth et al., 2006). The UV absorption spectra of sitting-atop metalloporphyrins differ from the normal square planar metalloporphyrins and can be spectrophotometrically monitored.

2.5. Applications of POPs

2.5.1. Gas separation and storage

Porous organic polymers aid in the adsorption and storage of gasses. Surface functionalization enhances the capacity and selectivity of a particular gas, which is crucial for gas separation and storage. Modified functional units can be found on the wall surfaces of POPs with regulated porosity and pore environment by using a various of synthetic approaches (Zhang et al., 2017).

2.5.1.1. Hydrogen storage

Oxidation of hydrogen in engine or fuel cells produces water, as a byproduct thus releasing no greenhouse gasses to the atmosphere. The utilization of hydrogen fuel cells is greatly limited by the lack of safe, convenient, and economical techniques for hydrogen storage (Ma & Zhou, 2010). Porous organic polymers are composites known to have a high surface area, which make them favorable for hydrogen storage. POPs can be synthesized with various synthetic routes that welcome a variety of functionalities. Co-polymers like HCPs consists of a fine pore structure where CMPs are 3-D amorphous rigid blocks with π-conjugated bonds, both showed moderate H_2 storage capacities (Chen et al., 2022). PIMs are synthesized by insufficient packing of monomers and have been extensively studied for H_2 storage due to their high surface area. Interestingly, PIM-1 showed to have long-term stability when storing H_2, with only a slight loss in hydrogen capacity and surface area after 400 days (1.7 wt% at 77 K and 100 bar) (Rochachat et al., 2019). Like PIMs, triptycene-based microporous polymers (TMPs) were synthesized to contain flexible benzylic bonds in their rigid backbone structure. TMPs could uptake H_2 at much lower pressure (2.21 wt% at 77 K and 1 bar), this is attributed to their high density microporous, which was more favorable compared to PIMs (Bera et al., 2018). Adequate H_2 storage by physisorption require extremely high surface area, hence microporous organic polymers were synthesized using various symmetrical monomers in a polycondensation reaction. This flexible synthetic route delivers purely organic sorbents with exceptional surfaces areas that can adsorb H_2 up to 3.7 wt% at 77 K and 15 bar (Wood et al., 2007).

2.5.1.2. Separation of CO_2/N_2 and CO_2 adsorption

POPs have been considered as one of the solutions for CO_2 capture, separation, and conversion due to characteristics like high porosity, low cost of synthesis and

tuneability. CO_2 has a smaller kinetic diameter compared to N_2, by controlling POP pore size, higher selectivity can be achieved by selecting a suitable adsorbent-adsorbate interaction (Bhanja et al., 2018). Various POPs have been studied for CO_2 capture such as perfluorinated CTFs which maintain stable adsorption capacity over several cycles of adsorption (Zhao et al., 2013). POP decorated with polar azo and hydroxy functional groups have shown promising adsorption of CO_2. Azo-bridged covalent organic polymers (azo-COPs) forms nanoporous networks with exceptional CO_2 selectivity at higher temperatures. The azo-COPs are heteroatom-rich (-N=N-) and exhibit very low affinity towards N_2 due to the entropic loss of N_2-gas molecules. As a result, they are extremely selective for CO_2 separation and capture (Patel et al., 2014).

2.5.1.3. Methane storage

In addition to hydrogen gas, methane is a potential gas used for clean energy. Although methane is considered a greenhouse gas, it is preferred over the use of other fossil fuels as it generates less emissions (Holmes & Smith, 2016). Various materials have been explored in the storage of methane such as activated carbons, metal-organic frameworks, and coordination polymers. Activated carbons are limited for gas storage by their pore size, tunability and low surface area (Tsivadze et al., 2018). There are two general methods for natural gas storage namely, liquefaction at low temperatures (LNG) and compression at high pressure (CNG) at room temperature. To decrease the CNG and LNG limitations, porous adsorbents can provide safer, simpler, and more cost-effective storage of natural gas at high pressure and ambient temperature (Makal et al., 2012). Hyper-cross-linked aromatic polymers are easy to synthesize at low costs and consists of ultra micropores, optimal for methane uptake (106 cm^3/g at 195 K and 1 bar) and storage. Recent studies have shown ketonimine-

linked COFs used for methane gas storage, resulted in methane uptake of 118 cc/g - 122 cc/g at 35 bars because of their high crystallinity and surface area. These COFs paved the road for further fine-tuning of building blocks, optimization of synthesis to potentially meet the targets set for commercial methane storage (Asokan et al., 2022).

2.5.2. Electrochemical energy storage

Due to unreliable energy supply, especially in South-Africa, the use of supercapacitors for energy storage have become crucial. This is because they provide high power densities, rapid charge-discharge speeds, and a long life cycle. There are two types of supercapacitors: electrostatic double layered capacitors (EDLC) and pseudocapacitors (PC). EDLCs use carbon derivative electrodes to store electrical energy electrostatically through charge separation in the double layer. This method of storage is purely electrostatic, which means that EDLC based devices exhibits high power density and long-term performances, but have low specific capacitance (Simon et al., 2008). Pseudocapacitors are a type of energy storage device that focuses on the charge transfer between the electrode and electrolyte. They store energy electrochemically through redox reactions or intercalation on the electrode surface by absorbing specific ions. PCs have high specific capacitance and energy densities due to faradaic processes but have a short cycle life (Wang et al., 2012). Combining the two types of capacitors, it creates hybrid supercapacitors, demonstrating the beneficial synergy of both PC and EDLC mechanisms and promotes adequate supercapacitor energy storage.

Hybrid supercapacitors have asymmetrical electrodes where one electrode has electrostatic properties while the other has electrochemical capacitance, both contributing to the total success of the supercapacitor hybrid (Bandyopadhyh et al., 2018). Efficient electrochemical energy storage principles are based on reversible

redox conversions of various materials. Modern technology has changed focus from inorganic electrodes like silicon, carbon materials, metal oxides, and tin to organic electrode materials (Kang & Son., 2020). There are two methods to incorporate redox-active functionality in POPs, the first being a predesigned building block approach and second, by a photosynthetic modification strategy. Formation of hallow POP materials having thin shell thickness, the electrolyte can diffuse into the materials enhancing the use of redox-active sites in materials. Due to the high surface area of POPs, its porosity and tunability shows promising utilization in pseudocapacitors and ultimately, in hybrid supercapacitors (Kang &Son, 2020).

2.5.3. Chemical sensing

Chemical sensing is critical in the chemical industry, for human health diagnosis, environmental safety, and food safety (Swager & Mirica, 2019). Traditional methods such as ion chromatography, gas chromatography, surface enhances Raman scattering methods, and mass spectrometry have been used for sensing and detection. These methods are limited due to high cost, a complication of instruments, and their time-consuming nature (Wang et al., 2022). POPs have been utilized as sensors to detect explosives, metal ions, anions, biological molecules, and enantiomers. The use of POPs has greatly evolved over the past decade as seen in Table 2.1. As early as 2012, POPs have been utilized to detect arene vapors (Liu et al.,2012). Fluorescent POPs have become popular over the years in sensing various chemicals including cyanide ions, picric acid, toxic pesticides and nitroaromatic compounds.

Table 2.1: *The chronological advancement of POPs used as sensors over the past decade.*

Year	Type of POP sensor	Chemicals for detection	Reference
2012	CMP	Arene vapors	(Liu et al.,2012)
	COP	Trinitrotoluene	(Xiang & Cao, 2012)
2013	COF	Picric acid	(Dalapati et al., 2013)
2014	Fluorescent HCP nanoparticles	Cyanide ion	(Li et al., 2014)
2016	Fluorescent 3-D COF	Picric acid	(Lin et al., 2016)
2017	Fluorescent COF	Triacetone triperoxide	(Rao et al., 2017)
2018	Fluorescent POP	Toxic pesticides	(Zhang et al., 2018)
2019	2-D Chemiresistive COF	NH_3, H_2S, NO an NO_2 gasses	(Meng et al., 2019)
2021	Electrochemiluminescence biosensors COF	microRNA-21	(Zhang et al.,2021)
2022	Fluorescent POP	Various nitroaromatic compounds	(Xiong et al., 2022)

There are five categories of POP-based sensors: 1) Fluorescent on sensors, 2) fluorescent off sensors, 3) ratiometric fluorescent sensors, 4) colorimetric sensors, and 5) chemiresistive sensors. Of these categories, fluorescent sensors are most common.

The interaction between POP and analyte structure, facilitated by strong covalent bonds, enables the sensor to exhibit rapid response, exceptional sensitivity, and effective selectivity, resulting in excellent reproducibility during applications (Wang et al., 2022).

2.5.4. Water treatment

The discharge of organic and inorganic pollutants into water systems is a serious problem that poses a great risk to both human health and the environment. Micro-organic pollutants such as pharmaceutical and personal care products that are released into water can have concerning health effects on the endocrine system. Wastewater treatments like reverse osmosis (Lee et al., 2012) and ultraviolet irradiation (Nihemaiti et al., 2018) have shown to have low efficiency and are very expensive. POPs can be designed to act as adsorbents according to the properties of the contaminants, thanks to their porous nature and tuneable structures (Sun et al., 2020). Hydroxyl-based POPs containing micro and mesopores have demonstrated exceptional adsorption capacities and reusability over 10 cycles. These POPs remain stable in the pH range of 1-14. The unique nanofiber-like morphology of these POPs allows for the cost-effective removal. Micro-organic chemicals such as diclofenac sodium, sulfamethoxazole, and acetaminophen have been successfully removed from water using these POP materials. (Ravi et al., 2022)

Phenol pollutants in water are particularly dangerous, as they are highly toxic, non-biodegradable, carcinogenic, and are classified as EDCs (Zala & Penn, 2004). Several methods, such as membrane separation (Li et al., 2021), ion exchange (Zhang et al., 2021), and electrochemical degradation, have been tested to remove phenolic pollutants from water in an easy and cost-effective way (Wu et al., 2020). These methods showed low adsorption capacities and require further improvement to

achieve the requirements for removing phenolic compounds in water. Various catechol-based monomers were used to synthesize POPs that were then tested for their ability to adsorb phenolic water pollutants. The composites exhibited large surface areas ranging from 800 mg/g – 1200 mg/g depending on the specific monomer building block used. The increased surface area resulted in an increased adsorption capacity. Additionally, these catechol POPs demonstrated an adsorption efficiency of over 80% after ten cycles and were much more efficient than any previously synthesized POPs (Zhao et al., 2023).

2.5.5. Heterogeneous catalysis

POPs have been widely studied as heterogeneous catalysts as they have excellent stability, tuneable pore size, high surface area, and simple functionalization. Compared to homogeneous catalysts, heterogeneous catalysts dominate the industrial chemical production due to their recyclability (Liu et al., 2023). POPs have generally been used in heterogeneous catalysis as i) the active catalyst containing π-conjugated backbone for light harvesting or as photosensitization, ii) as host matrix in order to store and stabilize active catalysts like metal nanoparticles, or iii) act as both active catalyst and host-matrices to ensure additional catalytic sites (Giri & Patra, 2022).

POPs like CMPs are promising heterogeneous catalysts for water splitting as they have π-conjugated backbones, allowing for large electron delocalization that favours light absorption and charge carrier transport (Li et al., 2016a). Hydrogen can be used as possible fuel in the future, but its use is limited by adsorption and storage, making water splitting important for hydrogen fuel cells. Dibenzothiophene dioxide containing CMPs with benzene cross-linker exhibit high photocatalytic activity with a hydrogen evolution rate (HER) of 2460 µmol/$h^{-1}g^{-1}$ under visible light. Adding Pt nanoparticles

as co-catalyst spikes HER remarkably to 9200 μmol/$h^{-1}g^{-1}$ and demonstrates the worthiness of POPs as heterogeneous catalysts for hydrogen production (Wang et al., 2018). The combination of metal oxides and POP photocatalysts still requires exploration due to some drawbacks of POPs in photocatalytic water splitting (Xu et al., 2018).

2.6. Nanoparticles

Nanoparticles (NPs) are particulate substances that have a dimension between 1 nm and 100 nm (Mohanraj & Chen, 2007). They have unique physical and chemical properties due to their increased surface area to volume ratio and are made from various materials like metal oxide ceramics (Holister et al., 2003). NPs consist of three layers: the surface layer, the shell layer, and the core layer. The surface layer can be functionalized with a variety of molecules, while the shell covers the central portion of the NP known as the core layer (Khan et al., 2017).

2.6.1. Iron oxide nanoparticles (Fe_3O_4) and their properties

Iron is the most abundant transition metal found in the earth's crust. Typically, iron oxide is cost-effective and has significant importance in biological and geological applications (Ali et al., 2016). Iron oxides are widely used as iron ore in thermite, durable pigments (colored concrete and paint), catalysis and hemoglobin in human bodies. Three most common forms of iron oxide are magnetite (Fe_3O_4), maghemite (γ-Fe_2O_3) and hematite (α-Fe_2O_3) (Laurent et al., 2008).

Hematite, also known as ferric oxide, is the oldest known iron oxide and is commonly found in rocks and soil. It is weakly ferromagnetic and consist of a rhombohedral or hexagonal crystal structure, as seen in Figure 2.10(a) (Can et al., 2012). Maghemite occurs in soil as a weathering product of magnetite. It is ferrimagnetic and consists of

a cubic or tetrahedral crystal structure, as shown in Figure 2.10(c). Magnetite is a black iron oxide known to have the strongest magnetism (ferromagnetic) of any transition metal oxide. Figure 2.10(b) shows the cubic crystal structure of magnetite. When soil contains magnetite, it may undergo weathering or heating, leading to the formation of maghemite. Maghemite is capable of forming continuous solid solutions with magnetite. It is characterized by a small band gap of 0.1 eV, and has particles that are smaller than 6 nm. Magnetite is highly unstable in the presence of oxygen as it can form maghemite (γ-Fe_2O_3) and should be kept under inert conditions (Laurent et al., 2008). At room temperature, magnetite is superparamagnetic and has shown promise in cancer diagnosis due to their biocompatibility, orderability and physiological stability (Marciello et al., 2016).

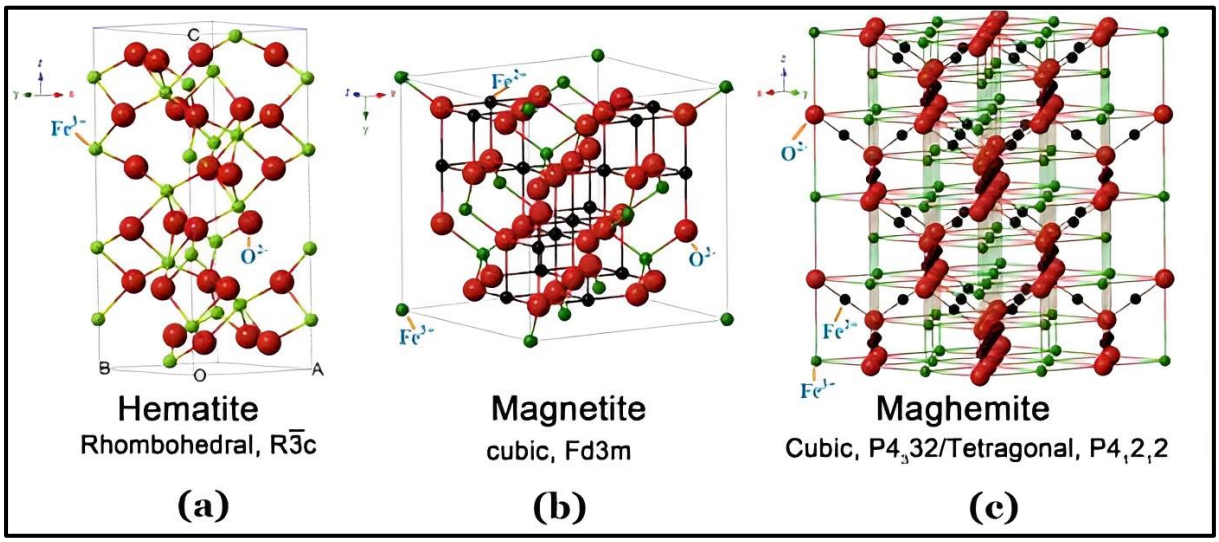

Figure 2.10: *Crystal structure of (a) Hematite, (b) Magnetite and (c) Maghemite*

Iron's magnetic properties can be explained through the use of an orbital diagram, as seen in Figure 2.11. A strong magnetic moment is created by the 3-D orbital, which holds four unpaired electrons. When iron atoms combine to form crystals, there are three main magnetic states that can occur. Initially, the atomic magnetic moments are randomly aligned, resulting in a paramagnetic crystal with zero magnetic moment.

When an external magnetic field is applied to iron crystals, some magnetic moments align to form a small net magnetic moment. This can cause ferromagnetism, anti-ferromagnetism, or ferrimagnetism in various materials (Teja & Koh, 2009). Magnetite is ferrimagnetic, meaning the magnetic dipole of the atoms on different sublattices are opposed and unequal, causing a spontaneous net magnetization. The magnetic properties of nanosized magnetite strongly depend on changes in crystal morphology, which affects magnetic coercivity. These properties can be controlled through various synthetic strategies (Cornell & Schwertmann, 2006).

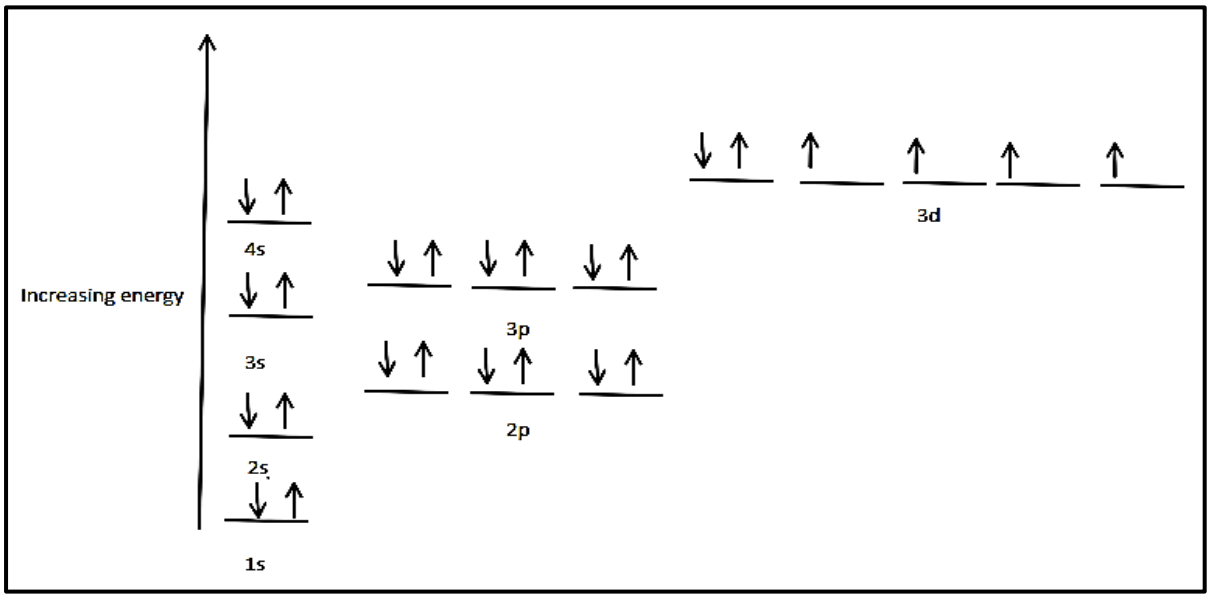

Figure 2.11: *Orbital diagram of iron showing four unpaired electrons in the 3d orbital.*

Iron oxide nanoparticles can be synthesized using physical, chemical and biological methods. In this study, we focused on the preparation that produces spherical nanoparticles. Table 2.2 summarizes the advantages and disadvantages of each preparation method. When defining the experimental settings, it is important to consider the uniformity of the nanoparticle sizes and the reproducibility of the process for commercial use without the need for further purification (Ali et al., 2016).

Table 2.2: *Various methods for the synthesis of magnetic iron oxide nanoparticles*

Methods used	**Advantages**	**Disadvantages**
Hydrothermal	Can control the shape and particle size easily. Stable in phosphate buffered saline solutions (without aggregation)	High temperature and pressure reaction conditions needed
Chemical coprecipitation	Easy and efficient method	Limited control of particle size distribution
Sol-gel	Precise control of size and internal structure	Weak bonding and low wear endurance

During hydrothermal synthesis, the size of the particles is mainly influenced by solvent, temperature, and reaction time. The larger nanoparticles can be observed with increased reaction time and water content. Particle size of Fe_3O_4 powders increases with increased reaction time, which favors grain growth. Additionally, a higher percentage water content produced larger particles (Chen & Xu, 1998). The rate of the reaction primarily depends on its temperature. At higher temperatures, nucleation occurs faster than grain growth, resulting in smaller particle sizes. It is crucial to investigate this method further as high temperature dependent synthesis may have an impact on the industrialization of these nanoparticles. However, this method has proven to supply stable nanoparticles with controllable particles size and no aggregation when placed in PBS buffer solution (Laurent et al., 2008).

The chemical coprecipitation method appears to be the easiest and most effective chemical pathway for the synthesis of magnetic nanoparticles (Daffe et al., 2018). A stoichiometric mixture of Fe^{2+} and Fe^{3+} salts are introduced into an aqueous medium yielding magnetite, equation 2.2.

$$Fe^{2+} + Fe^{3+} + 8\ OH^{-} \rightarrow Fe_3O_4 + 4\ H_2O \qquad \textbf{Equation 2.2}$$

Chemical coprecipitation synthetic strategy takes place in two phases. The first phase begins when the concentrations of the species reach critical supersaturation, leading to a burst of nucleation. The second phase involves the diffusion of solutes to the surface, causing slow growth of the nuclei. The particle number is determined by the end of the nucleation phase, and it does not change during particle growth. The particle size and distribution are controlled solely by kinetic factors that limit control over particle size, which happens during the very short nucleation period. Therefore, it is essential to separate these phases to produce monodispersed nanoparticles. (Laurent et al., 2008)

The third synthetic method considered for the preparation of Fe_3O_4 nanoparticles is the sol-gel synthesis and is based on the hydrolysis and condensation of molecular precursors in solution. After the precursors are formed, further condensation along with inorganic polymerization yield 3-D metal oxide networks in a wet gel. To obtain the crystalline product, heat treatments are required as the reaction occurs at ambient temperature. The properties of nanoparticles, such as their structure and kinetic parameters, depend on factors like solvent, temperature, concentration, pH, and the type of salt precursor used. These factors mainly impact the condensation of molecular precursor, which can result in larger Fe_3O_4 nanoparticles with a size between 30 nm to 50 nm (Lida et al., 2007). Further studies of the sol-gel method have shown that

size-controlled Fe_3O_4 nanoparticles with average diameter of 8 nm can be obtained by slowly releasing water for hydrolysis through esterification reactions and drying the solution in an autoclave under supercritical conditions (Lemine et al., 2012).

2.6.2. Applications of Fe_3O_4 nanoparticles

Iron oxides were originally used as coloring agents, but since then they have found numerous applications such catalysts, separation of bioactive molecules, and target drug delivery. Table 2.3 lists various chemicals that have been detected using Fe_3O_4 based electrocatalysts. Fe_3O_4 nanoparticles have been specifically used as sensors to detect multiple compounds like sunset yellow. This synthetic dye is commonly used in products like yogurt, candy, sweets, and soft drinks that contains disodium 6-hydroxy-5-[(4-sulfophenyl) azo]-2-naphthalenesulfonate. Fe_3O_4 nanoparticles have also been used to detect ascorbic acid, uric acid, and dopamine. To increase sensitivity on the GCE, Fe_3O_4 has been traditionally mixed with multiwalled carbon nanotubes. Graphene oxide in combination with Fe_3O_4 has also showed improvement of detection limits on GCE. Several techniques have been employed for the detection of EDCs, but DPV is the most favored one due to its high sensitivity. While there are studies on the use of Fe_3O_4 nanoparticle-based sensors for EDC detection, bisphenol A is the most commonly detected EDC.

Table 2.3: *Comparison of Fe_3O_4 based sensors for the detection of various chemicals.*

Chemicals tested	**Electrochemical method**	**Electrocatalyst used for detection**	**LOD (μM)**	**Reference**
Sunset yellow	DPV	Fe_3O_4-MWCNTs[a]/GCE	0.0014	(Shaikshavali et al., 2020)
Methomyl	CV	Ag-Fe_3O_4/GCE	20.8	(Gai et al., 2019)
Ascorbic acid	DPV	Fe_3O_4/rGO[b]/GCE	0.12	(Peik-See et al., 2014)
	DPV	Fe_3O_4/SFP/GCE	1.0	(Gao et al., 2021)
Uric acid	DPV	H-Fe_3O_4@C/GNS/GCE[d]	0.41	(Song et al., 2017)
	DPV	Fe_3O_4/SFP[c]/GCE	1.48	(Gao et al., 2021)
Dopamine	DPV	H-Fe_3O_4@C/GNS/GCE	0.053	(Song et al., 2017)
	DPV	Fe_3O_4/SFP/GCE	0.4	(Gao et al., 2021)
EE2	DPV	Au/Fe_3O_4@TA[e]/MWNT[a]/GCE	0.0033	(Nodehi et al., 2020)
Bisphenol A	CV	CS[f]-$_3O_4$/GCE	0.008	(Chunmei et al., 2011)
2-phenylphenol	CV	Fe_3O_4-NPs/$HMPF_6$[g]/CPE	0.006	(Karimi-Maleh et al., 2019)

[a] MWCNT/MWNT: multiwall carbon nanotubes, [b] rGO: reduced graphene oxide, [c] SFP: nitrogen self-doped sunflower plate-derived carbon, [d] H-Fe_3O_4@C/GNS/GCE: 3-D carbon-encapsulated hollow Fe_3O_4 nanoparticles homogeneously anchored on graphene oxide nanosheet, [e] TA: tannic acid, [f]CS: Chitosan, [g] $HMPF_6$: n-hexyl-3-methylimidazolium hexafluorophosphate

2.7. Porphyrin-based POPs and the incorporation of nanoparticles

The thermal and chemical stability of metalloporphyrin-based POPs contributes to their easy post-synthetic modification. On the other hand, to prevent aggregation of metal nanoparticles, they can be embedded within the POP structure (Kathiresan, 2023). Various POP materials like PIMs, HCPs, CMPs and COFs have been studied as support structures for Pd nanoparticles (PdNPs). The ladder structure and twisted backbone of PIMs do not provide pore confinement and NP growth, unlike HCPs and CMPs which can be easily functionalized. However, the pore size is still a limitation in controlling the size of PdNPs. CMPs based on porphyrins have shown to be an excellent directing group for the controlled growth of NPs with high stability and catalytic activity (Ju et al., 2019). COFs, due to their high crystallinity, have proven to be a promising supporting material for PdNPs growth. The success of PdNPs@POPs catalysts depends on the support material, Pd source, solvents, and reduction conditions (Tao et al., 2020)

The synthesis of POP-1 in a single pot, followed by incorporation of Fe_3O_4 nanoparticles by coprecipitation, resulted in the formation of highly magnetic porous organic polymers, as depicted in Figure 2.12. The Fe_3O_4 nanoparticles were evenly distributed on the substrate, which reduced agglomeration and increased their absorbance efficiency. POP-1 enriched with Fe_3O_4 nanoparticles showed to be highly magnetic and recyclability added to the promising LOD (0.08 - 0. 2 ng. g^{-1}) for the magnetic solid-phase extraction of pesticides (Wang et al., 2017).

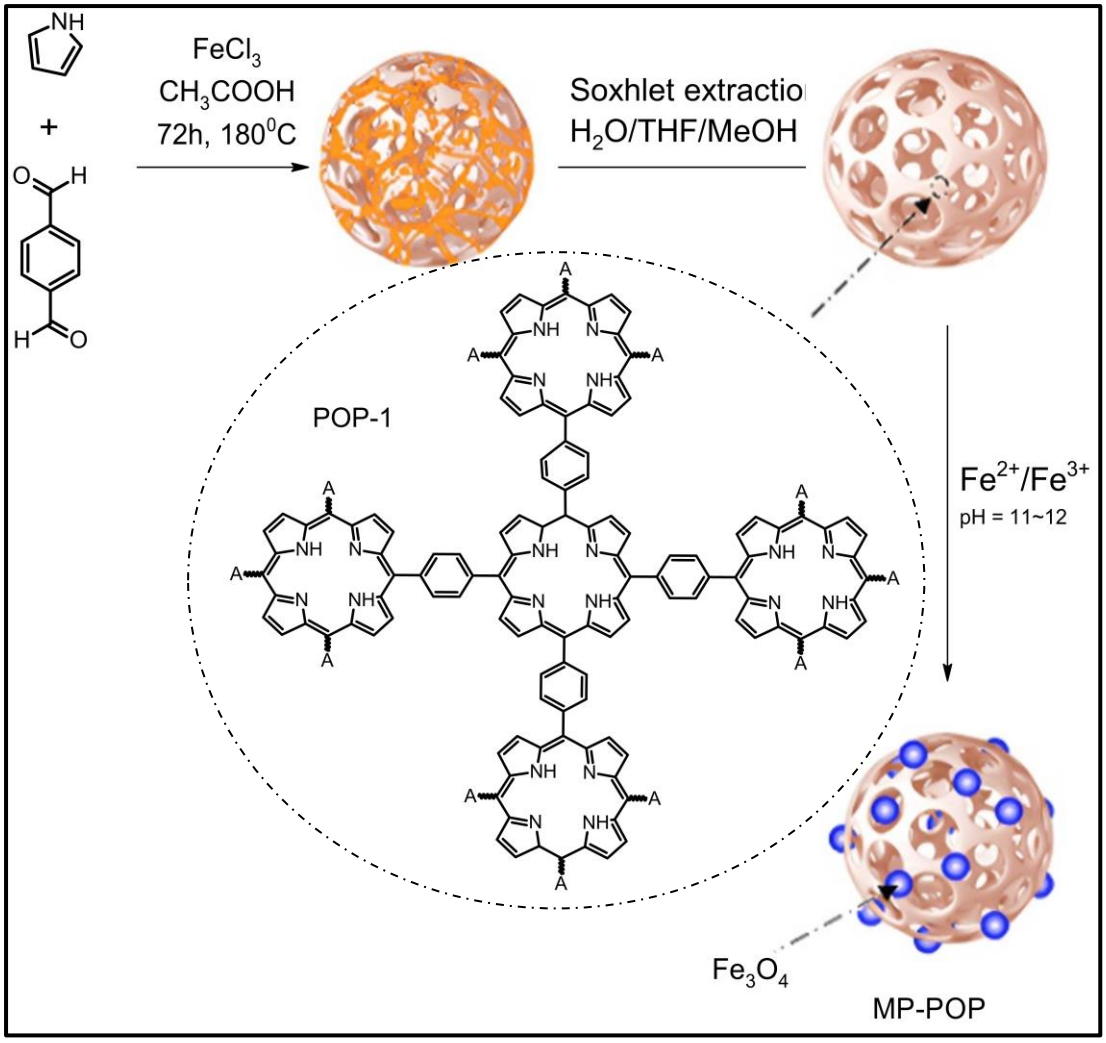

Figure 2.12: *Synthesis of POP-1 and MP-POP*

2.8. Endocrine disrupting chemicals

2.8.1. Overview and general sources

The endocrine system is regarded as the body's core control system because it creates, releases, and stores hormones to keep the body developing and functioning properly. The reproductive organs, thyroid, pituitary, and adrenal gland are the four primary organs of the endocrine system, as depicted in Figure 2.13 (Diamanti-Kandaraki et al., 2009).

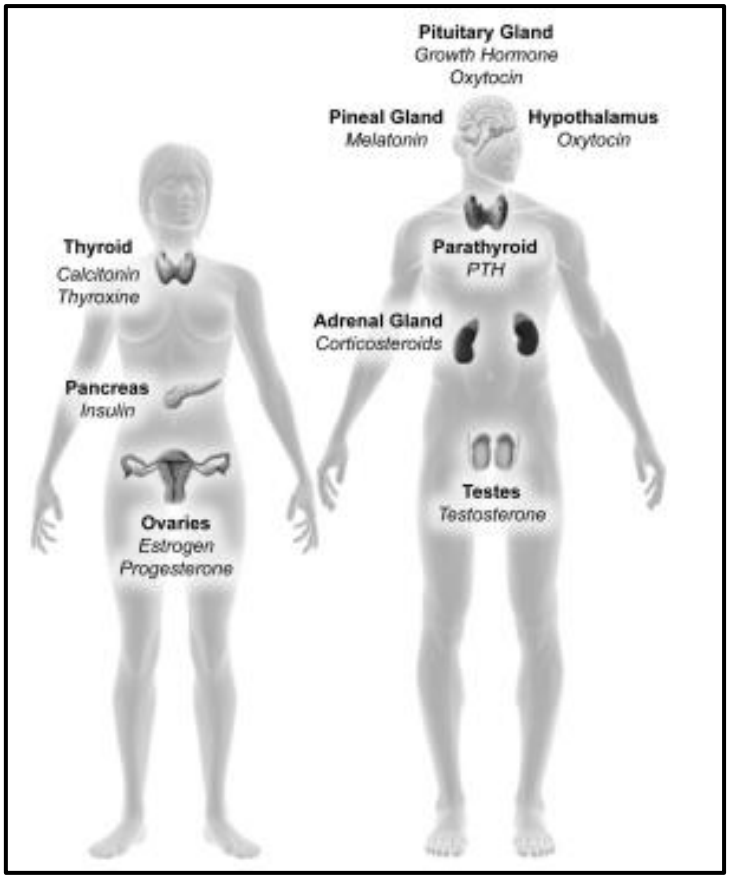

Figure 2.13: *The body's endocrine system.*

Endocrine disruptors were demarcated by the US Environmental Protection Agency in 1991 and were defined as external agents that interfere with natural hormones that maintain homeostasis, reproduction, and development (Crisp et al., 1998). Endocrine disruptive chemicals (EDC) are compounds that interfere with the natural operation of the endocrine system, potentially causing health risks. EDCs have various modes of operations; they can alter normal hormone levels, inhibit, or stimulate the production of metabolic hormones, or change the way hormones travel through the body (Schug et al., 2011). EDCs can cause an agonistic effect where normal hormone levels are altered as they mimic hormones and bind to a cellular receptor causing unnecessary cell response at the wrong time. These chemicals can also have an antagonistic effect on cellular responses where EDCs bind to the receptor but do not cause a response

and prevents normal hormone from binding. EDCs can alter normal amounts of hormones being circulated in the body and can interfere with normal synthesis or breakdown of hormones in the body's metabolic processes, by binding to transport proteins in the blood (Vandenberg et al., 2012).

The blocking or mimicking of endocrine hormones affects the functions of the endocrine system. Originally EDCs were thought to only influence nuclear hormone receptors like estrogen receptors, progesterone receptors, retinoid receptors, thyroid receptors, and androgen receptors. Still, their mode of action is much broader than initially recognized. EDCs can also influence mechanisms through transcriptional coactivators, enzymatic pathways involved in steroid biosynthesis, nonsteroid receptors, or their epigenetic impact on genes (Moral et al., 2008). EDCs, like hormones, can act at extremely low levels in tissue-specific ways or display non-traditional dose responses due to hormone receptor occupancy and saturation. When it comes to the health effects of EDCs, the age of exposure is critical. When exposed to these chemicals as an adult, higher dosages are required to cause toxicity, with effects happening only while the compounds are present in the body. However, exposure during development requires a low dose and has long-term consequences, even if the EDCs are eliminated from the body. The effects of these chemicals are worrisome in early stages of development as they can cause extreme effects years later that can lead to multigenerational inheritance of diseases (Skinner, 2011).

Endocrine disrupting chemicals are categorized based on their chemical features as shown in Table 2.4. EDCs are found in various food sources, personal care products, plastic manufacturing, food packaging, pharmaceuticals, pesticides, herbicides, fungicides, solvents and in synthetic hormones. There are six major categories of EDCs, and they are classified due to their chemical features which include parabens,

phthalates, bisphenols, perfluoroalkyl substances, polychlorinated biphenyls, and non-steroidal estrogens (Buoso et al., 2020).

Table 2.4: Categories of EDCs

Category	**Source**
Parabens	Food preservatives Personal care products
Phthalates	Personal care products Plastic manufacture, Resins
Bisphenols	Plastic manufacture, Resins Food packaging
Perfluoroalkyl substances	Food packaging Clothing Furniture
Polychlorinated biphenyls	Pesticides, fungicides, herbicides Solvents
Non-steroidal estrogens	Pharmaceuticals, synthetic hormones

Research has discovered links between exposure to EDCs and a range of illnesses, including obesity, diabetes, reproductive issues, breast and ovarian cancer, thyroid problems, and prostate issues. When animal models are tested, the effects of EDCs can impact not only the exposed individual but also their offspring through non-genomic modifications of the germ line (such as DNA methylation and histone acetylation). The Endocrine Society has expressed concern that EDCs pose a

significant challenge to the environment and ultimately to human health (Diamanti-Kandarakis et al. 2009).

2.8.2. Electrochemical detection of endocrine disrupting chemicals

Phenolic estrogens are the most common group of EDC pollutant, and the detection thereof has drawn great attention due to the impact on human health at very low concentrations (ngL^{-1}) (Yuksel, Kabay and Yuksel, 2013). Generally, urine samples can be used to test for the presence of endocrine disrupting chemicals. Previously, detection of EDCs were done using liquid chromatography-tandem mass spectroscopy (Arfaeinia et al., 2021), using an ultra-high performance liquid chromatography system interfaced with a triple quadrupole mass spectrometer in multiple-reaction monitoring mode or just a quadrupole mass spectrometer (De Toni et al., 2017).

Due to the severe health implications of these chemicals, along with the continuous increase of daily use of products containing these chemicals, electrochemical methods for detection have become appealing due to them being cheaper, portable, simpler, and accurate (Rama et al., 2021). Table 2.5 exhibits the detection of EDCs using electrochemical techniques. Various catalysts were used by modifying GCEs and screen-printed electrodes. Carbon-based materials such as multiwalled carbon nanotubes and graphene are commonly used as sensors, with DPV being the most sensitive electrochemical technique employed. MWCNT were coated on a GCE and showed the simultaneous detection of paracetamol, L-tyrosine and levodopa (Li et al., 2020). A modified GCE was used in combination with molecular imprinted polymer-based materials to detect the content of parabens in cosmetic products (Lorenzo et al., 2013). These sensor materials displayed potential in detecting a group of homologous compounds. The recoveries achieved ranged between 98% and 102%.

Furthermore, manganese phthalocyanine and polyaniline hybrid sensors were adopted to detect pesticides such as fenitrothion and eserine via square wave voltammetry (Akyüz and Koca, 2019). These catalysts were selective, sensitive, and stable. Moreover, they were easy to fabricate with high reproducibility.

Table 2.5: *Electrochemical detection of endocrine disrupting chemicals.*

Endocrine disrupting chemicals	**Electrochemical method**	**Electrocatalyst used for detection**	**LOD (µM)**	**Reference**
2-phenylphenol	DPV	MWCNT/GCE	2.8	(Baranowska & Bijak, 2013)
Dioctyl phthalate	DPV	MIP[a]/SPE[c]	9.0	(Sharif et al., 2022)
Diisonyl Phthalate	CV	MIPs[a]/GCE	0.027	(Zhao et al., 2018)
Diethyl phthalate	EIS	Graphene/GCE	$24x10^{-6}$	(Zhao et al., 2018)
Butylparaben	DPV	MWCNT[b]/GCE	0.5	(Lorenzo et al., 2013)
	SWV	MIPS/GCE	0.2	(Wang et al., 2010)
Paracetamol	DPV	MWCNTs-Nafion/GCE	0.5	(Li et al., 2020)
Levodopa			0.6	
Fenitrothion	SWV	ITO/MnPc-TA[d]/N_3-PANI[e]	0.049	(Akyüz and Koca, 2019)

[a] MIP: Molecular imprinted polymers, [b] MWCNT: Multiwalled carbon nanotubes, [c] SPE: Screen printed electrodes, [d] MnPc-TA: Terminal alkyne substituted manganese phthalocyanine thin film, [e] ITO: indium tin oxide, [f] N_3-PANI: 4-azido polyaniline

Chapter 3: Experimental methods

3.1. Chemicals and materials

Chemicals such as pyrrole, terepthaldehyde, iron (II) chloride, dichloromethane, methanol, tetrahydrofuran, zinc (II) chloride, iron (II) chloride tetrahydrate, iron (III) chloride hexahydrate, sodium chloride, di-sodium phosphate, monopotassium phosphate, tetrabutylammonium hexafluorophosphate, hydrogen chloride, ferric chloride, dimethylformamide, glacial acetic acid, polyvinylpyrrolidone, ammonia, ethanol, 2-phenylphenol, iron (III) chloride and ascorbic acid were purchased form Merck. Millipore water was used from an Elga LabPure Chorus II filter. Ethanol had 99% purity and pyrrole was distilled before used in reactions.

3.2. Experimental techniques

X-ray diffraction (XRD) analysis was conducted using a Bruker D2 PHASER-e diffractometer using Cu-Kα radiation (0.15418 nm). Scanning electron microscopy (SEM) and Energy-dispersive X-ray spectroscopy (EDX) were carried out on a crossbeam 540 FEG SEM microscope from Zeiss. Transmission electron microscopy (TEM) images were observed using a JOEL JEM 2100F. UV-Visabsorption measurements were taken on a CARY 100 BIO UV-Visspectrophotometer. FTIR spectroscopy was carried out using Brunker Alpha Fourier transform spectroscopy with platinum attenuated total reflectance (ATR) sampling accessory.

An Autolab potentiostat was used to carry out the electrochemical experiments. A three-electrode setup was employed to collect cyclic voltammetry data. The working electrode was a glassy carbon electrode and was polished with a slurry of alumina on a Buehler felt pad and rinsed with millipore water. The counter electrode was a platinum wire, while the reference electrode was a Ag/AgCl wire.

3.3. Synthesis of MPy-POPs and Fe_3O_4@MPy-POPs

The porphyrin based porous organic polymers were synthesized as reported in literature (Li, et al. 2020). The incorporation of Fe_3O_4 nanoparticles followed a similar procedure as previously reported (Wang, et al. 2018)

3.3.1. Synthesis of FePy-POP and ZnPy-POP

A one-pot synthetic route was followed for the synthesis of FePy-POP and ZnPy-POP. Freshly distilled pyrrole (1.48 mmol) and terepthaldehyde (1.48 mmol) was placed in a round bottom flask. Ferric chloride (1.78 mmol) was used for FePy-POP and zinc chloride (1.776 mmol) was used for ZnPy-POP synthesis and they were added in separate round bottom flasks. Glacial acetic acid (0.524 mmol) was added to the salt and flushed with nitrogen gas, followed by stirring for 6 hours under N_2 atmosphere. The reaction was placed in a high-pressure teflon tube in the oven for 72 hours at 180°C. The teflon tube was left to cool overnight. The product was washed using vacuum filtration using water, methanol, acetone, tetrahydrofuran and dichloromethane. The solid was dried at 80°C for 48 hours. Soxhlet extraction was used to purify the product using distilled water, dichloromethane, methanol and tetrahydrofuran respectively. The product was dried for 48 hours at 80°. The product was weighed and mass of 0.318 g and 0.372 g was determined for FePy-POP and ZnPy-POP respectively.

3.3.2. Synthesis of Fe_3O_4@FePy-POP and Fe_3O_4@ZnPy-POP

An aliquot of FePy-POP or ZnPy-POP was placed in a round bottom flask in the presence of distilled water (120 mL). The solution was stirred and purged with N_2 gas before $FeCl_3$ and $FeCl_2.4H_2O$ was added. The reaction was stirred for 10 minutes at

50°C. At this temperature, ammonia solution was added dropwise until a pH of 10-11 was achieved. The reaction was left to stir for another hour and the solution was vacuum filtered and washed thoroughly with distilled water and ethanol. The collected precipitate was placed in the oven at 60°C to dry and products Fe_3O_4@FePy-POP (0.284 g) and Fe_3O_4@ZnPy-POP (0.315 g) were collected.

3.4. Electrochemical analysis

3.4.1. Sunblock and apple peal sample preparation

Sunblock (1.015 g) was added to ethanol and sonicated for 1 hour to extract the compounds of interest. Thereafter, the mixture was added to a volumetric flask and diluted with a PBS buffer. The sunblock sample was used for the analysis of 2-phenylphenol. Refined apple peals (10 g) were added to methanol (50 mL) and sonicated for 2 hours. The collected residue was sonicated in methanol for another 2 hours for extraction of 2-phenylphenol and diluted with PBS buffer.

Chapter 4: Results and discussion

4.1. Synthetic strategy and characterization of MPy-POPs and Fe_3O_4@MPy-POPs

4.4.1. Synthesis

Scheme 4.1 shows the synthetic strategy used in this work. Pyrrole and terepthaldehyde were allowed to react under acidic conditions. The aromatic aldehyde was activated by protonation, followed by aromatic substitution on the activated carbon of pyrrole. This resulted in the formation of macrocyclic porphyrin blocks with free CHO groups through a condensation reaction. Further condensation led to the formation of an extended porous organic polymeric network structure which has been annotated as a blue sphere (Modak et al., 2012). The product was collected and purified by Soxhlet extraction to wash out short chain oligomers while leaving longer polymer chains to be collected (Samuel Watson Stahl, 2018). The purification process is difficult, tedious, and extremely time consuming. In the second reaction step, Fe^{2+} and Fe^{3+} salts were added to the MPy-POPs under basic conditions to promote the synthesis and complete growth of the nanoparticles crystals embedded into the pores of the MPy-POP framework.

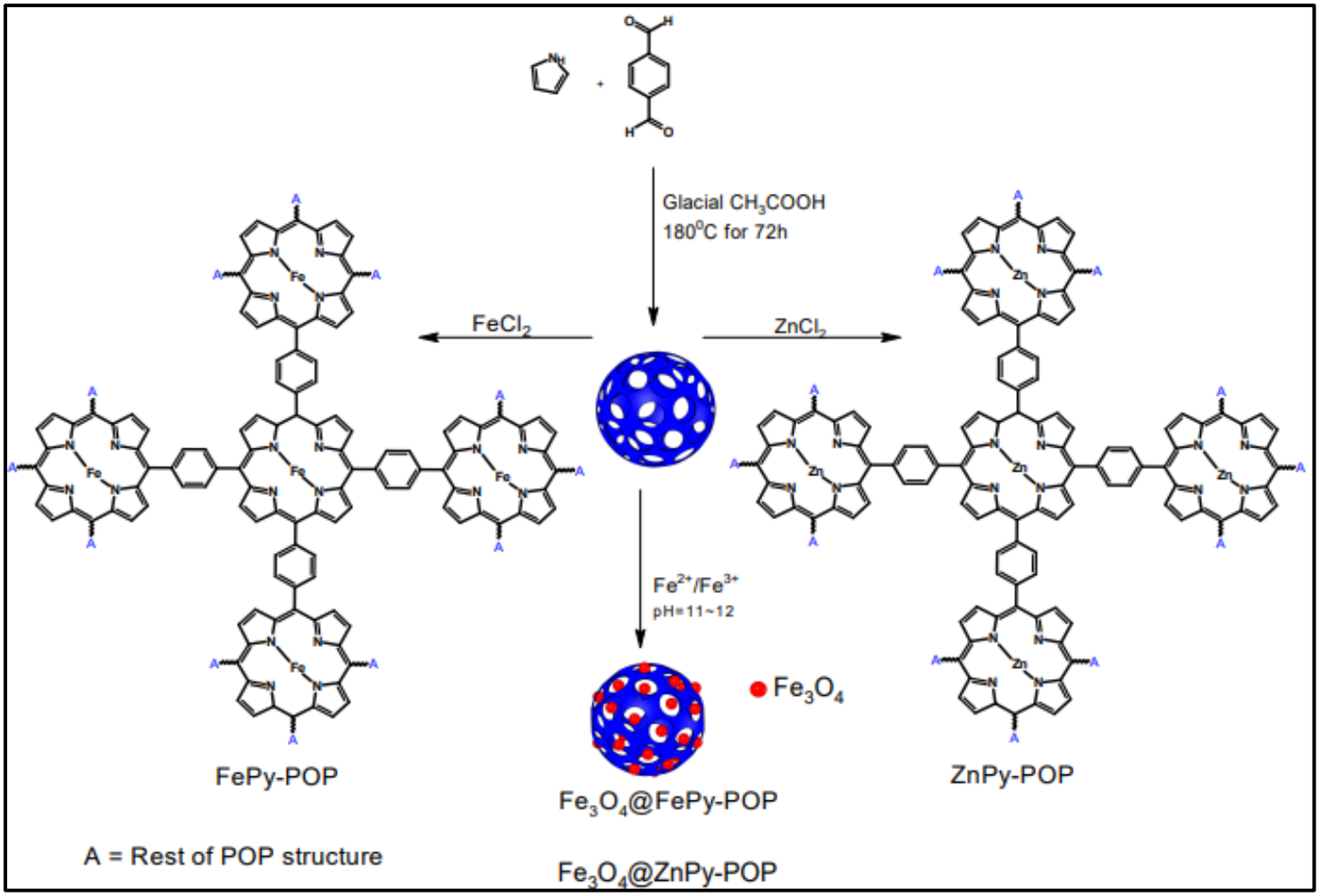

Scheme 4.1: Synthetic pathway of MPy-POPs and Fe_3O_4@MPy-POPs.

4.1.2. Powder X-ray diffraction (PXRD)

PXRD was used to assess the crystallinity and phase purity of FePy-POP, ZnPy-POP, Fe_3O_4@FePy-POP and Fe_3O_4@ZnPy-POP, and the results are displayed in Figure 4.1. In Figure 4.1(a), the XRD pattern for FePy-POP shows a broad peak at $2\theta \approx 10°$ and a slightly broad peak at $2\theta \approx 25°$ which relates to amorphous FePy-POP (Li et al., 2020). Figure 4.1(b) shows the PXRD pattern for Fe_3O_4@FePy-POP. The incorporation of nanoparticles into FePy-POPs gave rise to six sharp new diffraction peaks at 2-$\theta \approx 18.6°$, 30.6°, 35.8°, 37.35°, 43.6°, 53.9° and 57.4° and are indexed as (111), (220), (311), (222), (400), (422) and (511) respectively (JCPDS 19-0629). The

PXRD pattern for ZnPy-POP is displayed in Figure 4.1(c). The amorphous nature of ZnPy-POP was confirmed by a broad diffraction peak between $2\theta \approx 10°$ and $2\theta \approx 30°$. In Figure 4.1(d), Fe_3O_4@ZnPy-POP display similar diffraction peaks as Fe_3O_4@FePy-POP at $2\theta \approx 18.6°$, 30.6°, 35.8°, 37.35°, 43.6°, 53.9° and 57.4° due to Fe_3O_4 nanoparticles. The XRD patterns were able to confirm the highly crystalline nature and the unique cubic structure of Fe_3O_4 crystals present in the MPy-POP structures (Maryamdokh Taimoory et al.,2017). This is a clear indication that crystalline Fe_3O_4 nanoparticles are present in the amorphous MPy-POP pores forming the desired nanocomposites.

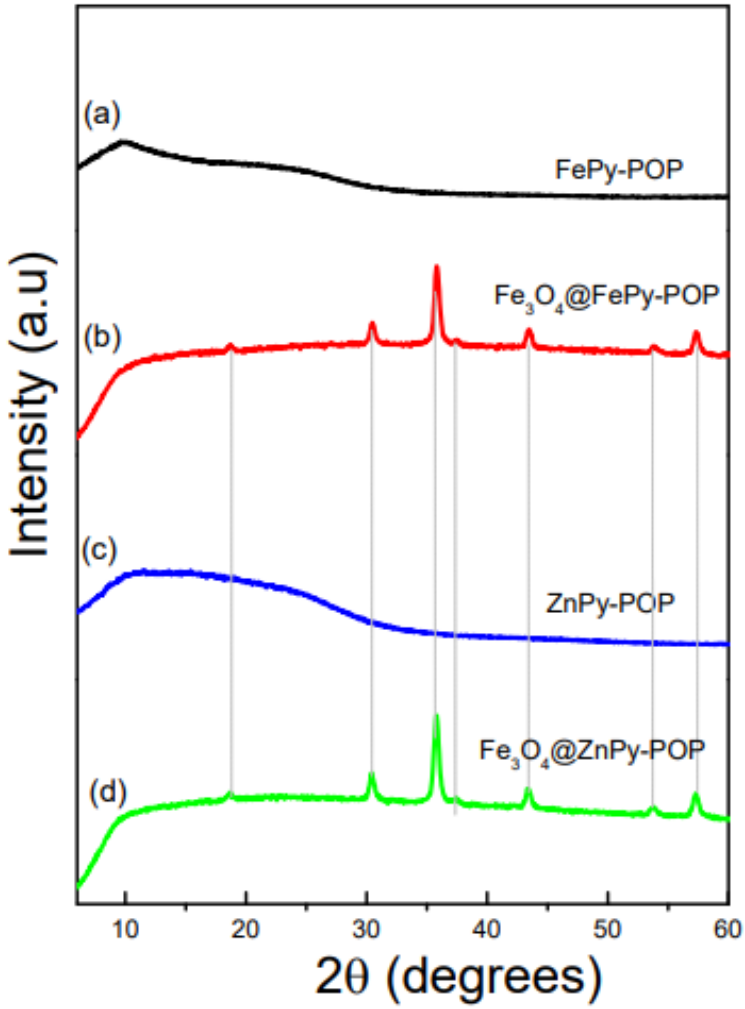

Figure 4.1: *XRD patterns of synthesized (a) FePy-POP, (b) Fe_3O_4@FePy-POP, (c) ZnPy-POP and (d) Fe_3O_4@ZnPy-POP*

4.1.3. Fourier transform infrared (FTIR) spectroscopy

FTIR was performed for all synthesized compounds and the results are shown in Figure 4.2. The FePy-POP spectrum in Figure 4.2(a) corresponds to the successfully synthesized FePy-POP spectra, as previously reported (Modak et al., 2011). The broad peak at 3000 cm^{-1} represents OH stretching and originates from water or alcohol used in the washing process. The peak at 1612 cm^{-1} corresponds to the stretching of C=N bond in the pyrrole ring, while the vibrational modes of phenyl rings (C=C) was observed at 1430 cm^{-1}. Additionally, a vibration band at 1268 cm^{-1} and 1044 cm^{-1} was due to C-N and N-H respectively. The bands between 700 cm^{-1} and 800 cm^{-1} were seen because of the C-H out-of-plane bending of phenyl rings forming part of the carbonyl backbone and the Fe-N coordination peak appeared at 562 cm^{-1} (Yao et al., 2021). In Figure 4.2(b), Fe_3O_4@FePy-POP exhibits a very faint peak at 3000 cm^{-1} which corresponds to OH stretching. Peaks at 1602 cm^{-1} and 1360 cm^{-1} are due to C=N in pyrrole and C=C in phenyl respectively. A peak at 416 cm^{-1} appeared after Fe_3O_4 nanoparticles were embedded in the FePy-POP structural pores, this peak represents the Fe-O stretch (Pintor Simamora et al., 2018).

In Figure 4.2(c), ZnPy-POP spectra is similar to FePy-POP and displayed Zn-N stretching at 564 cm^{-1}. Figure 4.2(d) shows the spectrum of Fe_3O_4@ZnPy-POP that is similar to Fe_3O_4@FePy-POP spectrum with a peak at 405 cm^{-1} characteristic to the Fe-O vibration. The appearance of metal oxide peaks proved successful incorporation of Fe_3O_4 nanoparticles into MPy-POPs and the formation of Fe_3O_4@FePy-POP and Fe_3O_4@ZnPy-POP composites.

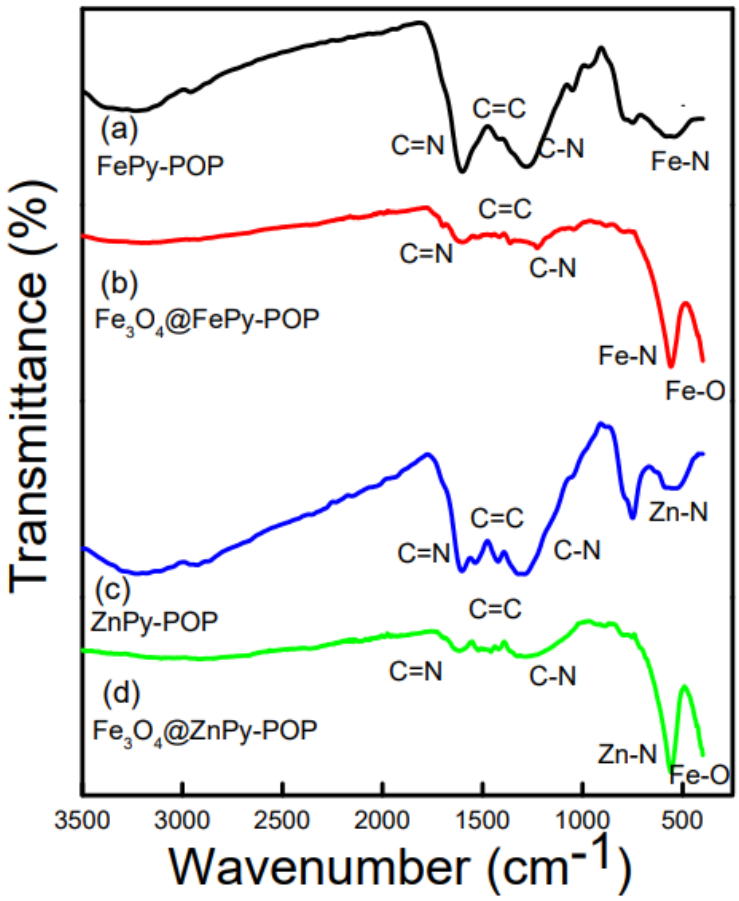

Figure 4.2: *FTIR spectra of (a) FePy-POP, (b) Fe_3O_4@FePy-POP, (c) ZnPy-POP and (d) Fe_3O_4@ZnPy-POP*

4.1.4. Scanning electron microscopy (SEM) and EDX

SEM was used to assess the morphology of the synthesized compounds and the results are depicted in Figure 4.3. Figure 4.3(a) shows the uniform spherical structure of FePy-POPs with a smooth surface as previously reported (Modak et al., 2011). After the FePy-POPs were enriched with Fe_3O_4 nanoparticles, the spherical structure of Fe_3O_4@FePy-POPs was maintained as shown in Figure 4.3(b). The surface of Fe_3O_4@FePy-POPs appeared rugged due to the nanoparticles surrounding the FePy-POP structure. Furthermore, Figure 4.3(c) displays ZnPy-POP as smooth and globular shaped and appears agglomerated and similar in size. The smooth surface of ZnPy-POPs becomes uneven when enriched with Fe_3O_4 nanoparticles, as shown in Figure

4.3(d). The Fe_3O_4@ZnPy-POP nanocomposite appeared completely covered with smaller spheres contributing to the uneven surface. The smooth spherical nature of FePy-POP and ZnPy-POP changed to a rugged spherical surface as seen in the SEM micrographs and serves as a clear indication of the successful incorporation and well dispersion of Fe_3O_4 nanoparticles onto FePy-POP and ZnPy-POP.

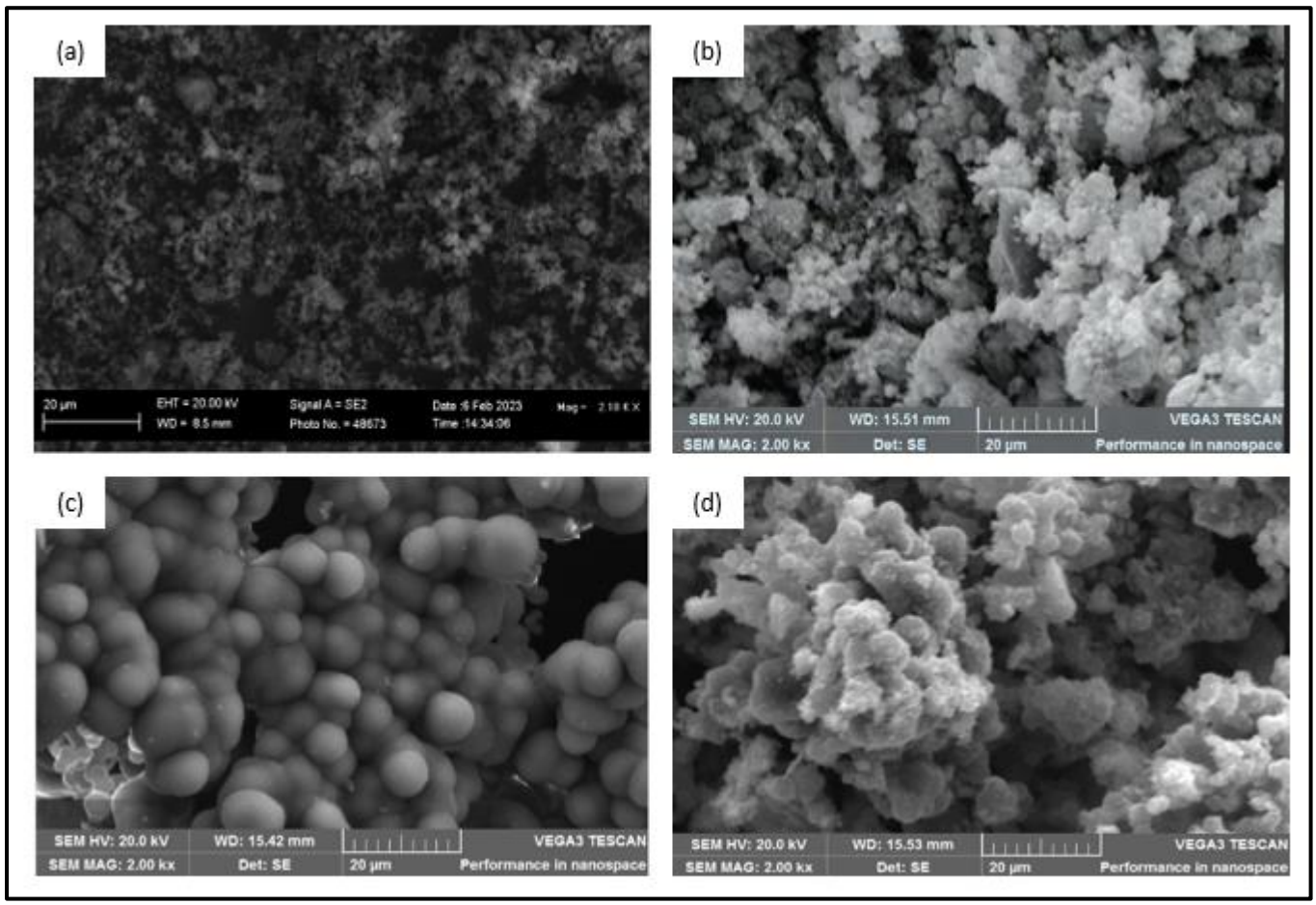

Figure 4.3: *SEM images of (a) FePy-POP, (b) Fe_3O_4@FePy-POP, (c) ZnPy-POP and (d) Fe_3O_4@ZnPy-POP*

Elemental analysis was preformed using EDX, and the results are presented in Figure 4.4. Figure 4.4(a) shows the EDX of FePy-POP, in which Fe is present at 0.5 wt%, furthermore O and N are present at 66.5 wt% and 33.0 wt% respectively. When Fe_3O_4

nanoparticles are incorporated (Figure 4.4(b)), the Fe peak became prominent at 29.6 wt% followed by O 22.9 wt%, confirming the enrichment of nanoparticles within the FePy-POP structure. The elemental analysis of ZnPy-POP, Figure 4.4(c) showed 14.5 wt% of Zn and 35.9 wt% of N. Enriching ZnPy-POP with Fe_3O_4 nanoparticles, Figure 4.4(d), revealed Fe at 25.8 wt% and O at 22.4 wt%. As a result of the dominating presence of Fe_3O_4 nanoparticles, the Zn peak decreased to 1.0 wt%. These findings further confirmed that the nanoparticles were successfully enriched within the POP structure.

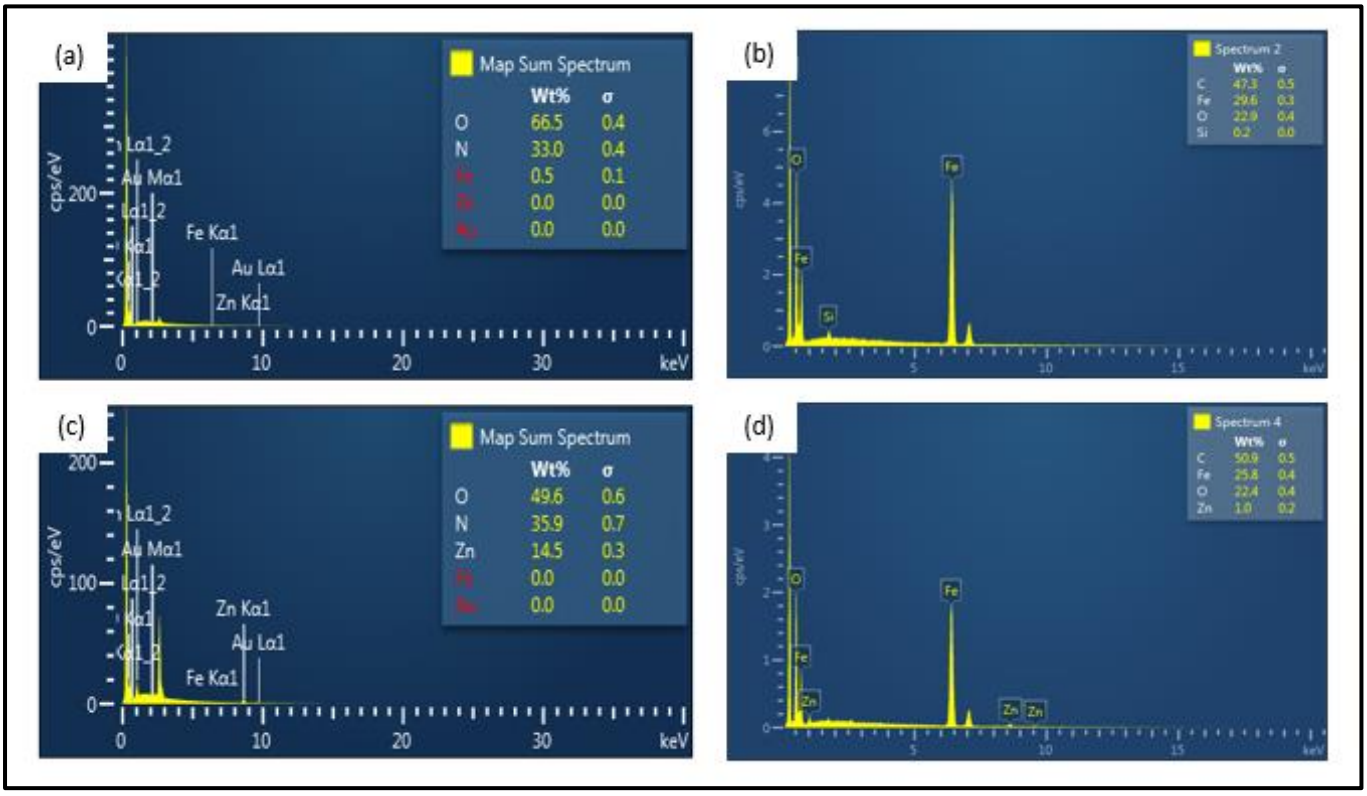

Figure 4.4: *EDX spectrum of (a) ZnPy-POP, (b) Fe_3O_4@ZnPy-POP, (c) FePy-POP and (d) Fe_3O_4@FePy-POP*

4.1.5. Transmission electron microscopy (TEM)

Figure 4.5 shows high-resolution TEM images of the composites. Figure 4.5(a) shows FePy-POPs as spherical particles distributed throughout the matrices. Some of the spheres have adhered to each other, forming larger particles that contain low electron density white spots due to the porous nature of POPs as previously reported (Modak et al., 2013). In Figure 4.5(b), it is clear that Fe_3O_4 nanoparticles have been incorporated in FePy-POP, as smaller spheres are abundant and completely covers the larger spherical FePy-POP structure. The TEM image for ZnPy-POP is shown in Figure 4.5(c) as having spheres packed over each other forming larger particles displaying porous features of ZnPy-POP. The complete coverage of the pores and the presence of smaller spheres in Figure 4.5(d) confirms incorporation of Fe_3O_4 nanoparticles onto ZnPy-POP.

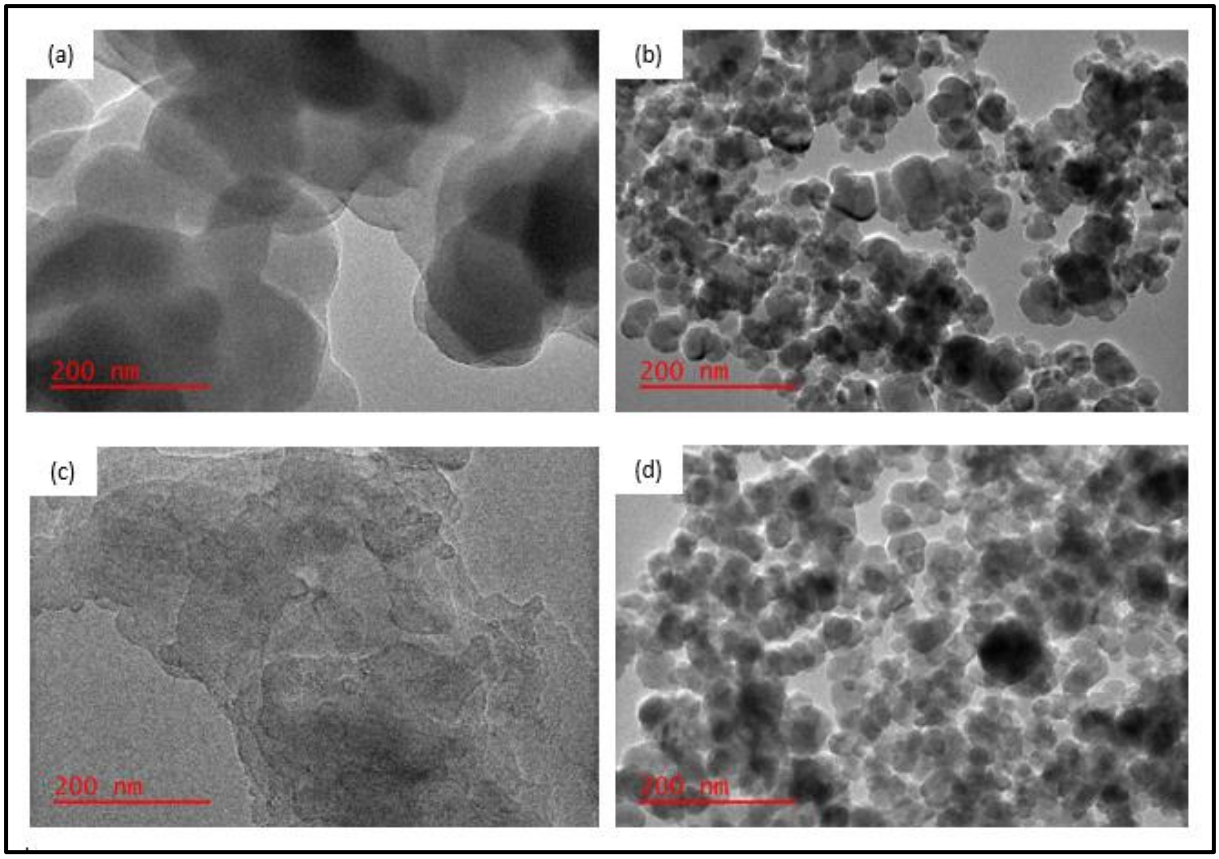

Figure 4.5: *TEM images of (a)FePy-POP, (b) Fe_3O_4@FePy-POP, (c) ZnPy-POP and (d) Fe_3O_4@ZnPy-POP*

4.1.6. Ultraviolet-visible (UV-Vis) spectroscopy

The absorption properties of MPy-POPs and Fe_3O_4@MPy-POPs were dissolved in dimethylformamide and analysed using UV-Vis spectroscopy, as shown in Figure 4.6. In Figure 4.6(a), the absorption spectrum for FePy-POP was illustrated. The peak at 227 nm was assigned to the Soret band or B band, while the peaks between 450 nm and 750 nm were identified as the Q band (Giovannetti, 2012). In Figure 4.6(b), the UV-Vis spectrum of Fe_3O_4@FePy-POP is shown to have a B band at 227 nm that is similar to FePy-POP. This indicates that the incorporation of the nanoparticles did not affect the absorption properties of the MPy-POP (Nagaraj et al., 2014). Figure 4.6(c) shows the absorption spectrum of ZnPy-POP with a B band at 300 nm and a shoulder

peak at 344 nm due to aggregation of the ZnPy-POP. Figure 4.6(d) displays the absorption spectra of Fe_3O_4@ZnPy-POP with a B band peak at 222 nm.

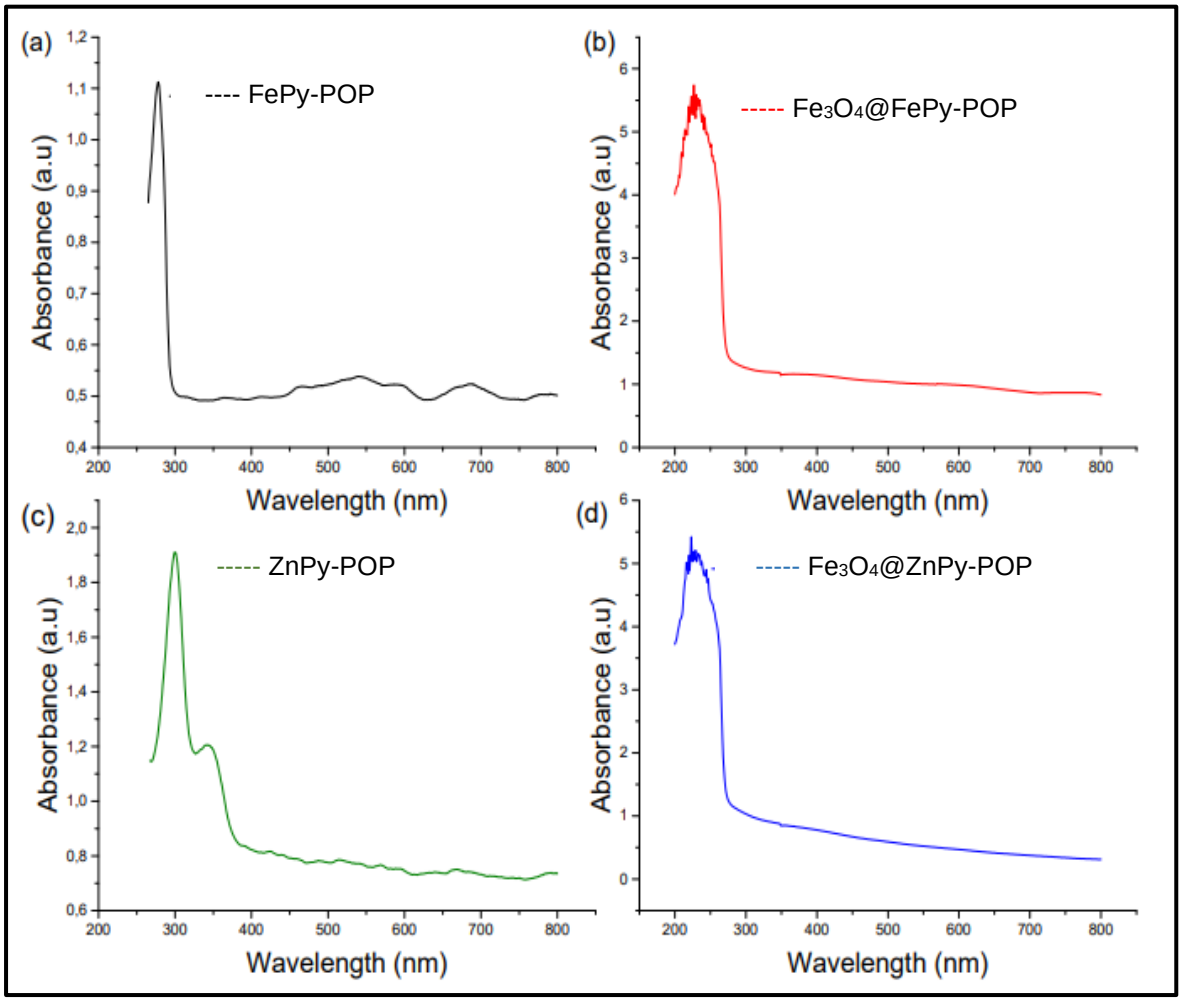

Figure 4.6: *UV-Visabsorbance of (a) FePy-POP, (b) Fe_3O_4@FePy-POP, (c) ZnPy-POP and (d) Fe_3O_4@ZnPy-POP*

Chapter 5: Electrocatalysis

5.1. Electrode modification

There are various methods available to modify the GCE for sensor development. In this work, electrodeposition on the GCE was the preferred method as the process is relatively inexpensive, fast and, easy (Cai et al., 2019, Rajendran et al., 2020). The method coats the designed material (in the polytop) as a thin film onto a conductive substrate. Scheme 5.1 shows the conditions used in this study.

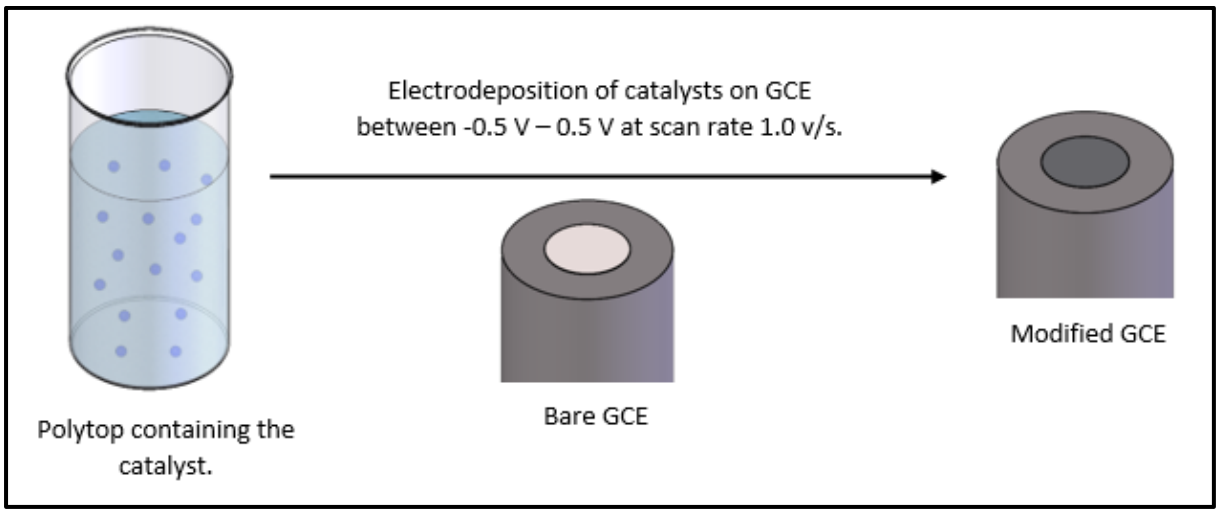

Scheme 5.1: *Graphical representation of the electrodeposition method.*

Figure 5.1 shows the voltammograms of FePy-POP during the electrodeposition process, cycled in the potential range between -0.5 V and 0.5 V vs Ag/AgCl. With an increasing number of scans, the intensity of the observed current increased, leading to the formation of a thin, uniform catalyst layer on the GCE surface. The current density on the GCE has influence in determining the thickness of the coating. Hence, the composition of the catalyst solution that governs the conductivity and impacts the success of electrodeposition (Filgueira et al., 2021).

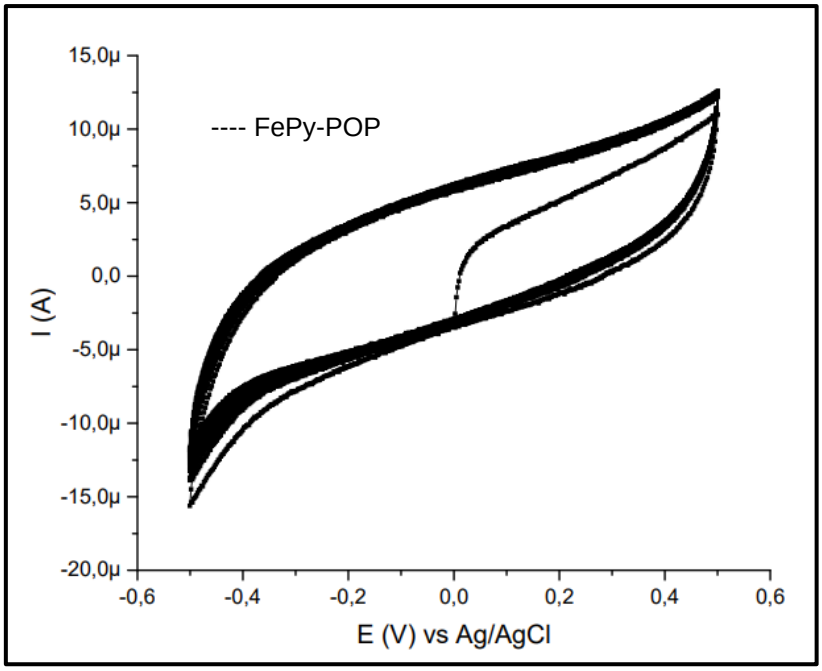

Figure 5.1: *Electrodeposition of FePy-POP on GCE between -0.5 V and 0.5 V at scan rate 1.0 v/s.*

5.2. Electrocatalytic oxidation of 2-phenylphenol

The synthesized MPy-POPs and Fe_3O_4@MPy-POPs were used as catalysts for the electrocatalytic oxidation of 2-phenylphenol. These catalysts facilitated electron transfer, reduced the overpotential, and increased catalytic currents since this oxidation does not occur on the bare GCE. The oxidation reaction of 2-phenylphenol were carried out at pH 6.8 for optimal catalytic conditions. Figure 5.2 illustrates the oxidation responses on the bare GCE compared to the GCE modified with catalyst materials. On the bare electrode, 2-phenylphenol was not detected, but upon modification with FePy-POP (Figure 5.2(a)), an oxidation potential at 0.61 V with a catalytic current at 2.98×10^{-5} A. In Figure 5.2(b), ZnPy-POP catalyzed 2-phenylphenol at a catalytic current of 4.15×10^{-5} A at an oxidation potential of 0.65 V. When Fe_3O_4 nanoparticles were incorporated into MPy-POPs, the oxidation potential of Fe_3O_4@FePy-POP in Figure 5.2(c) was 0.65 V with a catalytic current of

2.47× 10^{-5} A. Figure 5.2(d) shows that Fe_3O_4@ZnPy-POP catalyzed 2-phenylphenol at an oxidation potential 0.64 V with a catalytic current 2.96× 10^{-5} A.

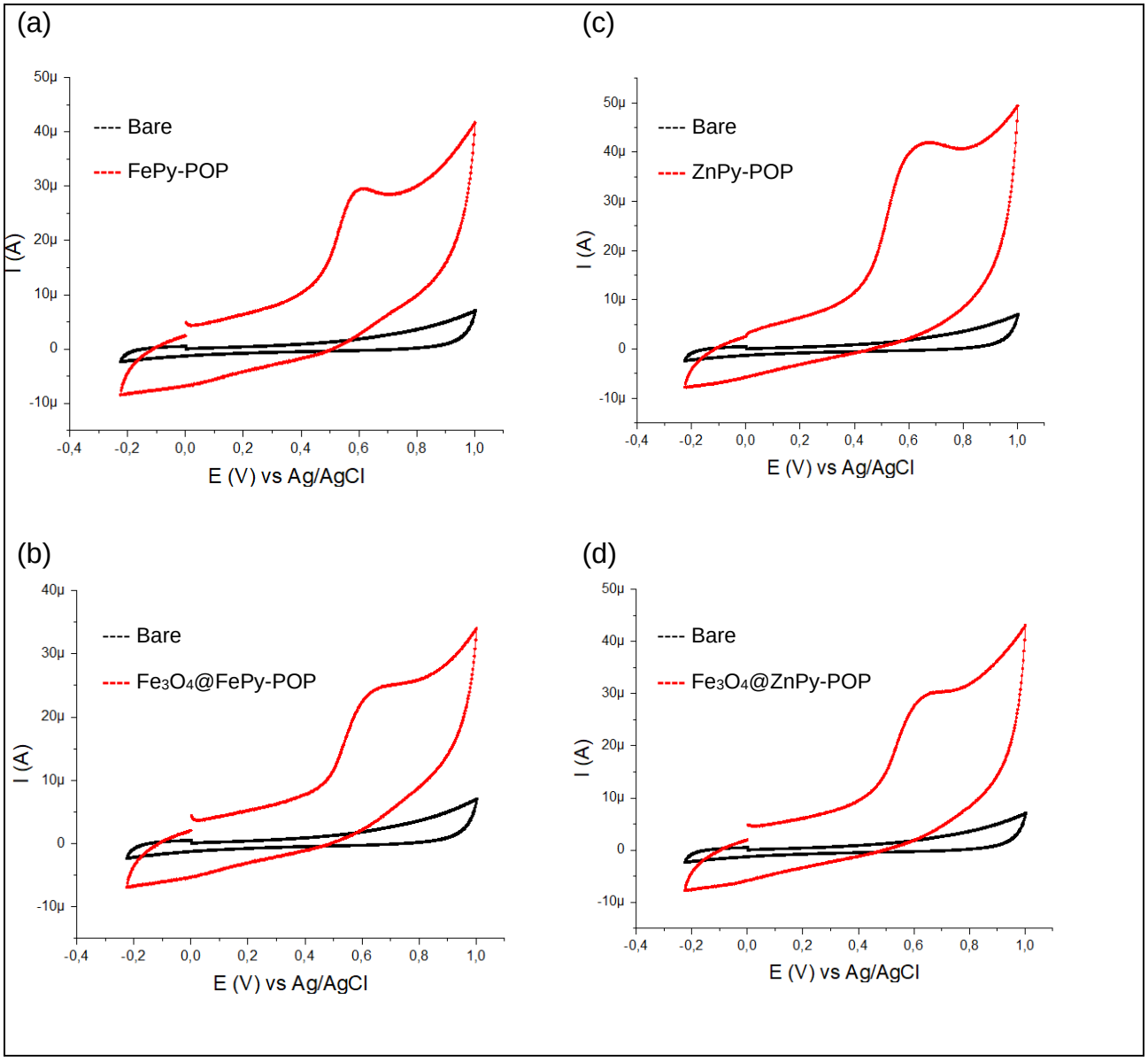

Figure 5.2: *Cyclic voltammograms of the bare GCE and (a) FePy-POP, (b) Fe_3O_4@FePy-POP, (c) ZnPy-POP and (d) Fe_3O_4@ZnPy-POP modified GCE for 2-phenylphenol oxidation in PBS at scan rate of 0.05 V/s.*

Table 5.1 compares the electrochemical oxidation of 2-phenylphenol on GCE modified with MPy-POPs and Fe_3O_4@MPy-POPs. FePy-POP had the lowest oxidation potential at 0.61 V and ZnPy-POP catalyzed 2-phenylphenol at a higher catalytic current of 4.15×10^{-5} A. The surface properties of the synthesized catalysts play a crucial role in their catalytic performance during the electrochemical analysis, particularly in detecting 2-phenylphenol in water (Prabhu et al., 2023). MPy-POPs, which contain metal centers, have more active sites, making them better at detecting 2-phenylphenol (Yang et al., 2022). The electrochemical oxidation of 2-phenylphenol occurs through an oxidation-reduction reaction that is mediated by the metal centers embedded into the MPy-POP and Fe_3O_4@MPy-POP framework.

Table 5.1: *Parameters for 2-phenylphenol oxidation on MPy-POP and Fe_3O_4@MPy-POP modified GCE at pH 6.8.*

Catalyst	**Ep (V) vs Ag/AgCl**	**Ip (A)**	**Limit of detection (mM)**	**b (mV/decade)**
FePy-POP	0.61	2.98×10^{-5}	2.6	474
ZnPy-POP	0.65	4.15×10^{-5}	0.75	304
Fe_3O_4@FePy-POP	0.65	2.47×10^{-5}	1.5	248
Fe_3O_4@ZnPy-POP	0.64	2.96×10^{-5}	1.4	181

Figure 5.3 shows the peak current against 2-phenylphenol concentration for the synthesized catalysts. The results revealed that the current increased linearly with increase in 2-phenylphenol concentration using the 3σ criteria. The limit of detection

ranged from 0.75 mM to 2.6 mM for the MPy-POP and Fe_3O_4@MPy-POP materials (Table 5.1). This is slightly higher in comparison to what is described in literature, Table 2.5. The allowed daily intake of 2-phenylphenol is 0.4 mg/kg of body weight, which suggests that all synthesized catalysts are suitable as sensors for detection of 2-phenylphenol in water (Álvarez et al., 2023). ZnPy-POP showed to have the lowest LOD followed by Fe_3O_4@ZnPy-POP, Fe_3O_4@FePy-POP and FePy-POP.

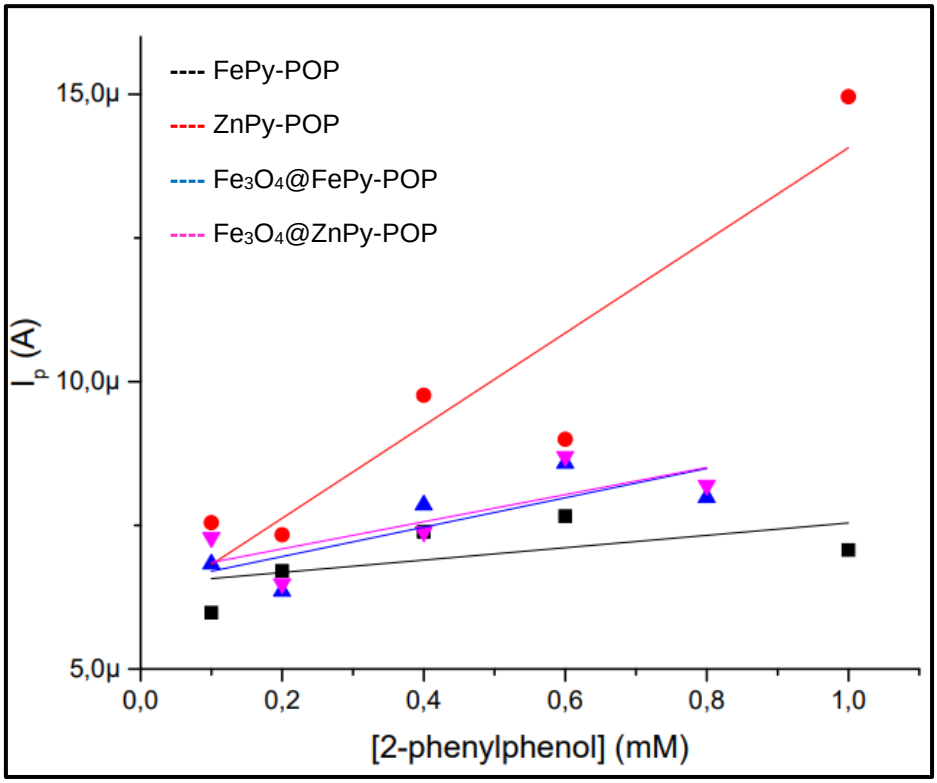

Figure 5.3: *Peak current vs concentration of 2-phenylphenol on MPy-POP and Fe_3O_4@MPy-POP modified GCE in pH 6.8 buffer.*

The catalytic process was further investigated using the graph of Ep vs log scan rate shown in Figure 5.4. To obtain information on the rate determining step, a Tafel slope was determined form Equation 5.1 for an irreversible diffusion-controlled reaction (Mohammad Ali Kamyabi et al., 2008).

$$Ep = \left[\frac{2.3RT}{2(1-\alpha)n_aF}\right] \times logv + K \qquad \textbf{Equation 5.1}$$

where *K* is a constant, v is the scan rate, *R* is the rate constant, *T* is the temperature, *F* is Faraday's constant, *Ep* is the peak potential, n_a is the number of electrons that is involved in the rate determining step and α the transfer coefficient. The Tafel equation describes the dependence of current on the overpotential and the gradient of Figure 5.4 gives $\frac{b}{2}$, where *b* is the Tafel slope (taf Faulkner and White, 2022).

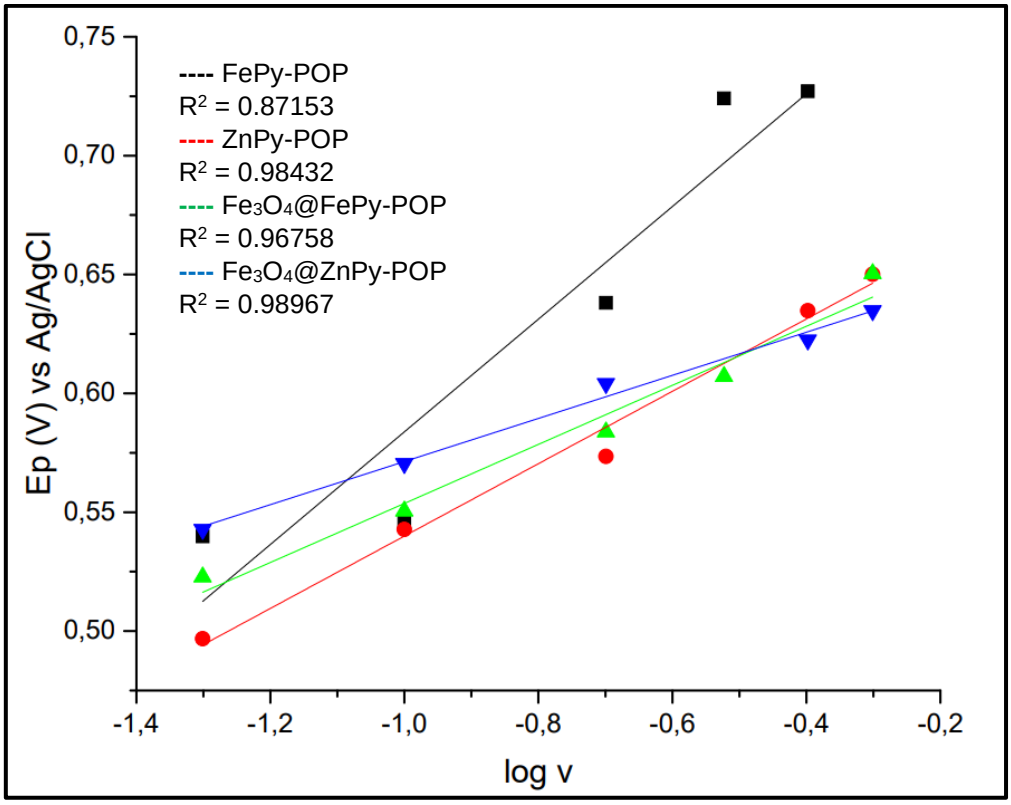

Figure 5.4: *Peak potential versus the logarithm of scan rate for the oxidation of 1mM 2-phenylphenol on MPy-POP and Fe_3O_4@MPy-POP modified GCE in pH 6.8 buffer.*

The Tafel slope, is calculated using the formula b= 2.3RT/ 2(1-α)nα F. The Tafel slopes for the synthesized composites were found to be between 181 – 474

mV/decade, as seen in Table 5.1. These values indicate strong catalyst-substrate (Sengeni Anantharaj et al., 2021).

5.3. Passivation studies

Figure 5.5 shows the passivation studies of the newly developed sensors. Figure 5.5(a) shows the catalytic current of FePy-POP decreased from 100% to 32% after two cycles and to 29% after the third cycle. ZnPy-POP passivated to 38% after the second cycle and to 34% after the third cycle, as seen in Figure 5.5(b). The catalytic current of Fe_3O_4@FePy-POP shown in Figure 5.5(c) decreased to 34% and ultimately to 33% after three cycles. In Figure 5.5(d), Fe_3O_4@ZnPy-POP also passivated after the second cycle to 37% and to 34% after the third cycle. These results are in line with the calculated Tafel slope values which predicted strong binding of the catalyst to the substrate. Hence, drastic passivation of the electrode surface was not surprising.

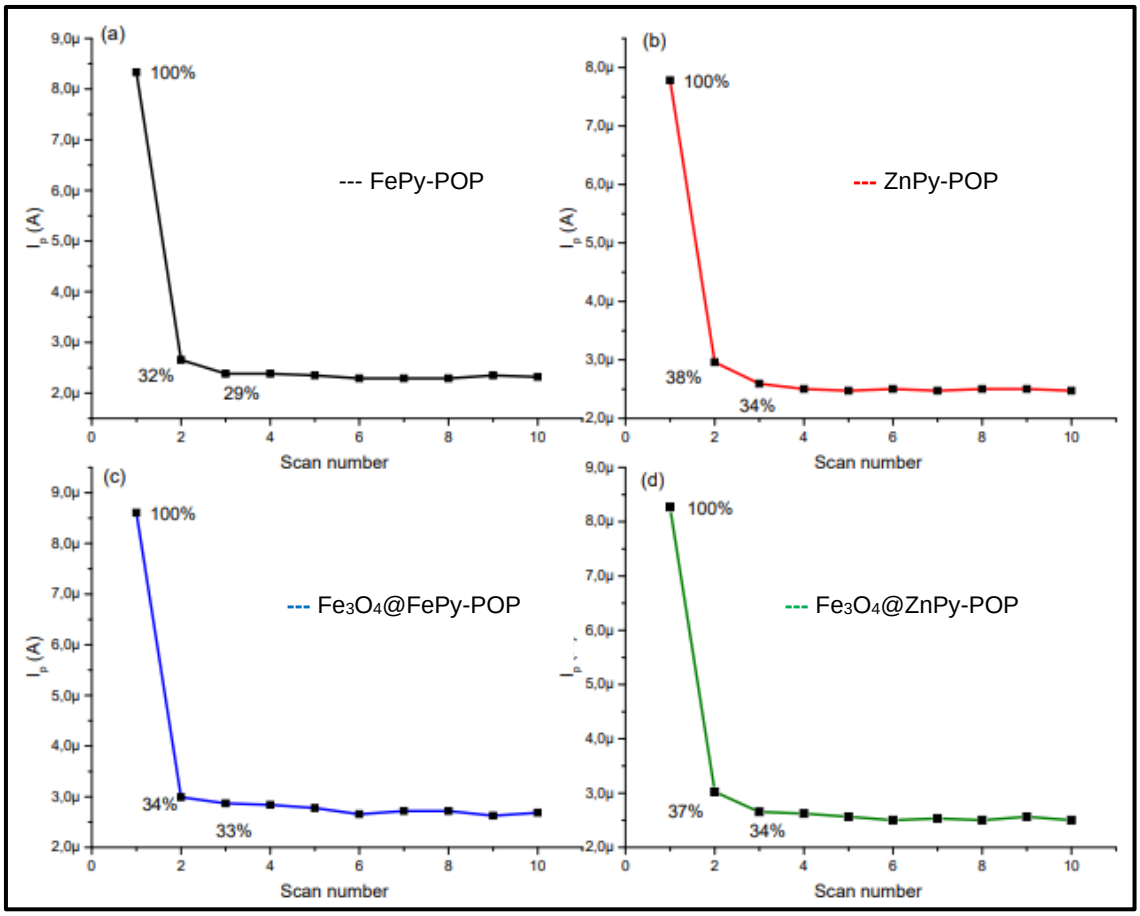

Figure 5.5: *Passivation of (a) FePy-POP, (b) ZnPy-POP, (c) Fe_3O_4@FePy-POP and (d) Fe_3O_4@ZnPy-POP on modified GCE in 1.0 mM 2-phenylphenol at 0.05 V/s.*

Scheme 5.2 shows the proposed electrocatalytic oxidation reaction mechanism for 2-phenylphenol. In the proposed scheme, two electrons are involved in the catalytic mechanism reaction which involves the formation of a radical and the resulting products which contribute to the passivation of the electrode surface.

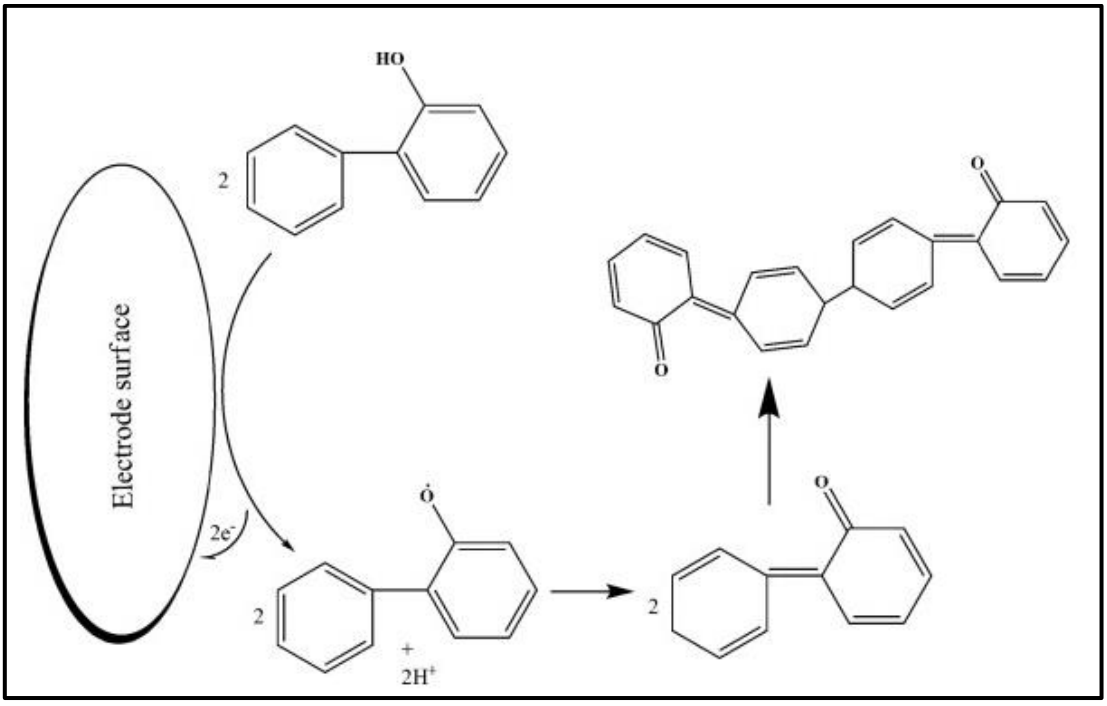

Scheme 5.2: *The electrocatalytic oxidation mechanism of 2-phenylphenol (Prabhu et al., 2023)*

The practical application of the modified GCEs were examined to quantify the detection of 2-phenylphenol in apple peels and sunscreen samples (Sun et al., 202). Figure 5.6(a) shows no significant catalytic responses were detected in the apple peel sample. The sunscreen sample shown in Figure 5.6(b), exhibit an oxidation peak at 0.61 V for ZnPy-POP and two oxidation peaks at 0.56 V and 0.82 V for FePy-POP. The Fe_3O_4@FePy-POP showed an oxidation peak at 0.57 V and Fe_3O_4@ZnPy-POP

at 0.57 V. FePy-POP showed the lowest oxidation potential. The catalysts proved to be sufficient to detect 2-phenylphenol in a real sample.

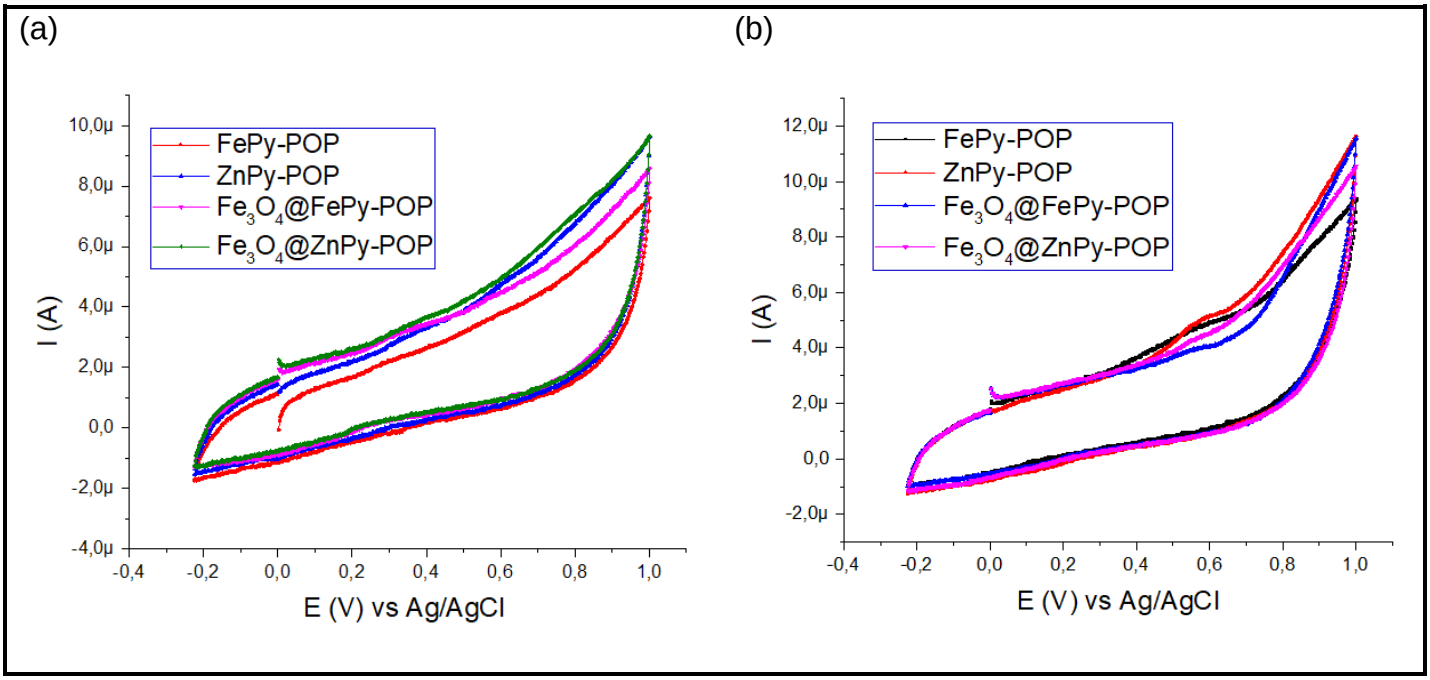

Figure 5.6: *Cyclic voltammograms of (a) apple peels and (b) sunscreen in PBS buffer at scan rate 0.05 V/s.*

Chapter 6: Conclusion and future work

6.1. Conclusion

The focus of this study was to synthesize and characterize various catalysts that can detect an endocrine-disrupting chemical, 2-phenylphenol. Synthesized MPy-POPs and Fe_3O_4@MPy-POP were chosen as catalysts due to their highly conjugate systems, chemical stability and their ability to bind with metals. Spectroscopic methods were used to confirm the successful formation of FePy-POP, ZnPy-POP, Fe_3O_4@FePy-POP and Fe_3O_4@ZnPy-POP. SEM and TEM images confirmed the expected spherical morphology of ZnPy-POP and FePy-POP. Upon incorporating spherical Fe_3O_4 nanoparticles into the MPy-POPs, they were observed to completely cover the MPy-POPs and reduce agglomeration. Elemental analysis showed successful incorporation of metals into the Py-POPs. PXRD confirmed MPy-POPs as amorphous while the nanoparticles in Fe_3O_4@MPy-POP displayed their crystalline nature. FTIR further confirmed the successful synthesis of the composites by showing characteristic fingerprints of the nanocomposites.

The MPy-POPs and corresponding Fe_3O_4 nanocomposites were immobilized on the surface of the GCE using electrode deposition technique. The modified electrodes were tested for its potential to oxidize 2-phenylphenol. The bare GCE could not detect the analyte, but the modified electrode detected 2-phenylphenol between 0.61 V and 0.65 V and catalytic currents ranging from 2.47 – 4.15 µA. The limit of detection varied between 0.75 – 2.6 mM. The FePy-POP was the most efficient catalyst oxidizing 2-phenylphenol at 0.61 V and Fe_3O_4@MPy-POPs was the least efficient with a catalytic potential at 0.65 V.

The catalysts were utilized for the detection of 2-phenylphenol in real samples. The sunblock sample showed detection, whereas apple peels did not exhibit any significant oxidation of 2-phenylphenol. FePy-POP was found to be a better catalyst as it resulted in detection of 2-phenylphenol in sunblock at lower oxidation potential.

The catalytic performance of FePy-POPs was found to be superior compared to the other synthesized catalysts. It has the potential to be a promising candidate for developing sensors for the detection of endocrine disrupting chemicals, like 2-phenylphenol in water.

6.2. Future work

The success of electro-catalysis depends on the materials used for electrode modification. Further research could be directed to minimize electrode fouling to achieve durability. Considering the synthetic route, as well as the structural composition of MPy-POPs and Fe_3O_4@MPy-POPs in detecting 2-phenylphenol, they prove to be very promising, however the purification methods can be optimized as they are very time consuming. Furthermore, other metals such as Ti, Cr, Co, and Ni metals can be used to coordinate with POPs as they all have partially filled 3d subshells that can accept electrons during electro-oxidation. A variation of nanoparticles can be utilized in the MPy-POP structures to lower the peak potential and increase catalytic currents. The Brunauer-Emmett-Teller method can be used to determine the surface area and pore size of the martials and monitor the effect nanoparticles will have on MPy-POPs. Additionally, pH studies can be done to investigate the effect of pH on the catalytic performance of the fabricated sensors. Alternative electrodes like screen printed electrodes can be used as a sensors substrate especially because we have seen in this work that these sensors are easily passivated and are likely to be used once.

References

2-Phenylphenol in Drinking-water Background document for development of WHO Guidelines for Drinking-water Quality. (2003). Available at: https://cdn.who.int/media/docs/default-source/wash-documents/wash-chemicals/2phenylphenol-background.pdf?sfvrsn=261b56f5_3 [Accessed 13 Aug. 2023].

Abdelnaby, M.M., Saleh, T.A., Zeama, M., Abdalla, M.A., Ahmed, H.M. and Habib, M.A. (2022). Azo-Linked Porous Organic Polymers for Selective Carbon Dioxide Capture and Metal Ion Removal. ACS Omega, 7(17), pp.14535–14543.

Akyüz, D. and Koca, A. (2019). An electrochemical sensor for the detection of pesticides based on the hybrid of manganese phthalocyanine and polyaniline. Sensors and Actuators B: Chemical, 283, pp.848–856.

Ali, A., Zafar, H., Zia, M., ul Haq, I., Phull, A.R., Ali, J.S. and Hussain, A. (2016). Synthesis, characterization, applications, and challenges of iron oxide nanoparticles. Nanotechnology, Science and Applications, Volume 9, pp.49–67.

Álvarez, F., Arena, M., Auteri, D., Binaglia, M., Anna Federica Castoldi, Chiusolo, A., Colagiorgi, A., Colas, M., Federica Crivellente, Chloé De Lentdecker, Isabella De Magistris, Egsmose, M., Fait, G., Franco Ferilli, Varvara Gouliarmou, Halling, K., Laia Herrero Nogareda, Ippolito, A., Frédérique Istace and Jarrah, S. (2023). Peer review of the pesticide risk assessment of the active substance metrafenone. *EFSA Journal*, 21(5).

Arfaeinia, H., Ramavandi, B., Yousefzadeh, S., Dobaradaran, S., Ziaei, M., Rashidi, N., & Asadgol, Z. (2021). Urinary level of un-metabolized parabens in women working in beauty salons. Environmental Research, 200, 111-771.

Asokan, K., Patil, M., Shatabdi Porel Mukherjee, Santhosh Sukumaran Babu, and T Nandakumar (2022). Scalable Mechanochemical Synthesis of β -Ketoenamine-linked Covalent Organic Frameworks for Methane Storage. 17(24).

Bandyopadhyay, S., Singh, C., Jash, P., Hussain, M. W., Paul, A., & Patra, A. (2018). Redox-active, pyrene-based pristine porous organic polymers for efficient energy storage with exceptional cyclic stability. Chemical Communications, 54(50), 6796–6799.

Baranowska, I. and Bijak, K. (2013). Voltametric determination of disinfectants at multiwalled carbon nanotube modified glassy carbon electrode. Journal of Analytical Chemistry, 68(10), 891–895.

Bard, A.J., Faulkner, L.R. and White, H.S. (2022). *Electrochemical Methods*. John Wiley & Sons, 137.

Ben, T., Ren, H., Ma, S., Cao, D., Lan, J., Jing, X., Wang, W., Xu, J., Deng, F., Simmons, Jason M., Qiu, S. and Zhu, G. (2009). Targeted Synthesis of a Porous Aromatic Framework with High Stability and Exceptionally High Surface Area. Angewandte Chemie International Edition, 48(50), pp.9457–9460.

Bera, R., Monda, S., Das, N. (2018). Triptycene based microporous polymers (TMPs): efficient small gas (H_2 and CO_2) storage and high CO_2/N_2 selectivity. Micropor. Mesopor. Mater., 257, 253-261

Bergman, Å., Heindel, J.J., Kasten, T., Kidd, K.A., Jobling, S., Neira, M., Zoeller, R.T., Becher, G., Bjerregaard, P., Bornman, R., Brandt, I., Kortenkamp, A., Muir, D., Drisse, M.-N.B., Ochieng, R., Skakkebaek, N.E., Byléhn, A.S., Iguchi, T., Toppari, J. and Woodruff, T.J. (2013). The Impact of Endocrine Disruption: A Consensus Statement

on the State of the Science. Environmental Health Perspectives, [online] 121(4), 104-106.

Bertolucci, E., Maria, A., Antonetti, C., Mirko Marracci, Tellini, B., Fabio Piccinelli and Visone, C. (2015). Chemical and magnetic properties characterization of magnetic nanoparticles, 1492–1496.

Bhaduri, S.N., Ghosh, D., Debnath, S., Biswas, R., Chatterjee, P.B. and Biswas, P. (2023). Copper (II)-Incorporated Porphyrin-Based Porous Organic Polymer for a Nonenzymatic Electrochemical Glucose Sensor. Inorganic Chemistry, 62(10), 4136–4146.

Bhanja, P., Modak, A. and Bhaumik, A. (2018). Porous Organic Polymers for CO_2 Storage and Conversion Reactions. ChemCatChem, 11(1), pp.244–257.

Biesaga, M. (2000). Porphyrins in analytical chemistry. A review. Talanta, 51(2), 209–224.

Buoso, E.; Masi, M.; Racchi, M. and Corsini, E. (2020). Endocrine-Disrupting Chemicals™ (EDCs) Effects on Tumour Microenvironment and Cancer Progression: Emerging Contribution of RACK1. International Journal of Molecular Sciences, 21(23), 9229.

Cai, Y., Wen, X., Wang, Y., Song, H., Li, Z., Cui, Y., & Li, C. (2021). Preparation of hyper-crosslinked polymers with hierarchical porous structure from hyperbranched polymers for adsorption of naphthalene and 1-naphthylamine. Separation and Purification Technology, 266, 118542.

Cai, Z., Yao, Q., Chen, X. and Wang, X. (2019). Nanomaterials With Different Dimensions for Electrocatalysis. Novel Nanomaterials for Biomedical, Environmental and Energy Applications, 435–464.

Can, M.M., Coşkun, M. and Fırat, T. (2012). A comparative study of nanosized iron oxide particles, magnetite (Fe_3O_4), maghemite (γ-Fe_2O_3), and hematite (α-Fe_2O_3), using ferromagnetic resonance. Journal of Alloys and Compounds, 542, 241–247.

Cao, Y., Wang, Y., Fu, Y., Zhou, F. and Huang, J. (2023). Fabrication of the hyper-crosslinked polymers chemically functionalized by 8-hydroxyquinoline and their efficient adsorptive removal of 2-naphthol from water. Separation and Purification Technology, 322, 124272–124272.

Chang Wan Kang and Seung Uk Son (2020). Redox-Active Porous Organic Polymers for Energy Storage. Bulletin of The Korean Chemical Society, 42(2), 159–167.

Chen, L.; Yang, Y.; Guo, Z.; Jiang, D. (2011). Highly Efficient Activation of Molecular Oxygen with Nanoporous Metalloporphyrin Frameworks in Heterogeneous Systems. Adv. Mater. 23, 3149− 3154.

Chen, L., Yang, Y. and Jiang, D. (2010). CMPs as Scaffolds for Constructing Porous Catalytic Frameworks: A Built-in Heterogeneous Catalyst with High Activity and Selectivity Based on Nanoporous Metalloporphyrin Polymers. Journal of the American Chemical Society, 132(26), 9138–9143.

Chen, X., Gao, J., & Jiang, D. (2015). Designed Synthesis of Porphyrin-based Two-dimensional Covalent Organic Frameworks with Highly Ordered Structures. Chemistry Letters, 44(9), 1257–1259.

Chen, X., Shi, Z., Hu, Y., Xiao, X., and Li, G. (2018). A novel electrochemical sensor based on Fe3O4-doped nanoporous carbon for simultaneous determination of diethylstilbestrol and 17β-estradiol in toner. Talanta, 188, 81–90.

Chen, Y., Fang, Y., Yu, J., Gao, W., Zhao, H., Zhang, X. (2021). A silsesquioxane-porphyrin-based porous organic polymer as a highly efficient and recyclable absorbent for wastewater treatment. J. Hazard. Mater. 406, 124769.

Chen, Z., Kirlikovali, K.O., Idrees, K.B., Wasson, M.C. and Farha, O.K. (2022). Porous materials for hydrogen storage. Chem, 8(3), 693-716.

Cheung, P., Sze Koon Lee and Kubiak, C.P. (2019). Facile Solvent-Free Synthesis of Thin Iron Porphyrin COFs on Carbon Cloth Electrodes for CO_2 Reduction. Chemistry of Materials, 31(6), 1908–1919.

Collins D.J., a Zhou S. Ma, H.C. (2010). Metal-Organic Frameworks, John Wiley & Sons, Inc, 249–266.

Cornell, R.M. and Schwertmann, U. (2006). The Iron Oxides: Structure, Properties, Reactions, Occurrences and Uses. 2nd ed. John Wiley & Sons.

Cote, A. P. (2005). Porous, Crystalline, Covalent Organic Frameworks. Science, 310(5751), 1166–1170.

Cousins, K., Zhang, R.W., (2019). Highly porous organic polymers for hydrogen fuel storage. Polymers 11 (4), 25.

Crisp, T.M., Clegg, E.D., Cooper, R.L., Wood, W.P., Anderson, D.G., Baetcke, K.P., Hoffmann, J.L., Morrow, M.S., Rodier, D.J., Schaeffer, J.E., Touart, L.W., Zeeman, M.G. and Patel, Y.M. (1998). Environmental endocrine disruption: an effects assessment and analysis. Environmental Health Perspectives, 106(suppl 1), 11–56.

Cui, S., Qian, M., Liu, X., Sun, Z., & Du, P. (2016). A Copper Porphyrin-Based Conjugated Mesoporous Polymer-Derived Bifunctional Electrocatalyst for Hydrogen and Oxygen Evolution. ChemSusChem, 9(17), 2365–2373.

Daffé, N., Choueikani, F., Neveu, S., Arrio, M.-A., Juhin, A., Ohresser, P., Sainctavit, P. (2018). Magnetic anisotropies and cationic distribution in $CoFe_2O_4$ nanoparticles prepared by co-precipitation route: Influence of particle size and stoichiometry. Journal of Magnetism and Magnetic Materials, 460, 243–252.

Dalapati, S., Jin, S., Gao, J., Xu, Y., Nagai, A. and Jiang, D.2013. An Azine-Linked Covalent Organic Framework. J. Am. Chem. Soc.135, 17310−17313.

Dai, Z., Sun, Q., Liu, X., Bian, C., Wu, Q., Pan, S., Wang, L., Meng, X., Deng, F. and Xiao, F.-S. (2016). Metalated porous porphyrin polymers as efficient heterogeneous catalysts for cycloaddition of epoxides with CO_2 under ambient conditions. Journal of Catalysis, 338, 202–209.

De Toni, L., Tisato, F., Seraglia, R., Roverso, M., Gandin, V., Marzano, C.,Foresta, C. (2017). Phthalates and heavy metals as endocrine disruptors in food: A study on pre-packed coffee products. Toxicology Reports, 4, 234–239.

Diamanti-Kandarakis, E., Bourguignon, J.-P., Giudice, L.C., Hauser, R., Prins, G.S., Soto, A.M., Zoeller, R.T. and Gore, A.C. (2009). Endocrine-Disrupting Chemicals: An Endocrine Society Scientific Statement. Endocrine Reviews, 30(4), 293–342.

Diercks, C. S., & Yaghi, O. M. (2017). The atom, the molecule, and the covalent organic framework. Science, 355(6328),1585.

Ding, S.Y., & Wang, W. (2013). Covalent organic frameworks (COFs): from design to applications. Chem. Soc. Rev., 42(2), 548–568.

Dong, Y.B., Guan, Q., Wang, G., Zhou, L.L., & Li, W.Y. (2020).: Nanoscale Covalent Organic Frameworks as Theragnostic Platforms for Oncotherapy: Synthesis, Functionalization, and Application. Nanoscale Advances, 2, 3656-3733.

Dong, Y., Jv, J.J., Li, Y., Li, W.H., Chen, Y.Q., Sun, Q., Ma, J.P. and Dong, Y.B. (2019). Nickel-metalated porous organic polymer for Suzuki–Miyaura cross-coupling reaction. RSC Advances, 9(35), 20266–20272.

Errahali, M., Gatti, G., Botta, M., Paul, G., Rolla, G.A., Canti, L., Fraccarollo, A., Maurizio Cossi, Angiolina Comotti, Piero Sozzani and Marchese, L. (2014). Microporous Hyper-Cross-Linked Aromatic Polymers Designed for Methane and Carbon Dioxide Adsorption. 118(49), 28699–28710.

Feng, X., Chen, L., Dong, Y., & Jiang, D. (2011). Porphyrin-based two-dimensional covalent organic frameworks: synchronized synthetic control of macroscopic structures and pore parameters. Chemical Communications, 47(7), 1979.

Filgueira, A., da, H., Alexandre, R., Alves, N., Regina, A. and Prasad, S. (2021). Influence of bath composition on the electrodeposition of amorphous Ni-Mo alloys using potassium-sodium tartrate as complexing agent. *The Canadian Journal of Chemical Engineering*, 99(S1).

Foster, A.D., Marzieh Tamaddondar, Jose Miguel Luque-Alled, Harrison, W.J., Li, Z., Gorgojo, P. and Budd, P.M. (2020). Understanding the Topology of the Polymer of Intrinsic Microporosity PIM-1: Cyclics, Tadpoles, and Network Structures and Their Impact on Membrane Performance. 53(2), 569–583.

Gai, K., Qi, H., Zhu, X., & Wang, M. (2019). Preparation of Ag-Fe_3O_4 nanoparticles sensor and application in detection of methomyl. E3S Web of Conferences, 118, 01002.

Gamal Mohamed, M., M. EL-Mahdy, A.F., G. Kotp, M. and Kuo, S.-W. (2022). Advances in porous organic polymers: syntheses, structures, and diverse applications. Materials Advances, [online] 3(2), 707–733.

Gao, P., Huang, Y., Zhang, Y., Sun, Q., Ruan, S., Yin, W., Pu, H., Yin, M. and Fa, H. (2021). Simultaneous Electrochemical Detection of Ascorbic Acid, Dopamine, and Uric Acid Using the Composite Materials of Fe_3O_4 and Nitrogen Self-Doped Sunflower Plate-Derived Carbon. NANO, 16(11), 2150127.

Geng, K., He, T., Liu, R., Tan, K. T., Li, Z., Tao, S., Jiang, D. (2020). Covalent Organic Frameworks: Design, Synthesis, and Functions. Chemical Reviews, 16, 8814-8933.

Germain, J., Fréchet, J.M.J. and Svec, F. (2007). Hypercrosslinked polyanilines with nanoporous structure and high surface area: potential adsorbents for hydrogen storage. Journal of Materials Chemistry, 17(47), 4989.

Giese, R. W. (2003). Measurement of endogenous estrogens: analytical challenges and recent advances. J. Chromatogr 1000, 401–412.

Giovannetti, R. (2012). The Use of Spectrophotometry UV-Vis for the Study of Porphyrins. Macro To Nano Spectroscopy, 6, 87-108.

Giri, A., Khakre, Y., Shreeraj, G., Dutta, T.K., Kundu, S. and Patra, A. (2022). The order–disorder conundrum: a trade-off between crystalline and amorphous porous organic polymers for task-specific applications. Journal of Materials Chemistry A, 10(33), 17077–17121.

Giri, A. and Patra, A. (2022). Porous Organic Polymers: Promising Testbed for Heterogeneous Reactive Oxygen Species Mediated Photocatalysis and Nonredox CO 2 Fixation. 22(9), e202200071.

Guo, Z., Sun, P., Xiao, Z., Lin, J., Shi, T., Liu, S., Sun, A. and Li, Z. (2018). Amorphous Porous Organic Polymers Based on Schiff-Base Chemistry for Highly Efficient Iodine Capture. Chemistry-an Asian Journal, 13(16), 2046–2053.

Hynek, J., Rathouský, J., Demel, J., & Lang, K. (2016). Design of porphyrin-based conjugated microporous polymers with enhanced singlet oxygen productivity. RSC Advances, 6(50), 44279–44287.

Hlisníková, H., Petrovičová, I., Kolena, B., Šidlovská, M., & Sirotkin, A. (2020) 'Effects and mechanisms of phthalates' action on reproductive processes and Reproductive Health: A Literature Review,' International Journal of Environmental Research and Public Health, 17(18), 6811.

Holister, P., Weener, J.W., Roman, C. and Harper, T. (2003). Nanoparticles. Technology white papers, 3, 1-11.

Hollis, O. L. (1966). Separation of Gaseous Mixtures Using Porous Polyaromatic Polymer Beads. Analytical Chemistry, 38(2), 309–316.

Holmes, D.E. and Smith, J.A. (2016). Biologically Produced Methane as a Renewable Energy Source. Advances in Applied Microbiology, 1–61.

Hwang, S. W.; Umar, Ahmad; Dar, G. N.; Kim, S. H.; Badran, R. I. (2014). Synthesis and Characterization of Iron Oxide Nanoparticles for Phenyl Hydrazine Sensor Applications. Sensor Letters, 12(1), 97–101.

Jiang, J.-X.; Su, F.; Trewin, A.; Wood, C. D.; Campbell, N. L.; Niu, H.; Dickinson, C.; Ganin, A. Y.; Rosseinsky, M. J.; Khimyak, Y. (2007). Conjugated Microporous Poly (Arylene ethynylene) Networks. Angew. Chem., Int. Ed.46, 8574– 8578.

Ji, W., Wang, T.-X., Ding, X., Lei, S., & Han, B.-H. (2021). Porphyrin- and phthalocyanine-based porous organic polymers: From synthesis to application. Coordination Chemistry Reviews, 439, 213875.

Ju, P., Wu, S., Su, Q., Li, X., Liu, Z., Li, G. and Wu, Q. (2019). Salen–porphyrin-based conjugated microporous polymer supported Pd nanoparticles: highly efficient heterogeneous catalysts for aqueous C–C coupling reactions. Journal of materials chemistry. A, Materials for energy and sustainability, 7(6), 2660–2666.

Ju, P.Y., Wu, S.J., Su, Q., Li, X.D., Liu, Z.Q., Li, G.H., Wu, Q.L. (2019). Salen-porphyrin-based conjugated microporous polymer supported Pd nanoparticles: Highly efficient heterogeneous catalysts for aqueous C-C coupling reactions. J. Mater. Chem. A 7 (6), 2660–2666.

Kathiresan, M. (2023) 'Metal-ion/metal nanoparticle-anchored porous organic polymers as efficient catalysts for organic transformations – a recent overview,' Chemistry – An Asian Journal, 18(8), e202201299.

Karimi-Maleh, H., Fakude, C. T., Mabuba, N., Peleyeju, G. M., & Arotiba, O. A. (2019). The determination of 2-phenylphenol in the presence of 4-chlorophenol using nano-Fe3O4/ionic liquid paste electrode as an electrochemical sensor. Journal of Colloid and Interface Science, 15:554, 603-610.

Kaur, P., Hupp, J. T., & Nguyen, S. T. (2011). Porous Organic Polymers in Catalysis: Opportunities and Challenges. ACS Catalysis, 1(7), 819–835.

Katekomol, P., Roeser, J., Bojdys, M., Weber, J., & Thomas, A. (2013). Covalent Triazine Frameworks Prepared from 1,3,5-Tricyanobenzene. Chemistry of Materials, 25(9), 1542–1548.

Khan, I., Saeed, K. and Khan, I. (2017). Nanoparticles: Properties, applications, and toxicities. Arabian Journal of Chemistry, 12(7).

Khan, U.S. et al. (2015) 'Transformation mechanism of magnetite nanoparticles', Materials Science-Poland, 33(2), 278–285.

Kuhn, P.; Antonietti, M.; Thomas, A. (2008). Porous, Covalent Triazine-Based Frameworks Prepared by Ionothermal Synthesis. Angew. Chem., Int. Ed, 47, 3450−3453.

Kyung S.S., Fritz, P. and Coskun, A. (2022). Porous organic polymers for CO2 capture, separation, and conversion. 51(23), 9831–9852.

Laurent, S., Forge, D., Port, M., Roch, A., Robic, C., Vander Elst, L., & Muller, R. N. (2008). Magnetic Iron Oxide Nanoparticles: Synthesis, Stabilization, Vectorization, Physicochemical Characterizations, and Biological Applications. Chemical Reviews, 108(6), 2064–2110

Lee C. O., Howe K. J. and Thomson B. M. (2012). Ozone and biofiltration as an alternative to reverse osmosis for removing PPCPs and micropollutants from treated wastewater, Water Res, 46, 1005 —1014.

Lee, J.S. M., & Cooper, A. I. (2020). Advances in Conjugated Microporous Polymers. Chemical Reviews, 4, 2171-2214.

Lemine, O. M., Omri, K., Zhang, B., El Mir, L., Sajieddine, M., Alyamani, A., & Bououdina, M. (2012). Sol–gel synthesis of 8nm magnetite (Fe3O4) nanoparticles and their magnetic properties. Superlattices and Microstructures, 52(4), 793–799.

Liao, L., Li, M., Yin, Y., Chen, J., Zhong, Q., Du, R., Liu, S., He, Y., Fu, W. and Zeng, F. (2023). Advances in the Synthesis of Covalent Triazine Frameworks. ACS omega, 8(5), 4527–4542.

Li, B., Su, F., Luo, H.-K., Liang, L., & Tan, B. (2011). Hypercrosslinked microporous polymer networks for effective removal of toxic metal ions from water. Microporous and Mesoporous Materials, 138(1-3), 207–214.

Li, Buyi; Gong, Ruini; Wang, Wei; Huang, Xin; Zhang, Wang; Li, Huanmin; Hu, Chunxiao; Tan, Bien (2011). A New Strategy to Microporous Polymers: Knitting Rigid Aromatic Building Blocks by External Cross-Linker. Macromolecules, 44(8), 2410–2414.

Lida, H., Takayanagi, K., Nakanishi, T., & Osaka, T. (2007). Synthesis of Fe3O4 nanoparticles with various sizes and magnetic properties by controlled hydrolysis. Journal of Colloid and Interface Science, 314(1), 274–280.

Li, H., Wu, X., Xu, Y., Tong, H. and Wang, L. (2014). Dicyanovinyl-Functionalized Fluorescent Hyperbranched Conjugated Polymer Nanoparticles for Sensitive Naked-Eye Cyanide Ion Detection. Polym. Chem. 5, 5949–5956.

Li, L., Cai, Z., Wu, Q., Lo, W. Y., Zhang, N., Chen, L. X., et al. (2016a). Rational design of porous conjugated polymers and roles of residual palladium for photocatalytic hydrogen production. J. Am. Chem. Soc. 138, 7681–7686.

Li, M., Zhao, H. and Lu, Z.-Y. (2020) ‘Porphyrin-based porous organic polymer, PY-pop, as a multifunctional platform for efficient selective adsorption and photocatalytic degradation of cationic dyes,’ Microporous and Mesoporous Materials, 292, 109-774.

Lin, G., Ding, H., Yuan, D., Wang, B., and Wang, C. (2016). Wang, A Pyrene-Based, Fluorescent Three-Dimensional Covalent Organic Framework. J. Am. Chem. Soc. 138, 3302−3305.

Liu, M., Guo, L., Jin, S., & Tan, B. (2019). Covalent Triazine Frameworks: Synthesis and Applications. Journal of Materials Chemistry A, 7(10), 5153-5172.

Liu, M., Huang, Q., Wang, S., Li, Z., Li, B., Jin, S. and Tan, B. (2018). Crystalline Covalent Triazine Frameworks by In Situ Oxidation of Alcohols to Aldehyde Monomers. 57(37), 11968–11972.

Liu, S., Chen, D., Zheng, J., Zeng, L., Jiang, J., Jiang, R., Zhu, F., Shen, Y., Wu, D. and Ouyang, G. (2015). The sensitive and selective adsorption of aromatic compounds with highly crosslinked polymer nanoparticles. Nanoscale, 7(40), 16943–16951.

Liu, S., Bai, J.L., Huo, Y.P., Ning, B.A., Peng, Y., Li, S., Han, D.P., Kang, W.J., Gao, Z.X. (2020a). A zirconium-porphyrin MOF-based ratiometric fluorescent biosensor for rapid and ultrasensitive detection of chloramphenicol. Biosensors and Bioelectronics, 149, 111-801.

Liu, T., Zhang, Y., Shan, Z., Wu, M., Li, B., Sun, H., Su, G., Wang, R. and Zhang, G. (2023). Covalent Organic Framework Membrane for Efficient Removal of Emerging Trace Organic Contaminants from Water. Nature Water. 1(12), 1059-1067.

Liu, X., Xu, Y., & Jiang, D. (2012). Conjugated Microporous Polymers as Molecular Sensing Devices: Microporous Architecture Enables Rapid Response and Enhances Sensitivity in Fluorescence-On and Fluorescence-Off Sensing. Journal of the American Chemical Society, 134(21), 8738–8741.

Li, X.; Huang, G.H.; Chen, X.J.; Huang, J.; Li, M.N.; Ying, J.N.; Liang, Y.; Yao, Y.; Li, Y.P. (2021). A Review on Graphitic Carbon Nitride (g-C3N4) Based Hybrid Membranes for Water and Wastewater Treatment. Sci. Total Environ. 792, 148462–148481

Li, Y., Duan, Q., Wang, H., Gao, B., Qiu, N., Li, Y. (2018a). Construction of two-dimensional porphyrin-based fully conjugated microporous polymers as highly efficient photocatalysts. J. Photochem. Photobiol. A 356, 370–378.

Li, Y., Duan, Q., Wang, H., Gao, B., Qiu, N., Li, Y. (2018a). Construction of two-dimensional porphyrin-based fully conjugated microporous polymers as highly efficient photocatalysts. J. Photochem. Photobiol. A 356, 370–378.

Li, Z.-Y., Gao, D.-Y., Wu, Z.-Y., and Zhao, S. (2020). Simultaneous electrochemical detection of levodopa, paracetamol, and l-tyrosine based on multi-walled carbon nanotubes. RSC Advances, 10(24), 14218–14224.

Lorenzo, M. Á., Sánchez Arribas, A., Moreno, M., Bermejo, E., Chicharro, M., & Zapardiel, A. (2013). Determination of butylparaben by adsorptive stripping voltammetry at glassy carbon electrodes modified with multi-wall carbon nanotubes. Microchemical Journal, 110, 510–516.

Lu, W., Yuan, D., Zhao, D., Schilling, C. I., Plietzsch, O., Muller, T., Zhou, H.-C. (2010). Porous Polymer Networks: Synthesis, Porosity, and Applications in Gas Storage/Separation. Chemistry of Materials, 22(21), 5964–5972.

Marciello, M., Luengo, Y., & P. Morales, M. (2016). Iron Oxide Nanoparticles for Cancer Diagnosis and Therapy. Nanoarchitectonics for Smart Delivery and Drug Targeting, 667–694.

Maria and Smith, K.M. (2023). Syntheses and Functionalizations of Porphyrin Macrocycles. Current Organic Synthesis, [online] 11(1), 3–28.

Marken, F., Carta, M. and McKeown, N.B. (2020) 'Polymers of intrinsic microporosity in the design of electrochemical multicomponent and multiphase interfaces,' Analytical Chemistry, 93(3), 1213–1220.

Maryamdokht Taimoory, S. et al. (2017) 'Importance of the inter-electrode distance for the electrochemical synthesis of magnetite nanoparticles: Synthesis, characterization, computational modeling, and cytotoxicity,' e-Journal of Surface Science and Nanotechnology, 15(0), 31–39.

Ma, S. and Zhou, H.-C. (2010) 'Gas storage in porous metal–organic frameworks for Clean Energy Applications', Chem. Commun., 46(1), 44–53.

McKeown, N.B. and Budd, P.M. (2006) 'Polymers of intrinsic microporosity (PIMS): Organic materials for membrane separations, heterogeneous catalysis, and Hydrogen Storage,' Chemical Society Reviews, 35(8), 675.

McKeown, N. B. (2017). The synthesis of polymers of intrinsic microporosity (PIMs). Science China Chemistry, 60(8), 1023–1032.

McKeown, N. B. (2020). Polymers of Intrinsic Microporosity (PIMs). Polymer, 122-736.

Meng Z., Stolz R. M. and Mirica K. A. (2019). Two-Dimensional Chemiresistive Covalent Organic Framework with High Intrinsic Conductivity. J. Am. Chem. Soc., 141, 11929−11937.

Modak, A., Mondal, J. and Bhaumik, A. (2013). Porphyrin-based porous organic polymer as bi-functional catalyst for selective oxidation and Knoevenagel condensation reactions. Applied Catalysis A: General, 459, 41–51.

Modak, A., Nandi, M., Mondal, J. and Bhaumik, A. (2011). Porphyrin-based porous organic polymers: novel synthetic strategy and exceptionally high CO2adsorption capacity. Chem. Commun., 48(2), 248–250.

Mohammad Ali Kamyabi, Shahabi, S. and Hosseini-Monfared, H. (2008). Electrocatalytic Oxidation of Hydrazine at a Cobalt (II) Schiff-Base-Modified Carbon Paste Electrode. Journal of The Electrochemical Society, 155(1), F8–F12.

Mohanraj, V. J., & Chen, Y. (2007). Nanoparticles - A review. Tropical Journal of Pharmaceutical Research, 5(1), 561-573.

Moral, R., Wang, R., Russo, I. H., Lamartiniere, C. A., Pereira, J., & Russo, J. (2008). Effect of prenatal exposure to the endocrine disruptor bisphenol A on mammary gland morphology and gene expression signature. Journal of Endocrinology, 196(1), 101–112.

Nagaraj B, Bahadur, K., M, K. and Yong R.L. (2014). Green fabrication of ferromagnetic Fe_3O_4 nanoparticles and their novel catalytic applications for the synthesis of biologically interesting benzoxazinone and benzthioxazinone derivatives. New Journal of Chemistry, 38(11), 5415–5420.

Nath, B., Li, W.H., Huang, J.H., Wang, G.E., Fu, Z.H., Yao, M.S., Xu, G., (2016). A new azodioxy-linked porphyrin-based semiconductive covalent organic framework with I-2 doping-enhanced photoconductivity. Crystengcomm 18 (23), 4259–4263.

Nihemaiti M., Miklos D. B., Hübner U., Linden K. G., Drewes J. E. and Croué J.-P. (2018). Removal of trace organic chemicals in wastewater effluent by UV/H_2O_2 and UV/PDS, Water Res., 145, 487 —497

Nodehi, M., Baghayeri, M., Ansari, R., & Veisi, H. (2020). Electrochemical quantification of 17α – Ethinylestradiol in biological samples using an Au/Fe_3O_4@TA/MWNT/GCE sensor. Materials Chemistry and Physics, 244, 122687.

Oliveras-González, C., Florent Di Meo, Arántzazu González-Campo, Beljonne, D., Norman, P., Maite Simón-Sorbed, Linares, M. and Amabilino, D.B. (2015). Bottom-Up Hierarchical Self-Assembly of Chiral Porphyrins through Coordination and Hydrogen Bonds. Journal of the American Chemical Society, 137(50), 15795–15808.

Ong, H.T., Samsudin, H. and Soto-Valdez, H. (2020). Migration of endocrine-disrupting chemicals into food from plastic packaging materials: an overview of chemical risk assessment, techniques to monitor migration and international regulations. Critical Reviews in Food Science and Nutrition, 1–23.

Patel, H.S., Sang Hyun Je, Park, J., Jung, Y., Coskun, A. and Yavuz, C.T. (2014). Directing the Structural Features of N2-Phobic Nanoporous Covalent Organic Polymers for CO2Capture and Separation. Chemistry: A European Journal, 20(3), 772–780.

Peik-See, T., Pandikumar, A., Nay-Ming, H., Hong-Ngee, L., & Sulaiman, Y. (2014). Simultaneous Electrochemical Detection of Dopamine and Ascorbic Acid Using an Iron Oxide/Reduced Graphene Oxide Modified Glassy Carbon Electrode. Sensors, 14(8), 15227–15243.

Pintor Simamora, Manullang, M., Jesinta Munthe and Juniastel Rajagukguk (2018). The Structural and Morphology Properties of Fe_3O_4/Ppy Nanocomposite. 1120, 12063–12063.

Prabhu, K., Malode, S.J., Shetti, N.P., Saravanan Pandiaraj, Abdullah Alodhayb and Muthumareeswaran Muthuramamoorthy (2023). Electro-sensing layer constructed of a WO_3/CuO nanocomposite for the electrochemical determination of 2-phenylphenol fungicide. Environmental Research, 236, 116710–116710.

Qian, Z., Wang, Z. J., & Zhang, K. A. I. (2021). Covalent Triazine Frameworks as Emerging Heterogeneous Photocatalysts. Chemistry of Materials, 33(6), 1909–1926.

Rajendran, S., Tuan Anh Nguyen, Saeid Kakooei, Yeganeh, M. and Li, Y. (2020). Corrosion Protection at the Nanoscale. Elsevier, 473-477.

Rama, R., Meenakshi, S., Pandian, K. and Gopinath, S.C.B. (2021). Room Temperature Ionic Liquids-Based Electrochemical Sensors: An Overview on Paracetamol Detection. Critical Reviews in Analytical Chemistry, 1–10.

Rao M. R., Fang Y., De Feyter St. and Perepichka D. F. Conjugated Covalent Organic Frameworks via Michael Addition−Elimination. J. Am. Chem. Soc., 2017, 139, 2421−2427.

Ravi, S. et al. (2022). Porous organic nanofiber polymers as superfast adsorbents for capturing pharmaceutical contaminants from water,' Environmental Science: Nano, 9(2), 730–741.

Rochat, S., Polak-Krasna, M., Tian, M., Mays, T.J., Bowen, C.R., Burrows, A.D. (2019). Assessment of the long-term stability of the polymer of intrinsic microporosity PIM-1 for hydrogen storage applications.Int. J. Hydr. Energy, 44, 332-337

Salata, O. (2004). Applications of nanoparticles in biology and Medicine. Journal of Nanobiotechnology, [online] 2(1), 3.

Samuel, W.S. (2018). The Effect of Soxhlet Extraction and Synthesis Temperature on Properties of Polyaniline. [online] ODU Digital Commons. Available at: https://digitalcommons.odu.edu/chemistry_etds/20?utm_source=digitalcommons.odu.edu%2Fchemistry_etds%2F20&utm_medium=PDF&utm_campaign=PDFCoverPages [Accessed 21 Oct. 2023].

Sarkar, C., Shit, S. C., Das, N., & Mondal, J. (2021). Presenting porous–organic–polymers as next-generation invigorating materials for nanoreactors. Chemical Communications, 57, 8550-8567.

Schug, T.T., Janesick, A., Blumberg, B. and Heindel, J.J. (2011). Endocrine disrupting chemicals and disease susceptibility. The Journal of Steroid Biochemistry and Molecular Biology, [online] 127(3-5), 204–215.

Scognamiglio, V., Antonacci, A., Patrolecco, L., Lambreva, M.D., Litescu, S.C., Ghuge, S.A. and Rea, G. (2016). Analytical tools monitoring endocrine disrupting chemicals. TrAC Trends in Analytical Chemistry, 80, 555–567.

Sebati, W., & Ray, S. (2018, October 24). Advances in Nanostructured Metal-Encapsulated Porous Organic-Polymer Composites for Catalyzed Organic Chemical Synthesis. *Catalysts*, *8*(11), 492.

Sengeni Anantharaj, Noda, S., Vasanth Rajendiran Jothi, Yi, S., Matthias Driess and Menezes, P.W. (2021). Strategies and Perspectives to Catch the Missing Pieces in Energy-Efficient Hydrogen Evolution Reaction in Alkaline Media. 60(35), 18981–19006.

Seo, M., Kim, S., Oh, J., Kim, S.-J., & Hillmyer, M. A. (2015). Hierarchically Porous Polymers from Hyper-cross-linked Block Polymer Precursors. Journal of the American Chemical Society, 137(2), 600–603.

Shaikshavali, P., Reddy, T. M., Lakshmi Narayana, A., Hussain, O. M., Venkataprasad, G., & Venu Gopal, T. (2020). A powerful electrochemical sensor based on Fe_3O_4 nanoparticles-multiwalled carbon nanotubes hybrid for the effective monitoring of sunset yellow in soft drinks. Journal of Food Measurement and Characterization, 14(6), 3319-3332.

Sharif, H.F.E.L., Patel, S.R., Ndunda, E. and Reddy, S.M. (2022). Electrochemical detection of dioctyl phthalate using molecularly imprinted polymer modified screen-printed electrodes. 1196, 339547–339547.

Shu, L., Yu, J., Cui, Y., Ma, Y., Li, Y., Gao, B. and Wang, H. (2022). Porphyrin-based conjugated microporous polymers with dual active sites as anode materials for lithium-organic batteries. International Journal of Hydrogen Energy, 47(20), 10902–10910.

Shultz, A. M., Farha, O. K., Hupp, J. T., & Nguyen, S. T. (2011). Synthesis of catalytically active porous organic polymers from metalloporphyrin building blocks. Chemical Science, 2(4), 686.

Sigen A, Yuwei Z.; Zhongping L.; Hong X.; Ming X., Xiaoming L.; Ying M. (2014). Highly efficient and reversible iodine capture using a metalloporphyrin-based conjugated microporous polymer. Chemical Communications, 50(62), 8495.

Simon, P., Gogotsi, Y. (2008). Materials for electrochemical capacitors. Nature Mater 7, 845–854.

Skinner M.K. (2011). Role of epigenetics in developmental biology and transgenerational inheritance, Birth Defects Res. C Embryo Today 93 (1), 51–55,

Street, M., Angelini, S., Bernasconi, S., Burgio, E., Cassio, A., Catellani, C., Cirillo, F., Deodati, A., Fabbrizi, E., Fanos, V., Gargano, G., Grossi, E., Iughetti, L., Lazzeroni, P., Mantovani, A., Migliore, L., Palanza, P., Panzica, G., Papini, A. and Parmigiani, S. (2018). Current Knowledge on Endocrine Disrupting Chemicals (EDCs) from Animal Biology to Humans, from Pregnancy to Adulthood: Highlights from a National Italian Meeting. International Journal of Molecular Sciences, 19(6), 1647.

Song, H., Xue, G., Zhang, J., Wang, G., Ye, B., Sun, S., Tian, L. and Li, Y. (2017). Simultaneous voltammetric determination of dopamine and uric acid using carbon-encapsulated hollow Fe_3O_4 nanoparticles anchored to an electrode modified with nanosheets of reduced graphene oxide. Mikrochimica Acta, 184(3), 843–853.

Song, K.S., Fritz, P.W. and Coskun, A. (2022) 'Porous organic polymers for CO_2 capture, separation, and conversion', Chemical Society Reviews, 51(23), 9831–9852.

Song, W., Zhang, Y., Chinh Hoang Tran, Ha Kyung Choi, Yu, D.-G. and Kim, I. (2023). Porous Organic Polymers with Defined Morphologies: Synthesis, Assembly, and Emerging Applications. 142, 101691–101691.

Soury, R., Chaabene, M., Jabli, M., Saleh, T.A., Ben Chaabane, R., Saint-Aman, E., Loiseau, F., Philouze, C., Allouche, A.R., Nasri, H. (2019). Mesotetrakis (3, 4, 5-trimethoxyphenyl) porphyrin derivatives: Synthesis, spectroscopic characterizations, and adsorption of NO_2. Chem. Eng. J. 375, 14.

Sun, J., Xu, L., Shi, Z., Zhao, Q., Wang, H. and Gan, T. (2021). Morphology-tunable hollow Mn2O3 nanostructures: highly efficient electrocatalysts and their

electrochemical sensing for phenolic endocrine disruptors via toughening of graphene oxide. Sensors and Actuators B: Chemical, 327, 128889–128889.

Sun, R., Feng S., Zhou B., Chen Z., Wang D., and Liu H. (2020). Flexible Cyclosiloxane-Linked Fluorescent Porous Polymers for Multifunctional Chemical Sensors. ACS Macro Lett., 9, 43−48.

Sun, Y., Li, Y., Wang, N., Xu, Q. Q., Xu, L., & Lin, M. (2018). Copper-based Metal-organic Framework for Non-enzymatic Electrochemical Detection of Glucose. *Electroanalysis*, *30*(3), 474–478.

Swager, T.M. and Mirica, K.A. (2019). Introduction: Chemical Sensors. Chemical Reviews, 119(1), 1–2.

Tanabe, K. K., Ferrandon, M. S., Siladke, N. A., Kraft, S. J., Zhang, G., Niklas, J., Nguyen, S. T. (2014). Discovery of Highly Selective Alkyne Semihydrogenation Catalysts Based on First-Row Transition-Metallated Porous Organic Polymers. Angewandte Chemie, 126(45), 12251–12254.

Tan, L. and Tan, B. (2017) 'Hypercrosslinked porous polymer materials: Design, synthesis, and applications,' Chemical Society Reviews, 46(11), 3322–3356.

Tao, R., Ma, X., Wei, X., Jin, Y., Qiu, L. and Zhang, W. (2020). Porous organic polymer material supported palladium nanoparticles. Journal of materials chemistry. A, Materials for energy and sustainability, 8(34), 17360–17391.

Teja, A. S., & Koh, P.-Y. (2009). Synthesis, properties, and applications of magnetic iron oxide nanoparticles. Progress in Crystal Growth and Characterization of Materials, 55(1-2), 22–45.

Thommes, M., Kaneko, K., Neimark, A.V., Olivier, J.P., Rodriguez-Reinoso, F., Rouquerol, J. and Sing, K.S.W. (2015). Physisorption of gases, with special reference to the evaluation of surface area and pore size distribution (IUPAC Technical Report). Pure and Applied Chemistry, [online] 87(9-10), 1051–1069.

Tian, Y., & Zhu, G. (2020). Porous Aromatic Frameworks (PAFs). Chemical Reviews, 120(16), 8934-8986.

Tsivadze, A Yu; Aksyutin, O E; Ishkov, A G; Men'shchikov, I E; Fomkin, A A; Shkolin, A V; Khozina, E V; Grachev, V A. (2018). Porous carbon-based adsorption systems for natural gas (methane) storage. Russian Chemical Reviews, 87(10), 950–983.

Vandenberg, L.N., Colborn, T., Hayes, T.B., Heindel, J.J., Jacobs, D.R., Lee, D.-H., Shioda, T., Soto, A.M., vom Saal, F.S., Welshons, W.V., Zoeller, R.T. and Myers, J.P. (2012). Hormones and Endocrine-Disrupting Chemicals: Low-Dose Effects and Nonmonotonic Dose Responses. *Endocrine Reviews*, [online] 33(3), 378–455.

Wang, G., Zhang, L., & Zhang, J. (2012). A review of electrode materials for electrochemical supercapacitors. Chem. Soc. Rev., 41(2), 797–828.

Wang H., Ding H., Meng X., Wang C. (2016). Two-dimensional porphyrin- and phthalocyanine-based covalent organic frameworks, Chinese Chem. Lett. 27,1376–1382

Wang, J., Jiao, C., Li, M., Wang, X., Wang, C. and Wu, Q. (2017). Porphyrin-based porous organic polymer modified with Fe_3O_4 nanoparticles as an efficient adsorbent for the enrichment of benzoylurea insecticides. Mikrochimica Acta, 185(1), 36.

Wang, S., Li, H., Huang, H., Cao, X., Chen, X. and Cao, D. (2022). Porous organic polymers as a platform for sensing applications. 51(6), 2031–2080.

Wang, Y., Cui, X., Zhang, P., Wang, Y. and Lu, W. (2023). Synthesis of porphyrin porous organic polymers and their application of water pollution treatment: A review. 29, 102972–102972.

Wang, Y., Cao, Y., Fang, C. and Gong, Q. (2010). Electrochemical sensor for parabens based on molecular imprinting polymers with dual-templates. Analytica Chimica Acta, 673(2), 145–150.

Wang, Z., Yang, X., Yang, T., Zhao, Y., Wang, F., Chen, Y., Zeng, J.H., Yan, C., Huang, F. and Jiang, J.-X. (2018). Dibenzothiophene Dioxide Based Conjugated Microporous Polymers for Visible-Light-Driven Hydrogen Production. ACS Catalysis, 8(9), 8590–8596.

Wood, C.D.; Tan, B.; Trewin, A.; Niu, H.; Bradshaw, D.; Rosseinsky, M.J.; Khimyak, Y. Z.; Campbell, N. L.; Kirk, R.; Stöckel, E.; Cooper, A.I. (2007). Hydrogen Storage in Microporous Hypercrosslinked Organic Polymer Networks. Chemistry of Materials, 19(8), 2034–2048.

Wu, Z.-S., Chen, L., Liu, J., Parvez, K., Liang, H., Shu, J., Müllen, K. (2013). High-Performance Electrocatalysts for Oxygen Reduction Derived from Cobalt Porphyrin-Based Conjugated Mesoporous Polymers. Advanced Materials, 26(9), 1450–1455.

Xia, J., Yuan, S., Wang, Z., Kirklin, S., Dorney, B., Liu, D.-J. and Yu, L. (2010). Nanoporous Polyporphyrin as Adsorbent for Hydrogen Storage. Macromolecules, 43(7), 3325–3330.

Xia, X., Sun, P., Sun, X., Wang, Y., Yang, S., Jia, Y., Peng, B. and Nie, C. (2021). Hyper-crosslinked polymers with controlled multiscale porosity for effective removal of benzene from cigarette smoke. e-Polymers, 22(1), 19–29.

Xie, X., Bu, Y. and Wang, S. (2016). Molecular imprinting: a tool of modern chemistry for analysis and monitoring of phenolic environmental estrogens. Reviews in Analytical Chemistry, 35(2), 87–97.

Xie, Y. et al. (2020). 'Iron-porphyrin-based covalent-organic frameworks for electrochemical sensing H_2O_2 and ph.', Materials Science and Engineering: C, 112, 110-864.

Xiang, Z and Cao, D. (2012). Synthesis of Luminescent Covalent–Organic Polymers for Detecting Nitroaromatic Explosives and Small Organic Molecules. Macromol. Rapid Commun., 2012, 33, 1184−1190.

Xiong, J.-B., Ban, D.-D., Zhou, Y.-J., Du, H.-J., Zhao, A.-W., Xie, L.-G., Liu, G., Chen, S. and Mi, L. (2022). Fluorescent porous organic polymers for detection and adsorption of nitroaromatic compounds. Scientific Reports, 12(1), 15876.

Xu, C., Zhang, W., Tang, J., Pan, C. and Yu, G. (2018). Porous Organic Polymers: An Emerged Platform for Photocatalytic Water Splitting, 6, 592.

Xu, S., Weng, Z., Tan, J., Guo, J. and Wang, C. (2015). Hierarchically structured porous organic polymer microspheres with built-in Fe_3O_4 supraparticles: construction of dual-level pores for Pt-catalyzed enantioselective hydrogenation. Polymer Chemistry, 6(15), 2892–2899.

Xu, X., Wang, S., Yue, Y., and Huang, N. (2020). Semiconductive Porphyrin-Based Covalent Organic Frameworks for Sensitive Near-Infrared Detection. ACS Applied Materials & Interfaces, 12(33), 37427–37434.

Xu, Y., Jin, S., Xu, H., Nagai, A., & Jiang, D. (2013). Conjugated microporous polymers: design, synthesis, and application. Chemical Society Reviews, 42(20), 8012.

WenyanZ., Luo Y., Wang H., Zhang D., Li Z. (2020). Porous Organic Polymers as Heterogeneous Catalysts for Visible Light-Induced Organic Transformations. Chinese Journal of Organic Chemistry, 40(11), 3777-3793.

Yang, L., Shao, L., Wu, Z., Zhan, P., & Zhang, L. (2023). Design and Synthesis of Porous Organic Polymers: Promising Catalysts for Lignocellulose Conversion to 5-Hydroxymethylfurfural and Derivates. *Polymers*, *15*(12), 2630.

Yao, X., Chen, K., Qiu, L., Yang, Z. and He, L. (2021). Ferric Porphyrin-Based Porous Organic Polymers for CO_2 Photocatalytic Reduction to Syngas with Selectivity Control. Chemistry of Materials, 33(22), 8863–8872.

Yuan, R., Yan, Z., Shaga, A., & He, H. (2021). Design and fabrication of an electrochemical sensing platform based on a porous organic polymer for ultrasensitive ampicillin detection. Sensors and Actuators B: Chemical, 327, 128949.

Yuan, Y. and Zhu, G. (2019) 'Porous aromatic frameworks as a platform for multifunctional applications', *ACS Central Science*, 5(3), 409–418.

Yu, C., Gou, L., Zhou, X., Bao, N. and Gu, H. (2011). Chitosan–Fe_3O_4 nanocomposite based electrochemical sensors for the determination of bisphenol A. Electrochimica Acta, 56(25), 9056–9063.

Yuksel, S.; Kabay, N.; Yuksel, M. (2013). Removal of bisphenol A (BPA) from water by various nanofiltration (NF) and reverse osmosis (RO) membranes. J. Hazard. Mater, 263, 307–310.

Zala S.M. and Penn D. J. (2004). Abnormal behaviours induced by chemical pollution: a review of the evidence and new challenges. Anim. Behav. 68, 649-664

Zhang, B., Wei, M., Mao, H., Pei, X., Alshmimri, S. A., Reimer, J. A., & Yaghi, O. M. (2018). Crystalline Dioxin-Linked Covalent Organic Frameworks from Irreversible Reactions. Journal of the American Chemical Society, 140(40), 12715-12719.

Zhang B., Yan J., Shang Y., and Wang Z. (2018). Synthesis of Fluorescent Micro- and Mesoporous Polyaminals for Detection of Toxic Pesticides. Macromolecules. 51, 1769−1776.

Zhang J. L., Yang Y., Liang W. B., Yao L. Y., Yuan R., and Xiao D. R. (2021).Highly Stable Covalent Organic Framework Nanosheets as a New Generation of Electrochemiluminescence Emitters for Ultrasensitive MicroRNA Detection. Anal. Chem,93, 3258−3265.

Zhang, K., Wang, Q., Zhou, Y., Gao, J., Li, C., & Jiang, X. (2020). A low-cost crosslinked polystyrene derived from environmental wastes for adsorption of phenolic compounds from aqueous solution. Journal of Molecular Liquids, 314, 113-641.

Zhang, W., Aguila, B. and Ma, S. (2017). Retracted Article: Potential applications of functional porous organic polymer materials. Journal of Materials Chemistry A, 5(19), 8795–8824.

Zhang, Z.Y.; Hu, W.J.; Ruan, W.J.; Ai, H.Y.; Yuan, B.L.; Fu, M.L. (2021). Highly Improved Dechlorination of 2,4-Dichlorophenol in Aqueous Solution by Fe/Ni Nanoparticles Supported by Polystyrene Resin. Chemosphere, 266, 128976–128983.

Zhao, X., Ju, X., Qiu, S., Hu, W., Yang, L. and Zhang, J. (2018). Fast and Sensitive Detection of Diisononyl Phthalate in Liquor Sample by Molecularly Imprinted Polymer Based Electrochemical Sensor. Russian Journal of Electrochemistry, 54(8), 636–643.

Zhao, X., Liu, Y., Zhu, Q., and Gong, W. (2023). Catechol-Based Porous Organic Polymers for Effective Removal of Phenolic Pollutants from Water. Polymers, 15(11), 2565–2565.

Zhang, Xu; Tang, Song; Qiu, Tian; Hu, Xiaojian; Lu, Yifu; Du, Peng; Xie, Linna; Yang, Yanwei; Zhao, Feng; Zhu, Ying; Giesy, John P. (2020). Investigation of phthalate metabolites in urine and daily phthalate intakes among three age groups in Beijing, China. Environmental Pollution, 260, 114005.

Zhao, X., Ju, X., Qiu, S., Hu, W., Yang, L. and Zhang, J. (2018). Fast and Sensitive Detection of Diisononyl Phthalate in Liquor Sample by Molecularly Imprinted Polymer Based Electrochemical Sensor. Russian Journal of Electrochemistry, 54(8), 636–643.

Zhao, Y., Yao, K. X., Teng, B., Zhang, T., & Han, Y. (2013). A perfluorinated covalent triazine-based framework for highly selective and water–tolerant CO_2 capture. Energy & Environmental Science, 6(12), 3684.

Zhou, D., Tan, X.Y., Wu, H.M., Tian, L.H., Li, M. (2019). Synthesis of C-C bonded two-dimensional conjugated covalent organic framework films by Suzuki polymerization on a liquid-liquid interface. Angew. Chem. Int. Edn 58 (5), 1376–1381.

Zhu, M.H., Chen, J.C., Huang, L.B., Ye, R.Q., Xu, J., Han, Y.F. (2019). Covalently grafting cobalt porphyrin onto carbon nanotubes for efficient CO_2 electroreduction. Angew. Chem. Int. Edn 58 (20), 6595–6599.